Journal of

POLISH CIMAC

SELECTED PROBLEMS OF DESIGNING AND OPERATING TECHNICAL SYSTEMS

Gdansk, 2009

This journal is devoted to designing of diesel engines, gas turbines and ships' power transmission systems containing these engines and also machines and other appliances necessary to keep these engines in movement with special regard to their energetic and pro-ecological properties and also their durability, reliability, diagnostics and safety of their work and operation of diesel engines, gas turbines and also machines and other appliances necessary to keep these engines in movement with special regard to their energetic and pro-ecological properties, their durability, reliability, diagnostics and safety of their work, and, above all, rational (and optimal) control of the processes of their operation and specially rational service works (including control and diagnosing systems), analysing of properties and treatment of liquid fuels and lubricating oils, etc.

CONTENTS

Introduction

In contemporary science we can observe higher and higher specialization in particular scientific disciplines. The specialization causes that research is conducted with not proper consideration of the knowledge from other scientific disciplines even if they belong to the same field of knowledge. Thus, specialists dealing with a subject from the „machine building and operating" discipline, study reluctantly the achievements of the related disciplines such as: „automation and robotics", „electronics", „electrical engineering", „energetics", „computer science", „mechanics" or " transport". Much more unconcerned is the knowledge from such disciplines as: „biocybernetics & biomedical engineering" and „biotechnology", although they are classified to the field of knowledge defined as „technical sciences". The situation is justifiable. It follows from the anxiety that studying developments in other disciplines may cause falling behind with developments in the discipline practiced by the given scientist. In consequence making a Doctoral Thesis is easier but Habilitation Thesis – much more difficult. Habilitation qualification can be achieved among others when a candidate in his/her research accomplishments can show application to for the first time the knowledge from any other field of knowledge, like for example. „mathematical sciences".

In each scientific discipline, independently which field of knowledge it belongs to, the science is being developed in result of applying proper scientific methods. However, apart from the specific methods, in each scientific discipline there are also used deductive and inductive methods if the created knowledge is supposed to be of essential for science cognitive properties. Deductive methods are used when it is necessary to prove a theorem. When a hypothesis (hypotheses) is (are) to be verified we apply inductive or deductive methods. As a rule the importance of the method called analogy is not appreciated. The analogy, however, enables searching for the common *rightness* (*premise*, *cause*) characterizing different research objects (being characteristic for particular scientific disciplines), while deduction consists in matching *consequence* (*result*, *conclusion*) to *rightness*, and *induction* – in matching rightness to *consequence*.

From this reason it can be interesting for many scientists and at the same time beneficial for development of technical sciences when the *Journal of POLISH CIMAC,* which is destined for papers concerning the knowledge enclosed in „machine building and operating" discipline, will present also these papers which are classified to the other scientific disciplines from the field of knowledge called „technical sciences", including "biocybernetics & biomedical engineering" and „biotechnology". Among such papers placed in this journal are: Identification of quasi-static cutting force of triticale-straws for designing use of scissor and finger cutting sets, Development of (plastic-, bio- and fibrous) energy-materials grinding, Analysis of frame stability as safety requirement, Increased power and energy losses in low voltage power line caused by load asymmetry, Decarburisation of ferrite laths during bainite reaction in ADI, Relations between BMD density and volumetric and fractal indicators of human trabecular bone, Energy cumulation under constant – amplitude and programmed loadings, Power Consumption investigation in disc refiner at waste paper treatment, Recirculation of beverage cartons, Influence of operational external loads on parameters of the surface geometric structure, Polyflow software use to optimize the parison thickness in blowing extrusion, Technical

condition monitoring of hor 6002 production line, Study of the technical state of a Francis turbine.

In that case we cannot exclude that after reading at least a few of the papers mentioned above, many readers will discover new opportunities for developing their own interests. That can happen, although the journal is addressed mainly to the people dealing with research on combustion engines and the systems ensuring their correct operation.

This is just what I cordially wish to all readers of our journal.

Editor-in-Chief
prof. Jerzy Girtler

CHOSEN SOLUTIONS OF COMPUTER LUMBAR SPINE SEGMENT MODELING

M. Araszkiewicz, T. Topoliński

Uniwersytet Technologiczno-Przyrodniczy
im. Jana i Jędrzeja Śniadeckich
ul. Ks. Kordeckiego 20, 85-225 Bydgoszcz, Poland
tel. 052 373-02-80, fax 052 374-93-27
e-mail:marasz@utp.edu.pl

Abstract

For many reasons Finite Element Method is very useful especially in biomechanical researches .One of them is difficulty of gaining real specimens for in vitro tests. The second one is that FEM provides relatively easy way to check how changing some parameters of spine geometry or materials, influences on spine segment behavior. Consider it, many research centers in whole world in last years started to prepare FEM models of spine. Some of them are quite simple, some are very advanced. This paper is a review of three chosen FEM lumbar spine models, made in different scientific centers in last years. Authors present their opinions about possibilities of using material coefficients of particular structures of spine in own model. It could be useful for anybody who wants to build proprietary spine model. Authors met many problems trying to obtain material coefficients from literature which may be adopted to own spine model. Models reviewed in this paper could be important assistance for creating own spine models.

Keywords: Finite Element Model, spine, lumbar, material coefficients, discs

1. Introduction

Finite Element Method is a wide spread method in situations where problems in testing of physical specimens exists. This problem appears very often in biomechanics, especially in human body investigations. The second advantage of FEM is that it makes possible easily conducts of qualitative research. The main disadvantage is that sometimes obtained results are not exact, and need physical, experimental verification [1,2,3].

There exist many of computer models publications. The more advanced the computer software and hardware is, the more sophisticated the models become. In this paper a few actual and modern computer models were reviewed, made in known world research centers.

2. Description of FEM model from universities in Ulm, Hamburg and Coventry (I)

This model was publicized in 2007 by the scientists from universities in Ulm, Hamburg and university in Coventry [1]. It is presented on Fig. 1. Ligaments which were included in the model: Anterior Longitudinal Ligament – ALL, Posterior Longitudinal Ligament - PLL, Ligamentum Flavum - FL, Interspinous - ISL, Supraspinous - SSL. VA means Vertebral Arch. Calculations were made in Ansys 10 program.

Values of material coefficients of particular model structures as intervertebral discs, vertebrae and ligaments, were assumed to achieve model behavior agreed with behavior of the real spine with at least 99% probability. Material coefficients of this model are presented on Tab.1.
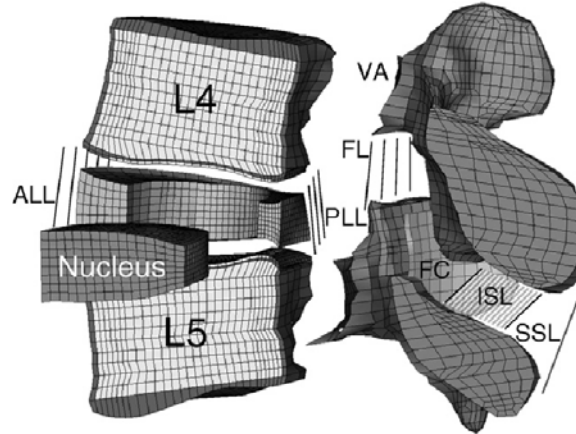
Fig. 1. Spine model from Ulm, Hamburg an Coventry, marked included ligaments [1]

Model imitates the following structures of spine:

1. **Vertebrae** were performed as built from cortical and cancellous bone included anisotropy of mechanical factors, with setting values of Young modulus and Poissons coefficient, including different values in different stress directions. Differences between anterior and posterior material of vertebrae were included.
2. The main **ligaments** were modeled: Anterior Longitudinal, Posterior Longitudinal, Capsular, Ligamentum Flavum, Interspinous and Supraspinous. Mechanical properties were taken from force-deflection curves placed in paper [4].
3. **Annulus fibrosus** were built from layers of fibers embedded in homogeneous substance. Fibers were composed in angle of 24º - 46º. Stiffness of fiber layers was higher at the outer side of disc, and decreased in center direction. Material of embedding substance was made using Mooney-Rivlin model, as almost uncompressible and with very low stiffness.
4. **Nucleus pulposus** was performed as incompressible solid, using linear material model. Material properties were Young modulus and Poisons coefficient.

Tab. 1. Material properties of spine structures [1]

Structure	Young and Kirchoff's modulus [MPa]	Poissons coef.
Cancellous bone	$E_{xx}=11300$, $E_{yy}=11300$ $E_{zz}=22000$ $G_{xy}=3800$, $G_{yz}=5400$ $G_{xz}=5400$	$\upsilon_{xy}=0,484$ $\upsilon_{yz}=0,203$ $\upsilon_{xz}=0,203$
Cortical bone	$E_{yy} = 140$, $E_{yy}=140$ $E_{zz} = 200$ $G_{xy} = 48,3$, $G_{yz} = 48,3$ $G_{xz} = 48,3$	$\upsilon_{xy}=0,450$ $\upsilon_{yz}=0,315$ $\upsilon_{xz}=0,325$
Posterior elements	$E=3500$	$\upsilon=0,25$
Bony endplates	$E=4000\text{-}12000$	$\upsilon=0,3$
Cartilaginous Endplates	$E=23,8$	$\upsilon=0,4$
Calibrated FEM model Annulus ground substance Nucleus pulposus Ligaments	 Mooney-Rivlin $c_1=0,18$, $c_2=0,045$ Mooney-Rivlin $c_1=0,12$, $c_2=0,03$ Calibrated force–deflection-curves	

Non-calibrated model		
Annulus-substancja	Neo-Hookean c=0,348, d=0,3	
Nucleus pulposus	E=0,2	υ=0,4999
Ligaments	Force–deflection-curves	

This model was calibrated using data from experimental investigations. Authors present results of verification of calibrated and non-calibrated model. Calibration indicates changing material coefficients of disc and ligaments structures. For non-calibrated model the accuracy was 82.8% for flexion and 77.1% for extension, which was found to be in good and satisfactory agreement. Calibrated model showed an accuracy of 96.8% and 93.8% for flexion and extension compared to the median value of the intact specimens.

3. Model from Laboratory of Orthopedic Hospital, in Berlin (II)
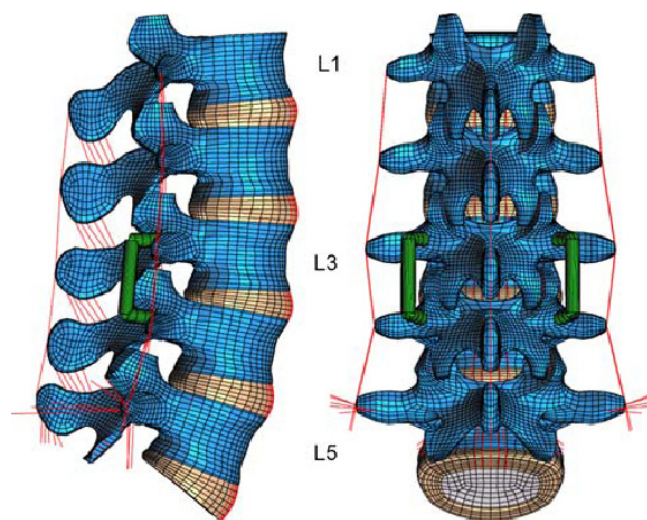
Fig. 2. Spine model from Berlin with implanted dynamic spine fixator [5]

Model publicized by scientist from Biomechanics Laboratory of Orthopedic Hospital in Berlin in paper from 2007 [5]. Models consist of 5 lumbar vertebras, discs and ligaments are depicted on Fig. 2. For particular parts of spine values of material coefficients are presented on Tab. 2. Calculations were made in Abaqus and as a postprocessor and preprocessor MSC/Patran program were used. Model was verified basing on comparison of calculations results with in vitro experiment.
Spine structures modeled were as following:

1. **Facet joints** had a gap of 0.5 mm and thin cartilaginous layer. Contact was simulated using "soft contact" with exponentially increasing of contact force.
2. **Nucleus pulposous** was createated as incompressible fluid. Compressibility was increased from $0,0005$ mm^2/N for healthy disc to $0,0503$ mm^2/N for slightly degenerated.
3. **Annulus fibrosus** was modeled from few layers of fibers, placed in concentric rings. Fibers were embedded in angle of 30º-150º. Stiffness of fibers increased with distance from center of the disc.
4. **Ligaments** were created as nonlinear 'spring' elements. Material properties were set on basis of force-deflection curves available in literature.

The model was calibrated using experimental data of Heuer, Shmidt et al. from 2006 year, for

11

different anatomical-reduction levels, loading directions and magnitudes. After calibration authors conduct comparison with four other publications, and assume good agreement between model and experimental data.

Tab. 2. Material properties of spine structures

Material	Young modulus [MPa]	Poissons coef.	Stiffness [N/mm]
Cortical bone	E=10000	υ=0,3	
Cancellous bone	E=200/140	υ=0,45/0,315	
Posterior bony elements	E=3500	υ=0,25	
Annulus fibrosus ground substance	Neo-Hookean C_{10} = 0.3448, D_1 = 0.3		
Annulus fibers	Nonlinear		
Nucleus pulposus (healthy)	Incompressible		
Nucleus pulposus (degen.)	Compressibe		
Ligaments	Nonlinear		
Pedicle screws (titanium)	E=110000	υ=0,3	
Dynamic fixation device			C=200
Rigid fixation device (titanium)	E=110000	υ=0,3	C=83000

4. Model from Uniwersity in Graz (III)
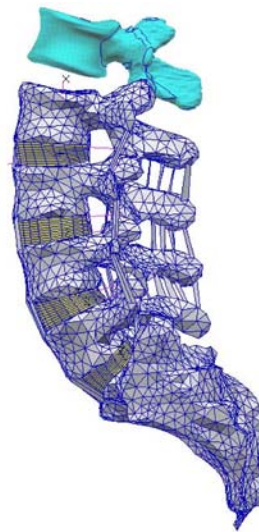
Fig.3.Geometry of the spine model from Graz [6]

This model was created in 2004 by scientists from University in Graz and from companies Sulzer and Zimmer. Was described in paper [6]. It consists of five lumar vertebras, discs and ligaments. Geometry of the model is depicted on Fig. 3. Authors included a sort of in vitro results which were used to achieve data to made force-deflection curves for particular ligaments. Finite element mesh was prepared in MSC Patran 2001 program, calculation were made in Abaqus. Model FEM results were verified and compared to in vitro experiment results.
Parts of spine were modeled as following :

1. Nucelus pulposous as well as annulus fibrosus were created using proprietary mathematical, material model, built on base of Cauchy-Green model.
2. Cartilaginous plates were 1mm thin, material coefficients were: E=23,8 MPa i υ=0,4.

3. Materiał of anterior and posterior bony elements was differentiated, for posterior elements coefficients were: E=3500 MPa, υ=0,25.

Mechanical properties applied to ligaments were set based on force-deflection curves gained from literature, including their different cross-sectional areas. Values of cross-sectional areas are presented in Tab. 3 with maximum and minimum. Differences between values point out that ligaments stiffness for spines may vary even few times.

Tab. 3. Values of cross-sectional areas of spine ligaments [6]

Ligament	Cross-sectional area minimum [mm^2]	Described study [mm^2]	Maximum [mm^2]
ALL	10,6	38	70
PLL	1,6	17	20
IT	1.8	6	10
FL	40	67	114
IS	12	35	60
SSL	6	30	59,8
CL	19	70	93,6
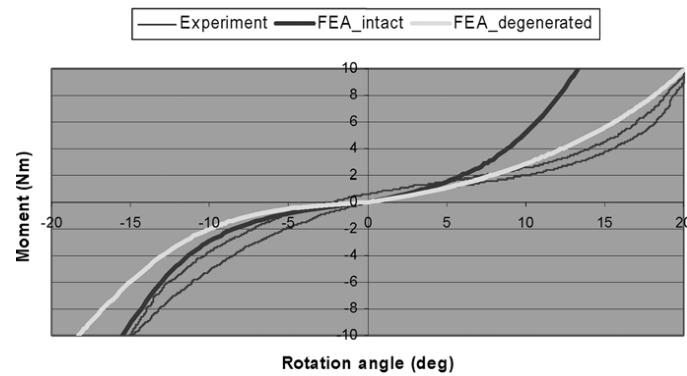
Fig.4. Force-deflection characteristic in flexion (+) - extension (-) movement
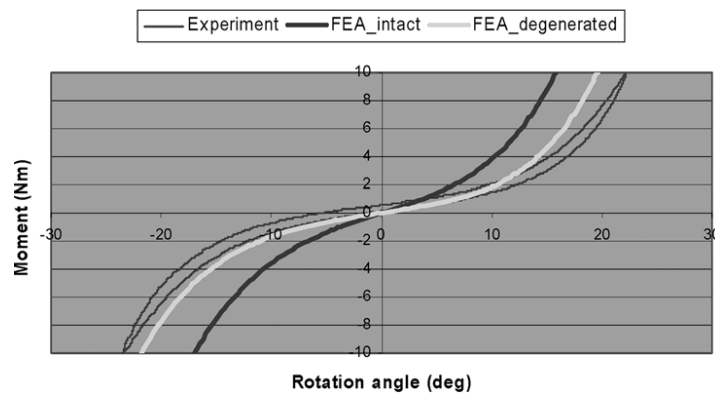
Fig.5. Force-deflection characteristic in lateral bending

Final computation results very good agreed with nonlinear stress-strain real spine curves. This model is the one of models for which whole curves were presented in paper, not only final values of deflection. Comparing curves gained in computation and in vitro experiment, it may be pointed out that model is slightly over stiffened for flexion-extension (Fig. 4) as well as for lateral bending (Fig. 5). Though, it seems that compatibility between computations and in vitro results is very good.

5. Conclusions

Models presented above are one of the most advanced and having good compatibility to real spines. For that reason they could be good example for building proprietary model. Many other spine models described in publications exists, some of them mathematically advanced, some relatively simple. Unfortunately information included in this publications are not enough to adopt to build own FEM model. That information often concerns the way geometrical data were gained, rarely describing in details applied material properties. In Tab.4 presented main disadvantages and advantages of models described above.

Tab.4 Features of described models

Model	Advantages	Disadvantages	Suggestions for own model
I	very high level of agreement with in vitro, advanced calibration procedure, bone anisotropy included	calibration only for flexion-extension	Useful calibration algorithms, material coefficients
II	validated and compared to many references, high quality of mesh in all segments	not included bone anisotropy	
III	very advanced material model of intervertebral disc, full characteristics included in paper,	not so good agreement to in vitro data as two other models	valuable force-deflection curves for ligaments, values of cross-sectional areas in paper

The most important for quality of model are proper material coefficients and characteristics for particular spine structures. For many reasons it is difficult to evaluate if the model is better or worse, but for sure, models in which only linear material models are used, are less accurate. Unfortunately many of old FEM spine models possess only linear material characteristics [7, 8]. Often models consists theoretically nonlinear material properties [9, 10], but their importance is not big enough to achieve nonlinearity of whole model.

For this reason such models can be used only in narrow range of load, in which nonlinearity could be ignored. Value of those models is small for applications in which real conditions have to be simulated, like flexion-extension together with lateral bending and axial rotations in wide range of load. Severe publications do not include full characteristics, only final values of deflection or force, even if model description gives impression that model is very advanced [11, 12].

References

[1]   Shmidt H. i in., *Application of a calibration method provides more realistic results for a finite element model of a lumbar spinal segment*, Clinical Biomechanics, 22, 2007

[2]   Shin D. S., Lee K., Kim D., *Biomechanical study of lumbar spine with dynamic stabilization device using finite element method*, Computer-Aided Design, 39, 2007

[3]   Yaoa J., Turteltaubb S. R., Ducheyne P., *A three-dimensional nonlinear finite element analysis of the mechanical behavior of tissue engineered intervertebral discs under complex loads*, Biomaterials, 27, 2006

[4]   Shirazi-Adl, A., Ahmed, A.M., Shrivastava, S.C., *Mechanical response of a lumbar motion segment in axial torque alone and combined with compression*, Spine, 11, 1986

[5]   Rohlmann A. i in., *Comparison of the effects of bilateral posterior dynamic and rigid fixation devices on the loads in the lumbar spine: a finite element analysis*, Eur Spine J.,16, 2007

[6]   Eberlein R., Holzapfel G.A., Frohlich M., *Multi-segment FEA of the human lumbar spine including the heterogeneity of the annulus fibrosus*, Computational Mechanics, 34, Springer-Verlag, 2004

[7]   Michael Y. i in., *Do Bending, Twisting an Diurnal Fluid Changes in the Disc Affect the Propensity to Prolapse ? A Viscoelastic Finite Element Model*, Spine, 21, 1996

[8]   Zhong Z.C., *Finite element analysis of the lumbar spine with a new cage using a topology optimization method, Medical Engineering & Physics*, 28, 2006

[9]   Haghpanahi M., Mapar R., *Development of a Parametric Finite Element Model of Lower Cervical Spine in Sagital Plane*, Materiały konferencji 28 IEEE EMBS Annual International, New York City, USA, Aug 30-Sept 3, 2006

[10]   Wang J.L., Parnianpour M. i in., *Development and validation of viscoelastic finite element model of an L2/L3 motion segment, Theoretical and Applied Fracture Mechanics*, 28, 1997

[11]   Little J.P. i in., *Nonlinear finite element analysis of anular lesions in the L4/5 intervertebral disc*, Journal of Biomechanics, 40, 2007

[12]   Sairyo K., *Buck's direct repair of lumbar spondylolysis restores disc stresses at the involved and adjacent levels*, Clinical Biomechanics, 21, 2006

IDENTIFICATION OF QUASI-STATIC CUTTING FORCE OF TRITICALE-STRAWS FOR DESIGNING USE OF SCISSOR AND FINGER CUTTING SETS

Andrzej Bochat

University of Technology and Life Sciences in Bydgoszcz
Mechanical Engineering Faculty
Department of Agricultural Engineering
al. Kaliskiego 7, 85-789 Bydgoszcz, Poland
e-mail:bochat@utp.edu.pl

Abstract

In the article there are presented empirical study results of quasi-static cutting force of triticale-straws. Research conducted on the testing machine INSTRON 8501 showed unambiguously that along with increase of cutting angle relevant to symmetry axis of straws in the range from 0 to 15^0, cutting force value approximately linearly decreases. In that case, it is necessary to check in an empirical way whether mentioned phenomenon occurs with cutting straws by means of scissor and finger cutting set (simultaneous cutting of a few dozen or a few hundred straws). Established change range of straw cutting angle is possible to realize during work of scissor and finger cutting set in field conditions.

Keywords: scissor and finger cutting sets, cutting, stalk of corn

1. Introduction

The basic working sets occurring in many agricultural machines are cutting sets of scissor and finger type. They are common in mowers, chaff cutters as well as combine-harvesters. Cutting plant material by scissor and finger cutting set is a special case of mechanical plant material division under the effect of outside forces crossing resistance of intermolecular material cohesion.

The essence of scissor and finger cutting set construction consists in the fact that the set includes a moving knifed slat and immovable finger bar. Cutters riveted to knifed slat have a shape of trapezium. Cutter edges are smooth or they have incisions.

Fingers fastened to finger bar are designed for separating cut material into portions. Fingers have cut-outs that enable plane and manoeuvrable motion of cutters and they also contract forward – in order to separate material easier. In some constructions there are riveted liners to fingers, which form anti-cutting edges. However, in other constructions this function is performed by side finger edges. Proper cutter sticking to liners is ensured by buttons screwed in to finger bar. Furthermore, the knifed slat is leaned on runner [1].

In figure 1 there is presented an exemplary section of scissor and finger cutting set.

Principle of operation of scissor and finger cutting set consists in the fact that fingers enter between cut plants and separate them into portions. Then, individual cutters squash straws or plant stems to side finger edges (anti-cutting edges) and cause cutting plants.

Rational and fast designing of energy-saving scissor and finger cutting sets with great efficiency

and stability is conditioned on analytic description of cutting process, occurring in these sets as well as empirical studies of plant material cutting process [1, 2, 3].

Results of *Ł.P. Kramarenko* [2] studies are assumption to conduct additional studies of plant material cutting process. *Ł.P. Kramarenko* has considered different cutting types in aspect of work and cutting resistance. He proved that while oblique cutting of straws and stems (at an angle of 45^0 to its symmetry axis) cutting force, and what follows – cutting work, is lesser in relation to cutting in perpendicular direction.
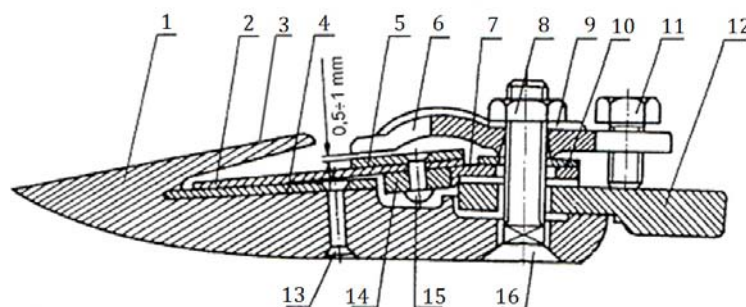
Fig.1. Cross-section of scissors-fingers cutting tool [1]:
1- finger, 2 – knife, 3 – top part of the finger, 4 – blunt edge, 5- plate of the knife, 6 – clamp of the knife slat,
7 – guide of the knife slat, 8 – screw cap, 9,10 – washers, 11-fasten screw, 12- finger bar, 13,15 – fasten rivet,
14 – knife slat , 16 - screw

In that case, it seems rational to study whether such relationship occurs also for angles of straw cutting, e.g.: 5^0, 10^0 and 15^0. Established change range of straw cutting angle results from the fact that it is possible to realize it during work of scissor and finger cutting set in field conditions.

Thus, as a purpose of research there was established empirical determination of triticale-straw cutting force at a different angle in relation to its symmetry axis in quasi-static cutting test as well as indicating possibilities of using these study results on the stage of designing scissor and finger cutting sets.

2. Plan and programme of research

In order to differentiate cutting force in quasi-static test of cutting straw there was planned an experiment. As independent variables in experiment there were established:
- straw cutting angle α,
- geometrical characteristics of stalk section: external diameter d_z and internal diameter d_w.
However, as an independent variable there was established straw cutting force P_{cj}.
The purpose of research was empirical differentiating of cutting force P_{cj} in quasi-static straw cutting test in order to establish relations:

$$P_{cj} = f(Fcj, \alpha), \tag{1}$$

where:
F_{cj} - area of straw section in cutting place,
α - straw cutting angle.

Straw cutting angle was changed in range from 0 to 15^0, where 5^0 (0^0, 5^0, 10^0, 15^0). The change range of straw cutting angle α established in research was earlier justified.

The research was conducted for the series of 30 selected at random triticale-straws with humidity of 12%.

Constant humidity was guaranteed through constant storage of specimens in air conditioning

cabinet. Total measurement number was 120. Prepared specimens of straw elements were 120 mm long each.

Special attention was paid to representative selection of straws for research. The whole population of straws designed for research was divided into five separate groups. From each group there were drawn 6 pieces of straw, resulting in 30 specimens for research. Such process course of random straw selection gave more probability of material representativeness for research.

After drawing straws there were done following measurements: weight of straw, weight of ear, length of individual sections of straw, length of ear, external and internal diameter of second and third straw section. The diameter of second and third straw section was measured in half length, in two perpendicular directions, differentiating the average of measurements. Diameter of the first section was measured after conducting cutting tests. On each straw there was performed four-times cutting research at different angles.

As a result of cutting process, there were obtained four straw sections with length of 10 mm. These sections were cut half in order to measure diameters. Diameters were measured in two perpendicular directions to each other. Exterior d_z and interior diameter d_w was differentiated as the average of eight measurements.

Research material had been prepared in such a way that quasi-static straw separation test was conducted on the section of straw corresponding to cutting height equalling 70 mm. This height corresponds with cutting height being realized by means of scissor and finger cutting set.

3. Research position

Empirical research of cutting force in quasi-static triticale-straw cutting test were conducted on the testing machine INSTRON 8501, belonging to equipment of Accredited Laboratory in Department of Machine Design in the University of Technology and Life Sciences in Bydgoszcz. In experiment there was used a cutting force sensor of own construction, which was fixed in the top handle of testing machine. In the bottom chuck there was fixed a frame of special cutting construction device. The device was designed in order to reflect a single element of scissor and finger cutting set, i.e. a cutter and anti-cutting edge. That is why, there were kept geometrical quantities in the device such as in a typical scissor and finger cutting set. For this reason a cutter and anti-cutting edge were made of original component elements of scissor and finger cutting set.

In figure 2 there was presented the view of device testing cutting force in quasi-static straw cutting test.
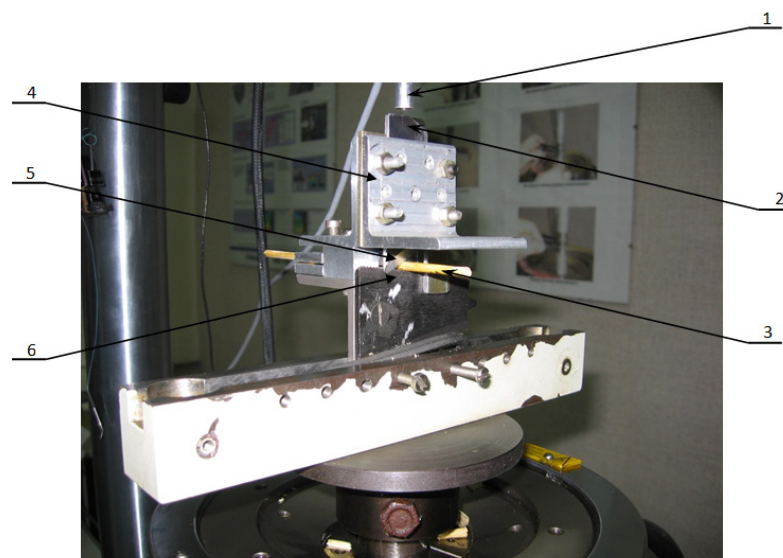
Fig. 2. View of attachment for testing cutting force in quasi-static trial of cutting:
1- mandrel of the force sensor, 2 – knife, 3 – material for cutting, 4 – body of the attachment,
5 – cutting edge, 6 – anti-cutting edge

A cutter in the device was binded to the top fixing handle of testing machine, i.e. force transducer, however an anti-cutting edge was fixed motionless in the frame of device, in the bottom handle of testing machine.

Additionally, the device made fixing the straw possible in such a way that straw cutting angle, i.e. an angle between cutting plane and straw axis, could be changed from 0 to 15^0.

4. Research methodology

Research of quasi-static cutting force was realized in such a way that a testing machine was suitably programmed in order to keep constant feed of top handle with fixed force transducer during surveying measurements. Mandrel of force sensor was influencing the top part of cutter, moving with the speed of 2 mm/s. Stalk of corn were fixed in two special (top and bottom) plates with made groove suitably at an angle of 0^0, 5^0, 10^0 and 15^0. The straw was fixed to such prepared plates and cutting process was realized at mentioned angles. Precision of angle measurement, while preparing plates, was $d\alpha = 0,5^0$. Cutting force was registered in a computer. Precision of force measurement was $dP = 0,01$ N.

Exemplar course of cutting force changes in the function of cutter dislocation in straw was presented in figure 3.
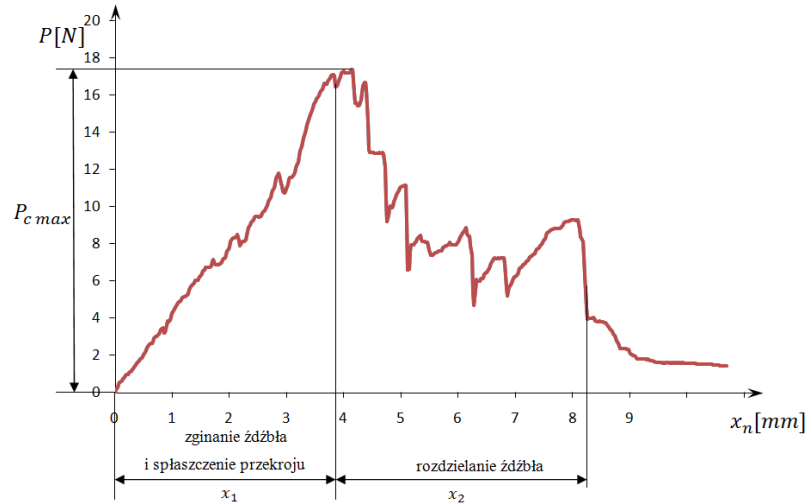
Fig. 3. Phases of cutting process trial

The quasi-static cutting test clearly shows two ranges of process course. In section x_1 the effect of straw deflection occurred and flattening its cross-section that lasts till the moment of reaching force P_{cmax}. Then, in section x_2 phenomenon of separating straw appears. The average force of separating straw is described by the relation:

$$P_{cj} = \frac{1}{x_2} \int_{x_1}^{x_1+x_2} P dx. \tag{2}$$

Cutting force P_{cj} was differentiated on the basis of results from discrete measurements of relation:

$$P_{cj} = \sum_{i=1}^{n} \frac{P}{n}, \tag{3}$$

where:
n – number of measuring points in the range of (x_1, x_1+x_2).

5. Analysis of study results

Conducted empirical studies proved that for all studied cases of cutting a single straw along with increase of straw cutting angle α, cutting force P_{cj} decreases approximately linearly.

In figure 4 there were presented exemplar study results of cutting force in quasi-static triticale-straw cutting test.
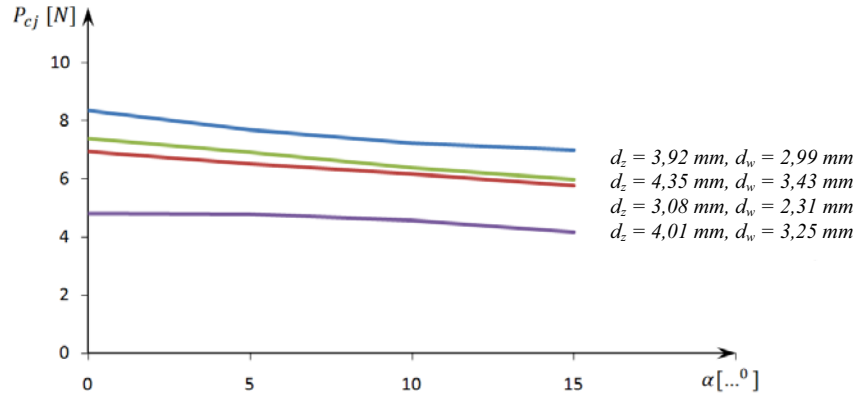
Fig. 4. Graph of the cutting force for different cutting angles of corn stalk to diameter

However, in figure 5 there was presented the dependence of straw cutting force P_{cj} on cutting angle α for three different cutting sections F_{cj}, i.e.: 3,5; 5,5; 7,5 mm^2.
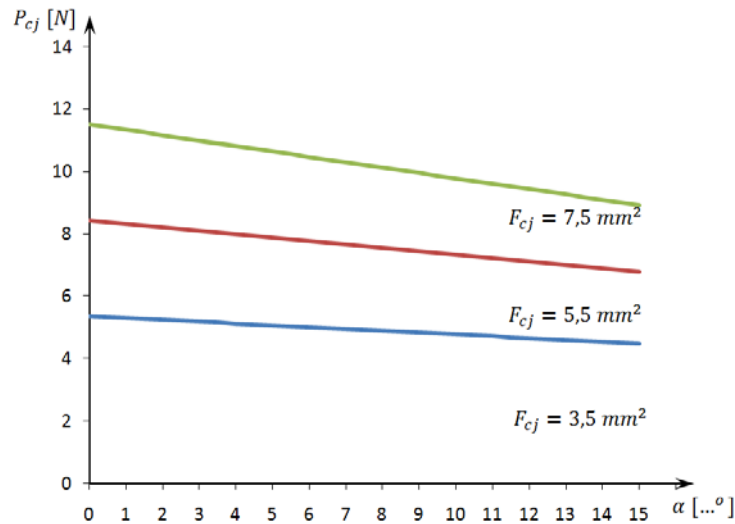
Fig. 5. Graph of the cutting force for different cutting angles and different cross-section area

Conducted analysis of multiple regression proved that static relation between variables of equation (1) has been already described in a satisfactory way on significant level $\alpha_{pi} = 0,05$ (correlation coefficient $R = 0,90$) by polynomial of the second degree in the form of:

$$P_{cj} = F_{cj} \left(1,5320 + 0,0118\,\alpha + 0,0015\,\alpha\,F_{cj} \right). \tag{2}$$

In figure 6 there were presented exemplar trusting sections for function regression $F_{cj} = 3,5$ mm^2.
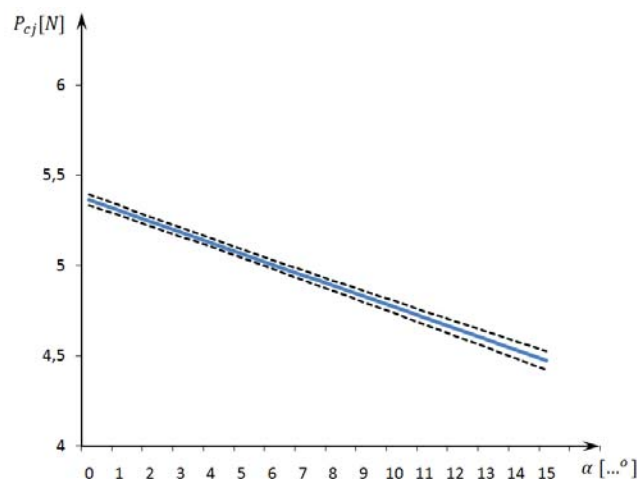
Fig.6. Graph of confidence interval for regression function to corn cross-section F_{cj} = 3,5 mm^2

6. Summary

Conducted empirical studies showed that for all cases of cutting a single triticale-straw, along with increase of straw cutting angle in relation to its symmetry axis (in the range from 0 to 15^0), cutting force in quasi-static test decreases approximately linearly.

In that case, it is necessary to conclude that it is intentional to check in empirical way whether mentioned phenomenon occurs with cutting straws by means of typical construction of scissor and finger cutting set or one should change its construction in order to decrease summary cutting force.

7. Literature

[1] Bochat A., Błaszczyk M., Zastempowski M., *Research issues of single straw and stem cutting process*, Chemical Engineering and Apparatus no. 1/2007.
[2] Chattopahyay P.S., Pandey K.P., *Mechanical properties of sorghum in relation to quasi-static deformation*, Journal of Agricultural Engineering Research, Vol.73, 1999.

THE CONDITION ASSESSMENT OF IN-SERVICE VANES OF GAS TURBINE NOZZLE UNIT WITH HELP OF DIGITAL ANALYSIS OF VANE SURFACE

Mariusz BOGDAN, Józef BŁACHNIO

Białystok Technical University
Faculty of Mechanical Engineering, Department of Automatics and Robotics
Wiejska 45c Street
15-351 Białystok, Poland,
marbog@doktoranci.edu.pl, jozef.blachnio@itwl.pl

Summary

The paper presents the methodology of condition assessment of in-service vanes of gas turbine nozzle unit with help of digital processing and analysis of vane surface. Included are 3D distribution graphs of basic RGB component colours (red, green and blue) for vane surface images registered with a digital camera (lab conditions) and with two types of commonly used videoscopes (working conditions). The graphs are coupled with results of examination of vane material. Considered were also both alteration of protective coating and core microstructure. The examinations were realised on metallographic sections with help of a SEM. The core microstructure was analysed mainly from the standpoint of modification of reinforcing phase γ' and alteration of phase γ and carbides. Size and distribution of phase γ' particles determines creep resistance properties (material criterion as the assessment criterion of vane condition). The analysis of images of gas turbine nozzle guide vane surface consists in counting of overheating area in relation to non-overheated area – the ratio is expressed in percentage terms (the criterion – the colour of the surface of a vane considered serviceable in relation to other distributions of colours on surfaces of vanes of different degree of overheating). The proposed approach is aimed at assessment of degree of overheating by reference to discolouration of vane surfaces after certain operational period.

Keywords: gas turbine vanes, digital image, phase γ'

1. The matter of considered problem

Turbine vanes are made of creep-resistant alloys with a nickel or cobalt matrix basis (superalloys). Their condition is examined (diagnosed) during operation or overhaul. The cause of damage to turbine vanes is often the material overheating as well as thermal fatigue caused by both excessive temperature and duration of its action, and also chemical aggressiveness of exhaust gas. As a result vane structure becomes modified, what leads to loss of material resistance. In general the structure modification consists in expansion of the γ' phase precipitations (the reinforcing phase – the component of microstructure having greatest influence on properties of superalloys). In special cases the expansion of the γ' phase leads to coagulation of precipitations and their dissolving in solid solution. In such conditions the material is characterised by lower creep resistance and the element, where this effect occurs, is exposed to damage, what generally results in dangerous turbine failure.

Generally, the overheating of vanes results from exceedance of admissible average temperature of exhaust gas as well as from irregular temperature distribution on the

circumference: e.g. as a result of improper fuel atomisation due to carbon deposit on injectors (fig. 1).

During operation and in repair workshops applied is the manual containing description of procedure for examination of turbine vanes overheating. According to the manual the preliminary examination of material overheating consists in visual inspection of vanes for detection of deformations, material defects, and before all, change of surface colour indicating the overheating of material.

The verification of diagnostician's decision is realised with a destructive method. The microstructure of examined element is analysed on metallographic section. In diagnostic examinations the vision
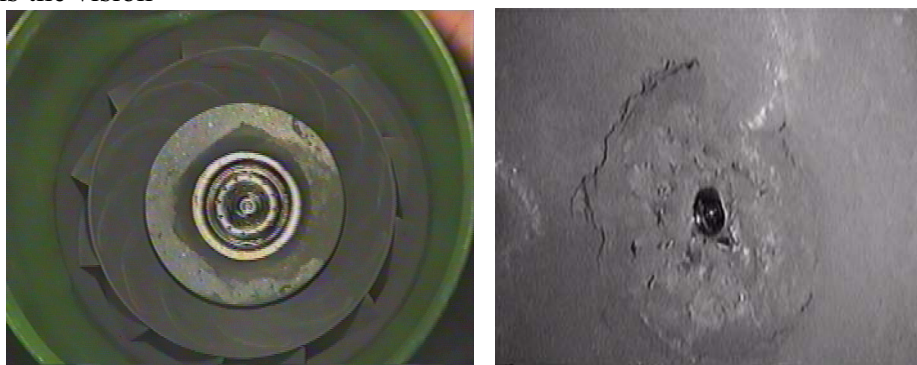
Fig. 1. General view of a combustion chamber injector: a – clean, b – covered with carbon deposit [1]

(the organoleptic method of condition assessment) is a subjective factor. Additionally, the colour is a physicopsychological phenomenon [2]. These facts cause that the assessment of vane condition made by a diagnostician can be crippled with great error. Therefore necessary is to develop an objective non-destructive computer-aided method of assessment of vane condition. Application of digital image recording technology combined with computer image analysis will contribute to higher credibility of results of turbine elements diagnostic as compared to currently used method of subjective assessment of condition made by a diagnostician. Additionally, application of a videoscope as an appliance for recording of vane surface image enables diagnosing of vanes without disassembly of a turbine.

2. Characteristics of examined object

Examined were stator vanes of a gas turbine of an aircraft jet engine. The vanes are made of ŻS-6K alloy of chemical composition shown in the table 1.

Tab. 1. Chemical composition of ŻS-6K alloy [3]

Chemical composition [%]										
C	**Mo**	**Cr**	**Ni**	**Co**	**Mo**	**W**	**Nb**	**Ti**	**Al**	**Fe**
0,16	4,0	11,0	the rest	4,5	10,3	5,0	-	3,0	5,5	1,0

The examined alloy is reinforced with cube-shaped γ' phase particles. The content of this phase amounts to ca. 64%. The alloy belongs to the group of cast nickel alloys (fig. 2).
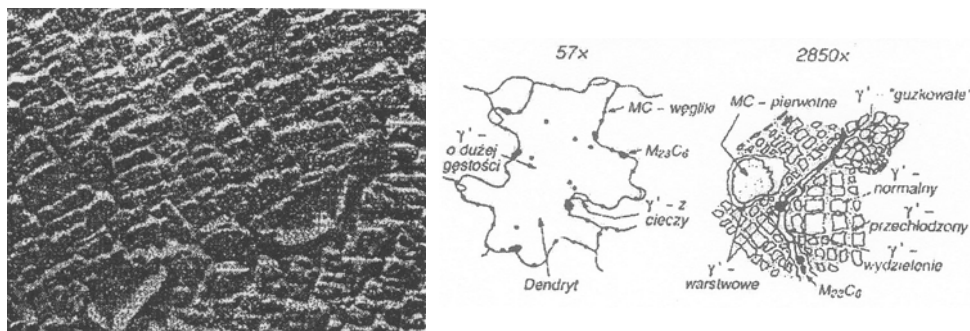
Fig. 2. Typical elements of the structure of cast nickel alloy [4, 5]

The important technological problem for this type of alloys it the thermal treatment, consisting mainly in homogenising annealing (structure homogenisation, increase of resistance and plasticity) [4]. The purpose of thermal treatment is also to obtain correct dispersion and shape of precipitations of γ' phase i.e. the main reinforcing phase. In many cases applied is also the protective coating, which allows increase of working temperature (by ca. 100K) and additionally protects the native material against harmful influence of high-temperature working medium (exhaust gas). During operation the coating changes its colour constantly. For recording of nature of these changes and acquisition of vane surface images used was following research equipment:

- digital camera Kodak Easy Share DX 7590;
- videoscope Olympus Iplex SA II (made in Japan);
- videoscope Everest XLG3™ VideoProbe (made in USA).

Fig. 3 shows an exemplary set of vane surface images of various overheating degree (according to hitherto applied classification of their technical condition). After long-standing operation the vanes made of ŻS-6K alloy are in various technical condition.
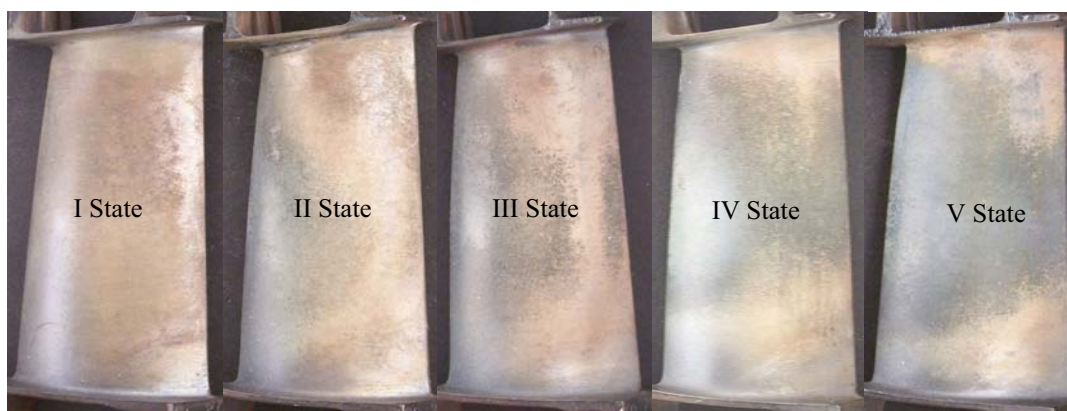
Fig. 3. Surface images made with digital camera Kodak Easy Share DX7590

3. Metallographic examination of in-service vanes of nozzle unit

To examine the microstructure of in-service vanes carried out were metallographic examination in laboratory conditions. The examinations were realised on metallographic sections with help of an optical microscope Neophot and a scanning microscope Hitachi S-3000N.

Fig. 4 shows the microstructure of coating and ŻS-6K alloy of a turbine vane in state I (vanes of uniform surface colour), and fig. 5 – in state V (vanes of multicoloured surface).
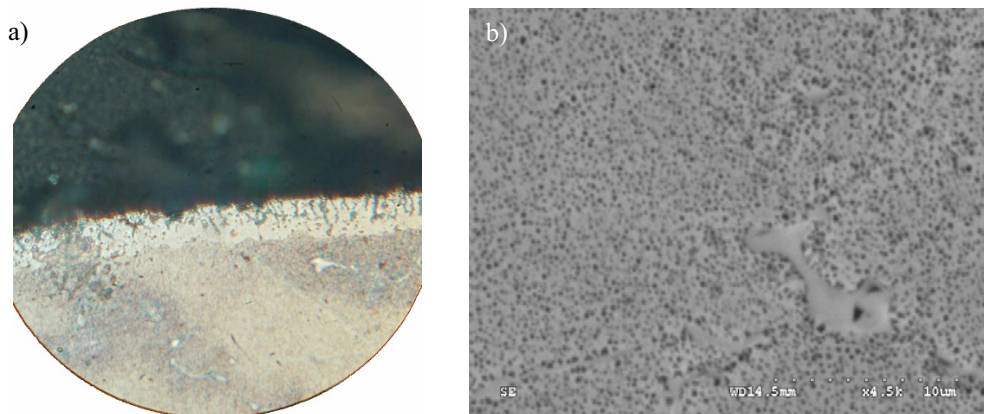
Fig. 4. Correct microstructure of turbine vane (state I): a) coating (magn. x450);
b) alloy ŻS-6K (magn. x4500)

Initially, after certain period of operation, the vane coating (fig. 4a) was not subject of degradation and its thickness differs only slightly from the thickness of the brand new coating. In the course of further operation the coating swells, and cracks appear due to thermal fatigue (fig. 5a).

The coating thickness gradually changes as a result of influence of working medium (exhaust gas) of high kinetic energy on vane material. The coating becomes thinner (fig. 6a), what results in loss of protective properties. As a result the temperature of vane material grows and the vane losses protection against chemical influence of exhaust gas. The vane becomes very sensitive to influence of exhaust gas. This leads to degradation of coating as well as of native material (fig. 6b).
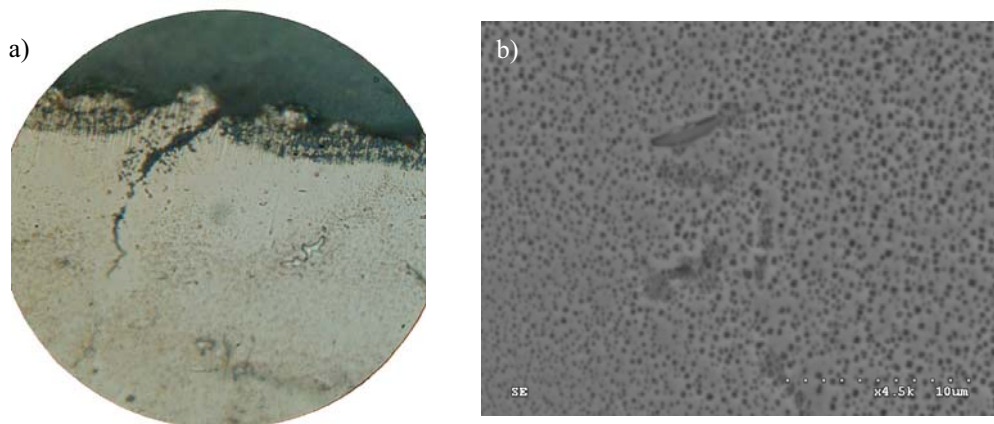
Fig. 5. Overheated microstructure of turbine vane (state V): a) coating (magn. x450);
b) alloy ŻS-6K (magn. x4500)

On the image of microstructure of ŻS-6K alloy were detected secondary precipitations of fine dispersion phase γ' (fig. 5b) formed after action of high-temperature exhaust gas. The morphology of γ' proves that if the critical temperature is exceeded, the alloy becomes overheated and in such case the vane cannot be considered as a serviceable one [6].
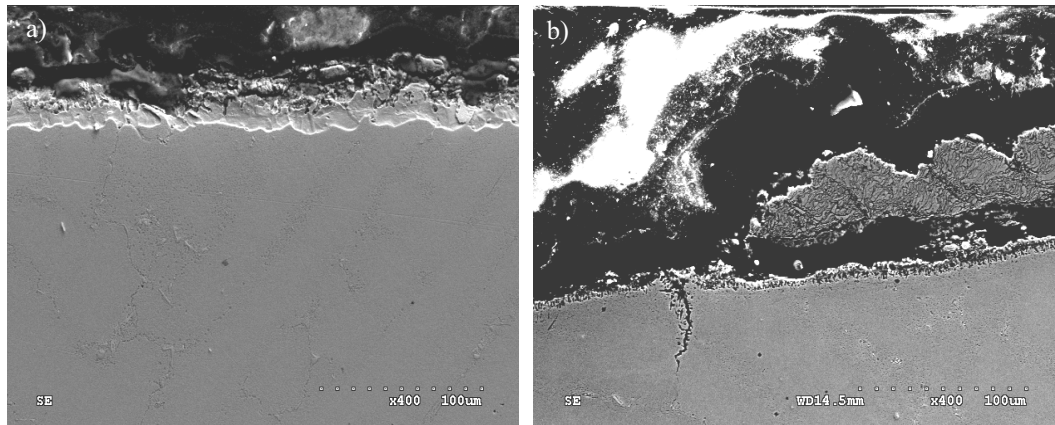
Fig. 6. Metallographic structure of surface layer of an in-service vane (state V):
a) reduction of coating thickness (magn. x450); b) thermal crack in coating, penetrating inside the vane
material (magn. x4500)

The examinations of coating microstructure (protective layer) and Ż6-SK alloy proved that influence of high-temperature exhaust gas caused decohesion of coating (fig. 5a, fig. 6) and modification of reinforcing phase *γ'* (fig. 5b). Results of examinations of vane microstructure proved that the vane No. 1 has correct structure and the vane No. 5 has overheated structure.

3. Method of scanning of images of in-service vanes surface

The process of destruction of a gas turbine vane starts with destruction of aluminium coating (shown on images of surface in the form of colour change – fig. 3). Digital images of surface of in-service stator vanes of a turbojet turbine were analysed for the purpose of determination of size of local overheating areas. Altogether were made five expositions for each state in guaranteed repeatable recording conditions for each appliance [7]. The stages of realisation of diagnostic method developed for the purpose of assessment of technical condition of examined turbine element (size of local overheating areas) are shown on fig. 7. As a criterion of degree of overheating was used the colour of vane surface in state V (overheated structure – metallographic examinations). Basing on prepared histograms (for each channel of digital image, i.e. red, green and blue – the RGB model) determined was the criterion threshold, which value was calculated on the base of saturation (position of maximum amplitude) for each individual component of RGB colour (R+G+B/3=162) – fig. 8.

Acquisition of images with help of: digital camera (laboratory conditions); videoscopes (working conditions): an American videoscope EVEREST -XLG, a Japanese videoscope OLYMPUS - IPLEX SA II

Metallographic examinations of vanes in metallographic states I-V

Calculation of histograms of distribution of basic RGB colours – determination of criterion plane

Scanning of images for states I - V in relation to selected colour profiles

Fig. 7. Realisation stages of diagnostic method of examination of in-service turbine vanes
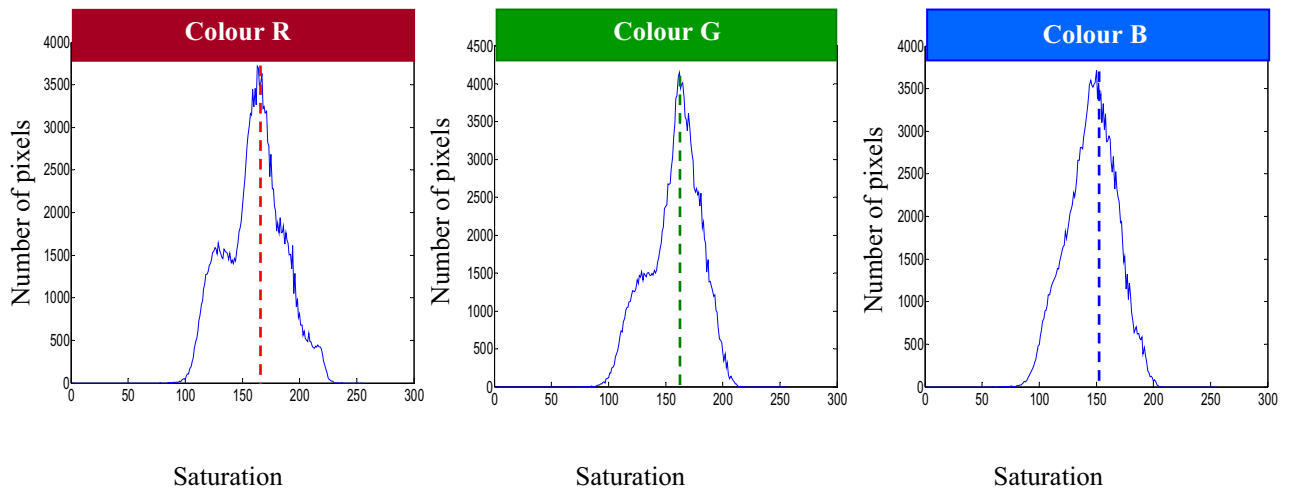
Fig. 8. Histograms of distribution of basic RGB colours for the vane in state V

The criterion threshold (plane value) was linked with 3D distribution of colour on surfaces of individual vanes in states I-V. As overheated surface points (pixels) were assumed these points, which value lies below determined plane. Figs. 9 and 10 shows graphical presentation of an exemplary assessment of overheated area for vanes in states I and VI, which images were recorded with digital camera. For better orientation adopted was the system of coordinates (where: x, y – size of vane image in pixels, z – saturation of RGB colour). The dashed line indicates irregular influence of temperature on examined vanes caused by wrong operation of injectors – disturbances in combustion process in combustion chamber.
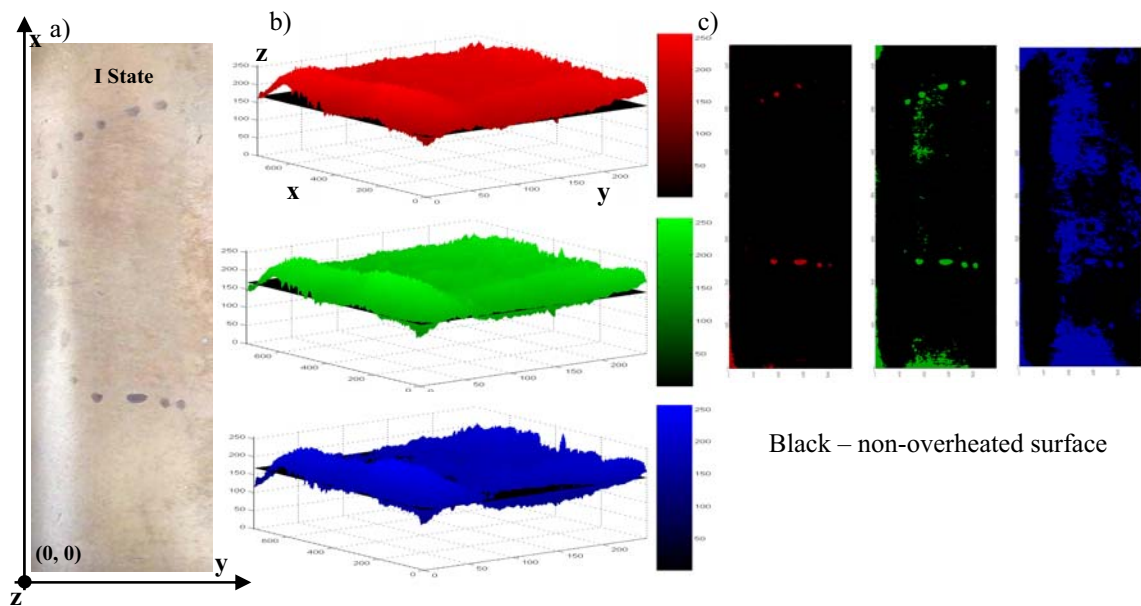
Fig. 9. Vane in state I: a) surface image; b) 3D distribution of basic RGB components; c) vane surface viewed from below – the result of introduction of criterion plane
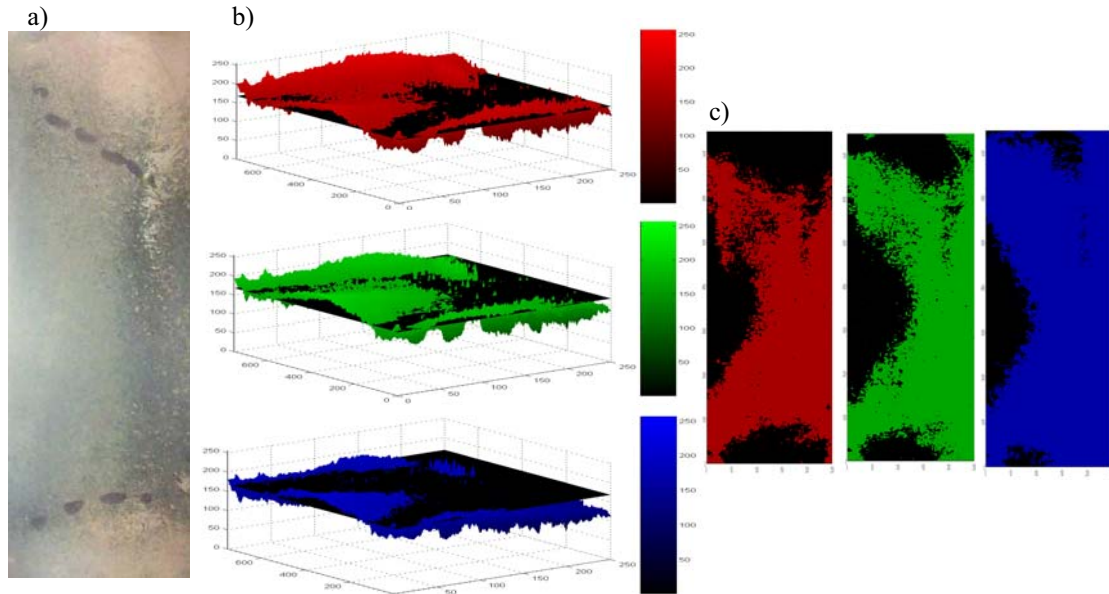
Fig. 10. Vane in state V: a) surface image; b) 3D distribution of basic RGB colours; c) vane surface viewed from below – the result of introduction of criterion plane

As the technical condition of vanes deteriorates, the overheated area increases (the set of image pixels) – figs. 9c, 10c. The introduction of the plane (criterion of overheating of vane material) to 3D graphs of distribution of RGB colours for images of surface of examined turbine element allows determination of overheated area/total area ratio (fig. 11). The same relation was determined for images recorded with two videoscopes (fig. 12).
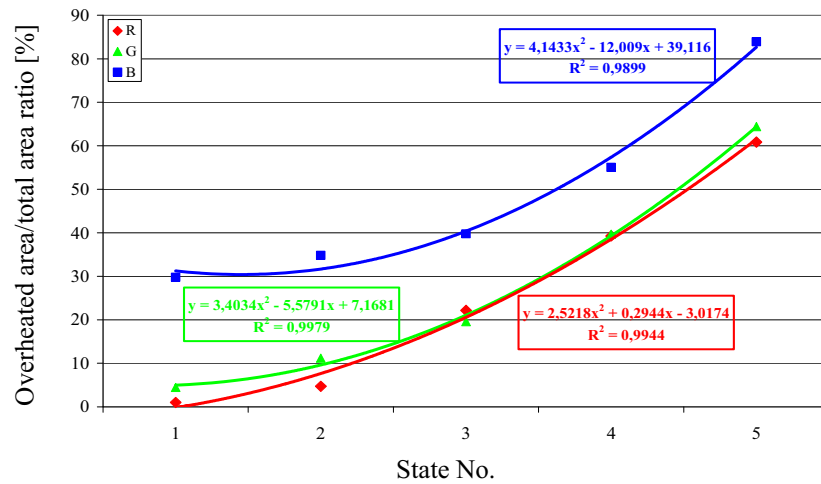
Fig. 11. Overheated area/total area ratio – images recorded with digital camera
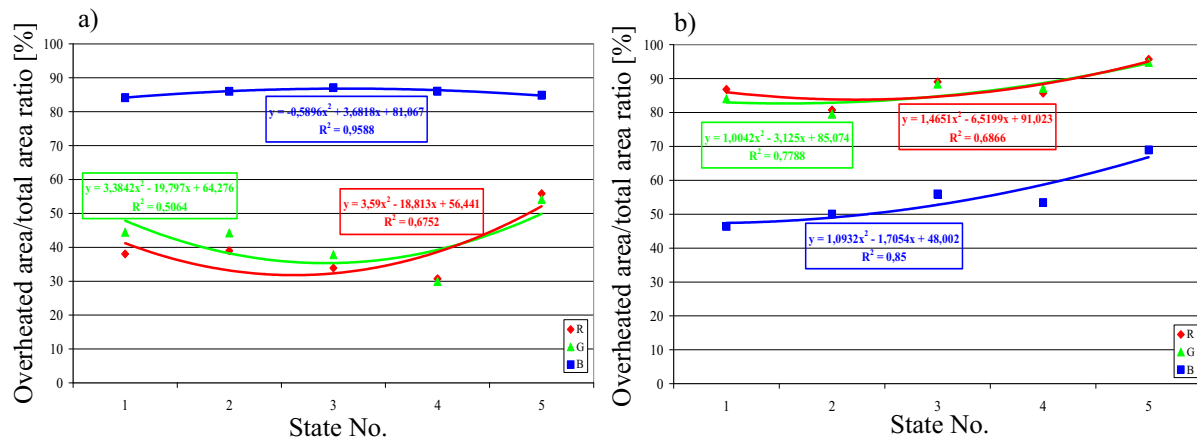
Fig. 12. Overheated area/total area ratio: a) images recorded with a Japanese videoscope; b) images recorded with an American videoscope

Summary

The above graphs prove that very good results were obtained for images of vane surface recorded in laboratory conditions with digital camera. The obtained graphs (fig. 8. 11) prove that changes of colour of vane surface reflect technical condition of examined turbine elements. Thus, application of described method improves credibility (objectivity) of assessment of vane condition in comparison with hitherto applied method. Percentage variations for individual states result from applied light and method of illumination of examined vanes. In laboratory conditions was used dispersed white light, and for videoscopes – concentrated light of another colour. Different is also the ability of colour recording by light-sensitive CCD matrixes installed in detection appliances. However, it is worth to note that application of endoscopes (i.e. videoscopes) for image acquisition can be useful for monitoring of vane condition (propagation of defects – technical condition of examined element) during periodical inspections without disassembling the turbine.

References

[1] Błachnio, J., *Technical analysis of failures and damage*, Basics of aircraft operation, Edited by J., Lewitowicz, Editions Air Force Institute of Technology, Vol. 4, pp. 181-264 Warszawa 2007 (in Polish).

[2] Hlebowicz, J., *Visual examinations. General principles and exemplary applications*, Warszawa, Editions Biuro Gamma, Warszawa 1997.

[3] Skočovský, P., Podrábský, T., Belan, J., *Operational degradation of aluminium-silicon layer of turbine vanes made from a Ni-based alloy,* The Archive of Machinery Technology and Automation, Vol. 24, No 1, pp. 45 – 52, Poznań 2004.

[4] Mikułowski, B., *Creep-resistant and heat-resistant alloys – superalloys,* Editions AGH, Kraków 1997.

[5] Sims, C.T., Stoloff, N.S, Hagel, W.C., *Superalloys II*, Wiley & Sons, New York 1987.

[6] Błachnio, J., Bogdan, M., *A non-destructive method to assess a degree of overheating of gas turbine vanes,* V International Scientific - Technical Conference Explo-Diesel and Gas Turbine'07, Journal of Polish CIMAC (2007), Vol. 2, No 2, pp. 43-50.

[7] Bogdan, M., Błachnio, J., *The Assessment of Degree of Gas-Turbine Vane Condition as Based on the Analysis of Light Reflected from the Vane Surface.* Archives of Transport. No 4, Vol 19, 2007, pp 5-16.

DEVELOPMENT OF (PLASTIC-, BIO- AND FIBROUS) ENERGY-MATERIALS GRINDING

Józef B. Flizikowski

University of Technology and Life Sciences
Al. Prof. S.Kaliskiego 7, 85-789 Bydgoszcz, Poland
tel., fax: +48 52 340-8255
e-mail: fliz@utp.edu.pl

Abstract

Summary: A general method of plastics-, bio-, and fibrous-materials grinders' development for energy engineering has been presented in this article. The method includes two beings: mathematical aiding an invention and working of a novelty. The common set is composed of characteristics, structure, relationships of knowledge about states and transformations, effectiveness and progress of the devices and machinery engineering, e.g. breaking up in the energy-materials recycling process. This innovation theory is identified by the valuation, estimation, testing and creative archiving the elaborated character and structure of the invention and grinders construction development.

Key words: *Grinding of waste, modelling of effectiveness, innovation, invention*

1. Introduction

The proposition of a devices construction, development methodology, applicable to polymer-, bio- and fibrous- energy-materials (PBFm) milling for energetic aims is discussed in this work. More then 7 million tones, or 30,3% of the post-consumer plastics waste, and 600 million tones of bio-, fibrous materials waste, was recovered as energy in EU25+Norway and Switzerland, up 1,5%% against 2008. Municipal incinerators remain the most common means of energy recovery. Capacity has been added as a consequence of the Landfill Directive and countries like Switzerland, Denmark, Germany and Sweden have above 75% of their post-consumer waste treated in energy recovery plants. Austria, the Netherlands and Belgium are all achieving around 60%. Other countries have less than 20% of their post-consumer waste recovered in energy recovery plants. This includes not only new Member States but also countries such as Finland, Greece, Ireland, Spain and the UK.

The methodology of the mathematically aiding: devices innovation in plastics and biomaterials wastes recycling for energy engineering, based on the system models (eq.1) needs the fulfilment of the methodical conditions and improvement possibilities: of the grinder and wastes beings in the recycling process [2, 11, 12]. The proposition of a devices construction, development methodology handles mathematical models of the beings.

The mathematical models of the machinery in the waste-energy engineering is the purpose of this study, and they include: elements and relations of the machinery, materials, processes, grinding and energy purposes, consequences of action as well as environment (and system self) influence, e.g. the ontology of invention of the (PBFm)-waste grinders in the recycling process.

2. Method of grinding development

The development of the devices and machinery design-construction in the innovation of the energy wastes engineering depends on an environment and system knowledge. The eco-energy development of grinding special system is carried on methodically, on the basis of the operation mathematical model [4].

The versatile equation including all the novelty beings in the operating systems, from idea till elimination, has the form:

$$L(\bar{H}, \bar{E}, \bar{R}, \Theta, t) = R(\bar{s}, \bar{z}, \Theta, t - t_0), \tag{1}$$

where:

$\bar{H}$ - performance, operation, functioning, working, action characteristics as output quantities (efficiency),

$\bar{E}$ - inner elements ((nS) construction) and outer elements (ready markets),

$\bar{R}$ - connections between/of elements (relations, reactions, correlations of machine, waste, environment and others system elements),

$\Theta-, (t_1 - t_0) -$ time,

$\bar{s}$ - intentional control of environment; acting-, information- and logistic system,

$\bar{z}$ - disturbances.

The left side of equation (1) (model) describes the properties of the devices, of the waste processing and product engineering, their features of physical nature that is adequate for the given action class in environment. These properties depend on the elements E_1, E_2, ..., E_m, on connections, relation between these elements R_1, R_2, ..., R_n, and they are functions of Θ and t (of the action and dynamical process time). The unknowns are the elements and relations of the set of energy characteristics H as output quantities, on which depends the evaluation of the innovation values of the idea, technology of the general efficiency of human, technical, energy-material, controlling action $P_d(t)$ and impact – also on generation of further novelties (inclusive of those from a PBF waste materials):

$$H = P_d(t)$$

The right side of equation (1) is a description of the inner and outer interference. It may depend on

a form of the wilful action – control by means of the signals from the set $\bar{s}$ (computer aided, actively), of the interaction: reciprocal action of the sets: waste, material – grinding and thermo process – system and technical conditions – environment - …objective; of the tension action – action of tensions (connected with potential difference), that causes compensatory processes (e.g. on a financial market); it may also occur as a disturbance of the system action

expressed by $\bar{z}$, or as consumption, state transformations in time.

Action characteristics - models

According to designation, the functional PBF-waste recycling for energy engineering spheres as technical system – is the whole of its external operating possibility:

- human potential $P^L(t)$,
- technical potential $P^T(t)$,
- energy – material (PBF-waste) potential $P^E(t)$,
- controlling potential $P^S(t)$.

Function of operating potential:

$$P_d(t) = \Phi\left[P^L(t), P^T(t), P^E(t), P^S(t)\right], \tag{2}$$

The following ones belong to indicators describing the operating potential (the description is limited to controlling potential exclusively, as the basic concept tool of designer's activity):

- temporary course of real executive possibilities, $\pi_d(t)$
- volume of operation used actively, usefully $M_d(t)$
- theoretical possibilities and operations needs, ε,

and especially:

$$P_d(t) = \pi_d(t) \cdot M_d(t) \cdot \varepsilon, \tag{3}$$

Operating (energy) environmental-system potential model - equation in the period (t_0, T):

$$P_d(T) = P_d(t_o) - \int_{t_o}^{T} p_d^E(t)dt - \int_{to}^{T} p_d^L(t)dt + \int_{t_o}^{T} p_d^R(t)dt, \tag{4}$$

where:

$P_d(t_o)$ - initial operating potential,

$p_d^E(t)$ - density of effectively used stream of potential,

$p_d^L(t)$ - density of lost stream of potential ,

$p_d^R(t)$ - density of recovered (or obtained from the environment) stream of potential.

Taking energetically PBF-waste grinding for energy engineering aims into account we obtain:

$$P_{em}(T) = P_{em}(t_o) - \int_{t_o}^{T} p_{em}^E(t)dt - \int_{t_o}^{T} p_{em}^L(t)dt + \int_{t_o}^{T} p_{em}^R(t)dt, \tag{4a}$$

where:

$P_{em}(t_o)$ – initial energy-material potential (*e-m*) of PBF-waste grinding system,

$p_{em}^E(t)$ – flux density of effectively used *e-m* raw, PBF-waste potential,

$p_{em}^L(t)$ – flux density of wasted and lost *e-m* PBF-waste potential,

$p_{em}^R(t)$ – flux density of *e-m* recreated potential, (or only retrieved from environment).

For design-construction development of grinder, the energy consumption, in technical system of PBF-waste grinding is represented as design-estimator and was calculated using the formula:

$$E_R = \frac{P_R v_R t'}{\eta_S \eta_P} , \tag{5}$$

where:

E_R - energy consumption of grinding by machine, $kJ \cdot kg^{-1}$;
P_R - load exerted on the material by the grinding force, N;
v_R - grinding velocity (the linear edge velocity), $m \cdot s^{-1}$;
t' - cycle time for disintegration of the material mass, $s \cdot kg^{-1}$;
η_s-, η_p - denote the efficiency of the motor and transmission, respectively, -.

This relation, like others found in the literature so far, does not take account of the specific characteristics of grinding in the case of recycling, arising from the objective of increasing the multiplicity of reuse of materials.

In the case of analysis of the overall effectiveness of multi discs grinding we employed the model [6, 7, 13]:

$$e_r = \frac{(\eta_{q-\acute{s}} - \eta_o) \cdot E_{brutto} \cdot \eta_s \cdot \eta_p}{(k_j \cdot v_r + \tau_{q-\acute{s}} \cdot A_{q-\acute{s}} + \varepsilon \cdot A_{q-\acute{s}} \cdot v_r^2) \cdot v_r \cdot t'} , \tag{6}$$

whereas in the case of special analysis - with the aim of modernization and development of the design of multi-disk PBF-waste shredders operating on the quasi-cutting principle - we employed a model representing an object-oriented relationship [11, 12, 14]:

$$e_r = \frac{\eta_{q-\acute{s}} \cdot E_{brutto} \cdot \eta_s \cdot \eta_p}{(k_j \cdot v_r + \tau_{q-\acute{s}} \cdot A_{q-\acute{s}} + \varepsilon \cdot A'_{q-\acute{s}} \cdot v_r^2) \cdot v_r \cdot t'} , \tag{7}$$

where:

E_{gross} - energy contained in the PBF-materials being processed, MJ·kg⁻¹;
k_j - coefficient of resistances to dead motion, N·s·m⁻¹;
τ_{q-s} - quasi-cutting stresses, N·m⁻²;
A_{q-s}-, A_{q-s}' - instantaneous and seconds cross-sectional PBF-waste area of quasi-cutting, m²;
ε - proportionality factor, N·s²·m⁻⁴;
η_{q-s} - material efficiency of the process of thermodynamic conversion of the quasi-cut product:

$$\eta_{q-\acute{s}} = \frac{T'_{wy/q-\acute{s}}}{T_{we/q-\acute{s}}} , \tag{8}$$

where:

$T'_{wy/q-s}$ - mass of the output material after quasi-cutting, kg;
$T'_{we/q-s}$ - mass of the input material before quasi-cutting, kg;
η_o - material efficiency of the conversion process without quasi cutting of the material:

$$\eta_o = \frac{T'_{wy}}{T_{we}} , \tag{9}$$

where:

T'_{wy} - mass of the output material without quasi-cutting, kg;
T'_{we} - mass of the input material without quasi-cutting, kg.

The energy effectiveness is defined thus:

$$E_e = \frac{L_{oi} - L_{oij}}{\dfrac{L_{oi} + L_{oij}}{2}} \tag{10}$$

where:

L_{oi}-, L_{oj}- successive instantaneous increments of the work of quasi cutting, N·m.

Fig.2: Intensive deformations (relations) model of pipe's as recycling element; v_R =0.01 m·s⁻¹ (except for rigid PVC-waste), 1 - motionless slat, 2 - draft of the hole in motionless slat; 3 - investigated sample; 4 - draft of the hole in moveable slat; 5 - moveable slat.
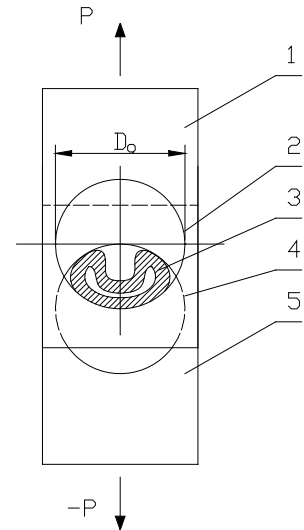
The mathematical descriptions of the variables given in equations (6) to (10) are obtained from experiments or from data contained in processing tables. The following characteristics of motors and transmissions are determined in operational trials:
- the kinematics' transmission, ratio of angles speed:

$$i_k = \frac{\omega_2}{\omega_1} , \tag{11}$$

- the dynamic transmission, ratio torque moment M_2 and M_1:

$$i_d = \frac{M_2}{M_1} , \tag{12}$$

- power N_1 and N_S at transmission input, equal to the power at the output of the motor:
$$N_1 = N_S = \omega_1 \cdot N_1, \tag{13}$$
- power N_2 and N_R at transmission output, equal to the grinding power:

$$N_2 = N_R = \omega_2 \cdot N_2, \tag{14}$$

- efficiency of the motor:

$$\eta_s = \frac{N_1}{N_E} = \frac{\omega_1 \cdot M_1}{N_E}, \tag{15}$$

- efficiency of the transmission (gears):

$$\eta_p = \frac{N_2}{N_1} = \frac{\omega_2 \cdot M_2}{\omega_1 \cdot M_1}, \tag{16}$$

- efficiency of the PBF-waste grinding process:

$$\eta_r = \frac{E_{m/q-\acute{s}}}{E_r}, \tag{17}$$

where:

$E_{m/q-s}$ - unit energy consumption for quasi-cutting in the conditions of the physical model (s. fig.2) to a defined form of the grinded product, kJ·kg^{-1};

E_r - unit energy consumption for quasi-cutting in machine conditions, kJ·kg^{-1};

N_E - electric power supplied to the motor, W.

The energy efficiency of PBF-waste grinding and thermo processing is determined similarly. The input energy of processing E_{we} is the sum of the energy contained in the charge material E_{we1}, and the energy supplied to it E_{we2} ($E_{we} = E_{we1} + E_{we2}$). The energy at process output E_{wy} is reduced by the energy losses E_{st}:

$$\eta_{ep} = \frac{E'_{wy}}{E_{we}} = \frac{E_{we} - E_{st}}{E_{we1} + E_{we2}} = \frac{E_{we1} + E_{we2} - E_{st}}{E_{we1} + E_{we2}}, \tag{18}$$

In the case of processing efficiency, the instantaneous values and the values occurring over the longer term are important. The mean value of the energy efficiency (or the mean energy efficiency) is sometimes called the energy efficiency in the literature [1, 2], but this is only justified when both efficiencies are equal to one another, e.g. in the case of auto-thermal processing.

Action characteristics – results and discussion

ERCO.net (*System of Efficient Administration of Energy Media Management*) is a modern information technology tool that enables the main objectives to be achieved for monitoring the states and transformations of energy in the break-up engineering, and that also allows the actuators to be controlled according to the rules and policy for the energy management system.
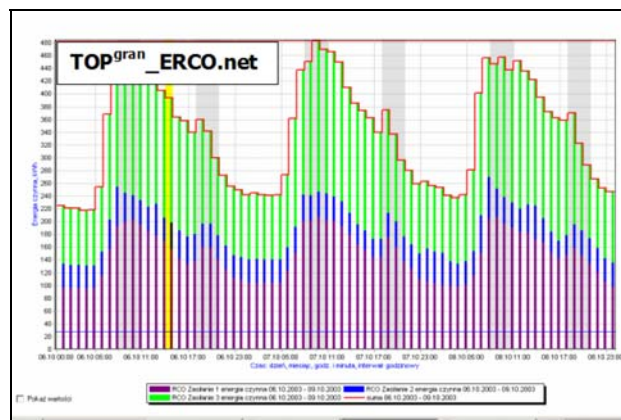
Fig.3: Characteristics-diagram of grinding and thermo process energy monitoring

This methodology is formation of the bases of knowledge about structural conceptions of multi-discs plastics-, bio- and fibrous-wastes grinders, and formations of energy-materials in recycling process (acc. to the IE-TEST-07 procedures, fig.4 [4]). Characterization of solutions - specific, unique and suitable - for using them in similar conditions of the mechanical wastes processing into the set geometrical form and dimensions of the granulated for energy product.

Fig.4: Solution: multi-discs grinders design-new-constructions for PBF-waste; elements and relations
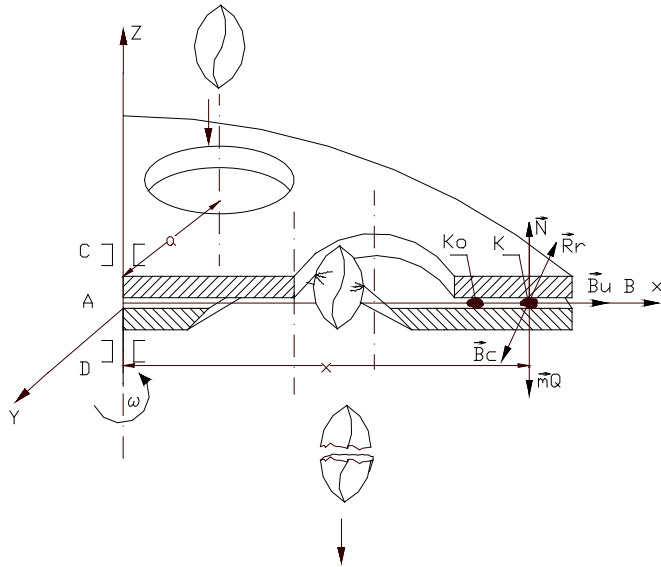
Given from experimental investigations results make up principles to shows selection onto settlement regarding to most suitable way of disintegration and solutions estimation of energy, work, effectiveness, energy consumptions and loads (Table 1).

Tab.1. Energy, effectiveness and efficiency grinding characteristics
of plastics- biomaterials- and fibrous waste

No.	Estimators of grinding development	Plastics waste	Biomaterials and waste	Fibrous waste
1.	Energy consumption of grinding by machine, E_R, kJ·kg^{-1}	655,4	137,8	212,9
2.	Effectiveness of multi discs grinding, e_r, -	68,7	116,1	98,6
3.	Material efficiency of the conversion process, η_0 -	0,14	0,13	0,07
4.	Efficiency of the PBF-waste grinding process, η_r, -	0,06	0,11	0,09
5.	Energy efficiency of PBF-waste grinding and thermo processing, η_{ep}, -	0,28	0,27	0,14

Also discerning analysis of sub-ranges of chart gives aids to selection optimal grinders' construction and way of disintegration. However general solution for every chart characteristics, described by 4-th degree equation assigned area of possible search:

$$H = a\,\Delta l^4 + b\,\Delta l^3 + c\,\Delta l^2 + d\,\Delta l + e$$
$$\text{for } R^2 > 0,95$$

The constructive features of the working set of the multiple discs grinder should be selected in such a way that the function achieves the maximal value (because of the e_R, η_0, η_r, η_e, indicator value) or minimal (because of the value of the unit energy consumption indicator E_R).
The point where the function value fulfils the required criterion is called problem solution: $x^* = (x^*_1, ..., x^*_n)$. The solution is, of course, from the permissible area:

$$x^* \in \Phi$$

The principle of the optimization support in the direction of getting the extreme solution can be defined:

$$\left\{ X^* \in \phi \right\} : \left\{ \underset{x \in \phi}{\wedge} Z(x) \geq Z\left(X^*\right) \right\},$$

in the case of minimization of energy consumption $(Z = E_R)$

$$\left\{ X^* \in \phi \right\} : \left\{ \underset{x \in \phi}{\wedge} Z(x) \leq Z\left(X^*\right) \right\}$$

in the case of maximization of energetic milling indicator, material and energy efficiency $(Z = e_R, \eta_0, \eta_r, \eta_e)$.

Solution

We attribute a great part to creative individuality- building, to aiding formation processes, by modern systems of grinding design development, design engineering, production, operation, recirculation, tests and estimation. A specific area of coexistence of the (Pw) plastics-, (Bw) biomaterials-, (Fw) fibrous waste and machinery construction, grinding parameters (LT, LO, LR, PK, PR, PLOT, PLOR, PPMT, PPMR, GPK, ST) is the engineering of wastes break-up in recycling process (tab.2). Many thousands years of tradition, ontology and construction development of the

Tab. 2. The PBF-waste grinding and grinders parameters

Symbol	TOP^{gran}_TEST_07 - New Solutions, Product conception	Pw	Bw	Fw
LT	Number of shields, -	5	5	5
LO	Number of openings in the first row of the first shield, -	9	9	9
LR	Number of rows, -	2	2	2
PK	Angular velocity, rad·s^{-1}	11,34	8,83	21,5
PR	Row radius, m	0,065	0,065	0,065
PLOT	Increase of the number of openings between shields, -	2	2	2
PLOR	Increase of the number of openings between rows, -	2	2	2
PPMT	Increase of the radius of rows between shields, m	0,003	0,003	0,003
PPMR	Increase of the radius of rows in a shield, m	0,002	0,002	0,002
GPK	Angular velocity gradient, , rad·s^{-1}	2,00	1,50	4,00
ST	Shields' diameter, m	0,255	0,255	0,255

grinding, mills ensure better and better setting in order and pro-innovation conjectures. There is constantly so much to be composed and innovated.

3. Summary and comment

The use of plastics, biomaterials fibrous materials is expected to continue and increase, driven by: potential for development, innovation, energy saving potential and positive contribution to climate protection, quality of life enhancement, enabling of affordable products.

Our most important task in the waste management area is to divert combustible waste from landfill. Plastics are particularly important to recover, as they offer many options including recovering the calorific content of the material. For recovery, mechanical recycling will remain the preferred method for homogeneous plastics waste streams, whereas for a number of mixed streams different energy recovery options are preferable. Both methods save resources and CO_2 emissions. The methodology of the devices development in plastics, biomaterials, fibrous materials recycling for energy engineering, based on the system model (1) needs the fulfilment of the methodical conditions and improvement possibilities: of the grinder and PBFm and materials beings in the recycling process.

The first condition of development of the product creative methodology of PBF-waste break-up

in the recycling process for energy engineering is model description of the objective, of the solution essence (idea), processing of the conception, construction, production and monitoring of the machine novelty, e.g. in the **TOP^{gran}** computer environment corresponding to the idea of the systems for integrated manufacturing of the machinery components.

There exists discrepancy between the calculated construction indicators and energetic efficiency indicators – determined for the machine built on the basis of the carried out support procedures. The discrepancy achieves the value of even several percent (the obtained result is the most adventageous when the discrepancy between the calculated construction and the constructed mill with the energy – consumption $E_R = 655,4 kJ \cdot kg^{-1}$ – with the criterion $E_R < 700 \ kJ \cdot kg^{-1}$ is 6,4%). In the process of searching for processing machines properties, it is necessary to include the following procedures:

- to use the scientific basis of machine construction and exploitation,
- to create new solutions on the basis of individual ideas taking into consideration the nature of needs,
- to take into consideration the complexity of technical systems to implement the stated processing function – steering, drive, service, repairing, power supply, damages, scrapping and others.

Plastics make up around 10% by weight of the feed but as much as 50% of the calorific content thanks to their high specific calorific value. The last 10 years have seen a remarkable change in the approach to waste management across Europe. As a result, there has been a significant increase in the recycling of all materials as well as more recovery of energy from combustible waste. The situation with respect to PBF-waste is no exception, and as this work demonstrates, both recycling and energy recovery of plastics-, bio- and fibrous waste continue to increase.

References:
1. Kamyk, W., *PhD-Work (in polish),* UTP Bydgoszcz, 2008,
2. Chun, J.J.Yi, Moon, Y.H., *Application of neural networks to predict the width variation in a plate mill,* Journal of Material Processing Technology, April 2001,
3. Flizikowski, J.B., *Dissertation on construction (in polish),* Publishers ITE, Radom 2002,
4. Flizikowski, J.B., Flizikowski, A., Kamyk, W., *Ontology and Development of Food Grinder Construction. (in polish)*, Inżynieria Maszyn 20/03, pp. 223-226, Bydgoszcz 2003,
5. Flizikowski, J.B., *Global Algorithm of Machinery Innovation. (in polish),* Publishers BTN, Bydgoszcz 2006,
6. Flizikowski, J.B., Kopacek, P., *Innovation of Multi-disk Food Break-up. (in polish),* Inż. i Ap. Chem. 46, pp.46-47, No 1/2007,
7. Flizikowski, J.B., Kowalski, A., *Precise Drive of Food Grinders. (in polish),* Inż. i Ap. Chem. 46, pp. 48-49, No 1/2007,
8. Flizikowski, J.B., Lis, A., *Optimisation of Multi-disk Grinder. (in polish),* Inż. i Ap. Chem. 46, pp. 450-52, No 1/2007,
9. Kazimierczak, G., Pacula, B., Budzyński, A., *Solid Edge. Computer-aided Design. (in polish),* HELION, Gliwice, 2004,
10. Macko, M., *Effect of Design Features of Multi-disk Unit on Usable Characteristics of Breaking up Process of Plastics Pipe Recyclates. (in polish),* Dysertacja WM-ATR, Bydgoszcz 2000,
11. Mazurkiewicz, A., *Transformation of Knowledge in Machinery Construction and Operation. (in polish),* Publishers ITE, Radom 2002,
12. Ostwald, M., *The Elements of Construction Optimisation. (in polish),* Publishers PP, Poznań, 2003,
13. Xiao D., Xu, H., *An Integration of Ontology-based and Policy-based Network Management for Automation,* CIMCA-IAMTIC'06, 2006,

14. Cempel, C., Natke, H.G., *Energy model of social system with production and recycling Eco Energy Processor (EEP),* Inter. Jour. of System Science, vol. 33, No 2, pp.87-95, 2002,

ANALYSIS OF FRAME STABILITY AS SAFETY REQUIREMENT

Henryk Holka, Mariusz Kukliński

University of Technology and Life Sciences in Bydgoszcz
al. Prof. S. Kaliskiego, 85-796 Bydgoszcz, Poland
tel.: +48 52 3408292, fax.: +48 52 340825
e-mail: holka@utp.edu.pl, mariusz.kuklinski@utp.edu.pl

Abstract

This work is an analysis of an accident that occurred in a warehouse during loading of a new multi-level storing frame. The frame was designed in a professional design office with aid of computer program. It is of great importance to carry out checking procedures at various steps of the computerized design process. In this article two different methods were applied in order to calculate the critical buckling force. Then the results were compared. The Euler's and the Rayleigh's method yielded convergent results. The both methods proved that the critical buckling force would be exceeded if the frame was fully loaded. Since the frame began to incline when it was loaded only in 80%, other reasons of buckling must also be considered. Although we can't eliminate designer's mistake, it is more probable, that the buckling resistance of the frame was reduced by inappropriate operation of hydraulic stackers. The photographs show that the construction was so tightly loaded with palettes, that the overloading was the most probable cause of the catastrophe. The bending moment originated during the loading process could also reduce the buckling resistance of the construction.

Keywords: frame stability, buckling, Euler method, Rayleigh's method

1. Introduction

At present, development of computer technology and professional CAD/CAM codes the ability of applying appropriate design and simulation software is a constitutive part of engineering education. However, the practical use of this software requires a detailed training. A cursory study is not satisfactory and may lead to catastrophic consequences in operation of designed constructions. The analyzed case of collapsed multi-level frame for palettes storing shows that a stability analysis is an indispensable part of a design process. The majority of commercial civil engineering software includes modules of a stability analysis. Nevertheless, it is instructive to compare and evaluate most known and applied methods of stability and buckling analysis that may serve as a handy check of computerized design process. The other problem is an appropriate and strictly observed system of loading and unloading multi-level storing frames. It is essential for a safe life cycle operation of this type of construction to preserve the loading limits. When the maximum utilization of storing space of warehouses turns a main objective and substitutes a safety criterion, damage may be very extensive.

The inspiration for the present work was collapsing and the total destruction of a multi-level storing frame that was 16,44 m long, 9,60 m deep and 8,00 m high. The frame provided three levels for storing palettes. The construction consisted of u-channel bearing columns with tops connected by horizontal square section tubes. As it is shown in fig.1, the palettes were stored side by side without leaving any distance between them. Palettes stored with maximum concentration

might cause an overloading of the construction. The other reason might be an inappropriate system of loading the construction with palettes. The loading and unloading of multi-level high storing frame was performed by telescopic hydraulic stackers. Operators controlled the process with help of camera and, in case of inattention; the forks of stacker might hit a bearing column and cause the loss of stability or deformation and local buckling of u-channel column.

In the time of the catastrophe the frame was loaded in 80% with palettes of 7700 N unitary weight. The process of frame destruction, since the moment of light noticeable inclination of the first external span until the complete destruction, lasted about two hours. In order to preserve the content of the palettes stays between the frame and the building's girders were installed. The static forces in the curved frame were so great, that the bearing columns began to crack. The enclosed picture (fig. 2.) shows the extension of destruction caused by buckling of bearing columns.

Fig. 1. Palettes stored in the multi-level frame

Fig. 2. Destroyed multi-level storing frame after collapsing

2. Definition of construction stability and its analysis

We consider a dynamic system described by set of regular differential equations:

$$\dot{\mathbf{y}} = \mathbf{f}(\mathbf{y}, t) . \tag{1}$$

If the vectorial function $\mathbf{f}$ does not depend in explicit way from time t, then the system is stationary. Otherwise the system is nonstationary. Accepting the partial solution $\widetilde{y}(t)$ of the above-mentioned equation as equation of undisturbed motion, and the remaining solutions y(t) as disturbed motion equations, we observe the evolution of disturbances $y_i(t_0) - \widetilde{y}_i(t_0)$, i = 1,..., m, for the initial moment t = t_0. For so defined solutions Liapunov (1892) introduced the following definition of stability:

Undisturbed motion $\widetilde{y}(t)$ of system (1) we call stable in relation to variables y_1, y_2,...,y_m if for every ε > 0 exists δ > 0 such, that for every solution y(t) of the system (1) satisfying condition $\left\| y(t_0) - \widetilde{y}(t_0) \right\| < \delta$, inequity $\left\| y(t) - \widetilde{y}(t) \right\| < \varepsilon$ is valid for every t ≥ t_0 [1].

According to the above-mentioned definition, small variations from the initial conditions remain finite in time for stable motion. Equations of disturbed motion we express by means of deviations $x_i(t) = y_i(t) - \widetilde{y}_i(t)$. Substituting this equation to (1) and expanding the right side of the resulting equation into the Tylor series we receive the equation of disturbed motion in the vectorial form:

$$\dot{\mathbf{x}} = \mathbf{A}(t)\mathbf{x} + \eta(\mathbf{x}, t) , \tag{2}$$

where the coefficients $a_{ij}(t) = \partial f_i / \partial y_j$ are estimated for y= $\widetilde{y}(t)$, and η_i are higher order derivatives from the Tylor expansion. Taking into account exclusively linear equation $\dot{\mathbf{x}} = \mathbf{A}(t)\mathbf{x}$ we carry out a linearization of equation of disturbed motion.

The linear analysis of stability called singular values method permits a determination of theoretical buckling resistance (the point of bifurcation) of the ideally linear elastic construction. However, imperfections and nonlinearities present in the majority of real constructions inflict, that buckling occurs before they achieve their theoretical buckling resistance. Therefore, in everyday engineering practice a nonlinear buckling analysis should be applied, which is available in professional engineering software. The finite element method (MES) is predominantly used in civil engineering software. The application of MES in stability analysis is clearly presented in [2].

However, the aim of this article is to present and compare methods that evaluate the correctness of computer procedures. The analyzed case of collapsed frame serves as an example.

3. Euler's method of buckling analysis

Stability of steel structures is the essential safety criterion during their design and life cycle operation. The research on the structure stability dates from 1744, when Euler published his work on bar's stability. The classical method of buckling analysis still bears his name. It is a simple method that assumes one of four buckling types. As it was noticed in the first paragraph the frame collapsed by inclination of the construction in the plane of figure 3. Since the tops of bearing columns were joined by horizontal square section tubes and the base of each column was fixed in the ground, we assume that in the analyzed case the first derivatives of deflection line equals zero at external points of each column. It is evident from fig. 3, that the buckling length of the column is the same as in the second Euler's buckling type i.e. the buckling coefficient μ=1. As forces in the analyzed column are applied between nodes, we predict that the buckling coefficient of the column should be even less than one (μ<1). Fig. 3 presents the sketch of the analyzed frame. In the

case of the internal column four palettes of the same level rest their corner on the same column (see fig. 1.). Therefore we admit that the single column is loaded with the weight of one palette on each level.
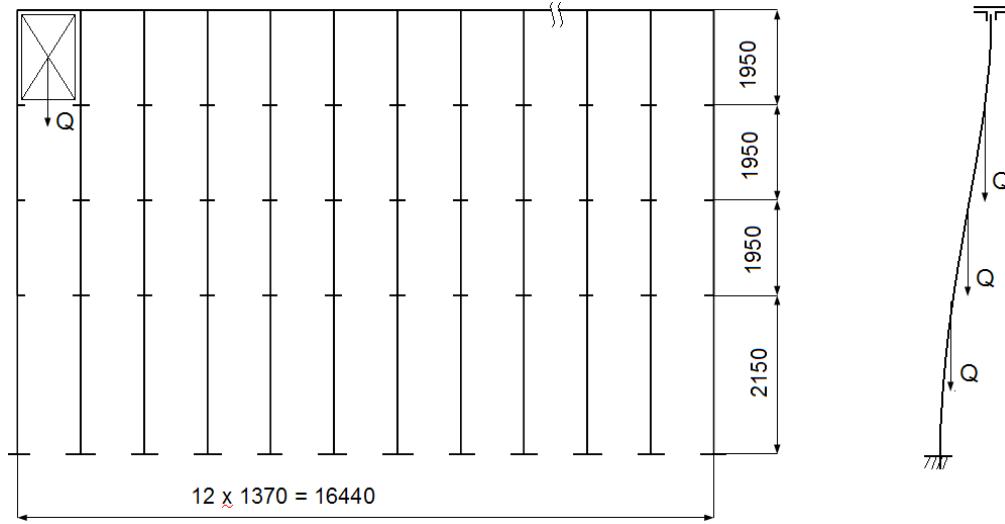
Fig. 3. The scheme of the multi-level storing frame and its buckling model

The geometrical data of u-shaped bearing columns are as follows: cross section area F = 3,48 cm^2, moment of inertia of the cross section I$_x$ = 41,04 cm^4, radius of inertia i = 3,43 cm.

Stress of pure compression caused in the column by the loading 3Q amounts to:

$$\sigma_c = \frac{3Q}{F} = \frac{3 \cdot 0,0077}{0,000348} = 66,37 \quad MPa.$$

The stress caused by buckling is greater than originated by pure compression. The measure of the column strain is the critical force it can support without buckling. The value of this critical force is given by the subsequent formula:

$$P_{kr} = \frac{\pi^2 \cdot E \cdot I_x}{L_w^2}. \tag{3}$$

In this formula L$_w$ is the buckling length of a column and it can be written as L$_w$ = L·μ, where L is a real length of the column. For the adopted buckling type the value of buckling coefficient μ we calculate by means of the following formula:

$$\mu = \frac{1}{2 - \left(\dfrac{Q}{Q_t}\right)^{0,25}} = \frac{1}{2 - \left(\dfrac{7700}{23100}\right)^{0,25}} = 0,805, \tag{4}$$

where Q is the weight of a single palette and Q$_t$ is the total load of a column. Consequently the buckling length L$_w$ = 0,805·8,0 = 6,44 m. The slenderness of a column is given by the formula:

44

$$s = \frac{L_w}{i} = \frac{644}{3,43} = 187,7 \, . \tag{5}$$

The boundary slenderness we compute assuming the proportionality limit σ_{prop} = 235 MPa and elastic modulus E = 205·10³ MPa:

$$s_{gr} = \pi \cdot \sqrt{\frac{E}{\sigma_{prop}}} = \pi \cdot \sqrt{\frac{205 \cdot 10^3}{235}} = 92,74 \, . \tag{6}$$

Since the column slenderness is greater than boundary slenderness, we may use the Euler formula (3) to calculate the critical buckling force, which results P_{kr} = 19980 N. For the internal fully loaded column we have:

$$Q_t = 3Q = 23100 \, N > P_{kr} = 19980 \, N \, . \tag{7}$$

The stability analysis carried out by Euler's method reveals that the critical force P_{kr} for internal columns of the structure is exceeded. Treating the case more precisely, we notice that 38 external columns are loaded only with forces P = Q/2 on each level and 4 corner columns only with forces P = Q/4 on each level. This slightly increases the stiffness of the frame. The critical force calculated for the whole structure approximately equals the total load of the frame.

On the other hand the palettes, probably of varying weight, were stored side by side increasing the load of the single column. Applying the formula (4) was also an approximation. Concluding we may say, that the frame was in the state of boundary stability and any incorrectness in loading process might cause the buckling. Because of adopted approximations we also calculated the critical buckling force applying Rayleigh's method.

4. The Rayleigh's method of stability analysis

Our purpose is to check the stiffness of the frame against buckling. The analysed structure has in fact infinite number of degrees of freedom. To find the buckling criterion we may reduce the problem to a single column treated as a single degree of freedom (SDOF) system. This method is called Rayleigh's method and it assumes, that during free vibrations a column adopts a single shape function $\psi(x)$, changing only the amplitude A(t). So the function y(x) = ψ(x)·A(t) determines the position of all points of bearing column. Applying the boundary conditions of the deflection line of a column we assume the shape function in the following form:

$$\Psi(x) = 0,5\left(1 - \cos\frac{\pi x}{L}\right). \tag{8}$$

Applying the principle of virtual work we formulate the equation of motion of generalized SDOF system:

$$\delta W_E = \delta W_I \, , \tag{9}$$

where δW_E is the virtual external work done by external loadings on their corresponding displacements. It includes the work of excitation force on palette's mass (m_Q), the work of palette's inertia force on its displacement $\delta y(x_i)$ and the work of palette's weight on its

displacement δe_i. δW is the virtual internal work done by internal bending moments $M(x, t)$ on their corresponding changes in curvature $\delta y''(x)$. The analysed model is presented in fig. 4.
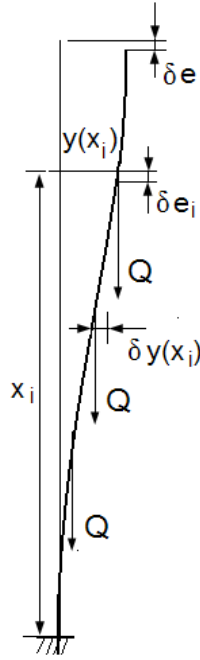
Fig. 4. The model of bearing column as a generalized SDOF system

In our model we neglect the weight of the frame elements supposing that they are much smaller than the weight of the palettes and we assume the constant stiffness of the columns EI. Now we may write the virtual external and internal work in the subsequent form:

$$\delta W_E = -\sum_i m_Q \ddot{y}(x_i,t) \cdot \delta y(x_i) + \sum_i m_Q \ddot{y}_{EX}(t) \cdot \delta y(x_i) + \sum_i Q_i \cdot \delta e_i \qquad (10)$$

$$\delta W_I = \int_0^L M(x,t) \cdot \delta y''(x) dx . \qquad (11)$$

In the generalized SDOF system we may write the following relations:

$$\begin{aligned}
y(x,t) &= \Psi(x)A(t) & \dot{y}''(x,t) &= \Psi''(x)\dot{A}(t) \\
y'(x,t) &= \Psi'(x)A(t) & \delta y(x,t) &= \Psi(x)\delta A \\
y''(x,t) &= \Psi'(x)A(t) & \delta y'(x,t) &= \Psi'(x)\delta A \\
\ddot{y}(x,t) &= \Psi(x)\ddot{A}(t) & \delta y''(x,t) &= \Psi''(x)\delta A
\end{aligned} \qquad (12)$$

that are the consequence of adopting the shape function $\psi(x)$.

According to the Euler-Bernouli hypothesis plane sections remain plane after deformation. We assume this hypothesis as well as the linear relation between damping stresses and strain velocity. Made assumptions lead to the following relation [3]:

$$M(x,t) = EI\left[y''(x,t) + c \cdot \dot{y}''(x,t)\right], \qquad (13)$$

where c is a damping constant.

The displacements of buckling forces δe_i we calculate from the following relation [3]:

$$\delta e_i = \int_0^{x_i} y'(x,t)\delta y'(x)dx \,. \tag{14}$$

Finally the equation of motion of the column has the form:

$$m_G \ddot{A}(t) + c_G \dot{A}(t) + k_G A(t) = P_G(t) \,, \tag{15}$$

where:

$m_G = \sum_i m_Q [\Psi(x_i)]^2$ - generalized mass

$c_G = c \cdot EI \int_0^L [\Psi''(x)]^2 \, dx$ - generalized damping

$k_G = EI \int_0^L [\Psi''(x)]^2 \, dx - Q\left\{ \int_0^{x_1} [\Psi'(x)]^2 \, dx + \int_0^{x_2} [\Psi'(x)]^2 \, dx + \int_0^{x_3} [\Psi'(x)]^2 \, dx \right\}$ - generalized stiffness

$P_G(t) = -\ddot{y}_{EX}(t) \sum_i m_Q \cdot \Psi(x_i)$ - generalized effective load.

The column will lose its stability when the generalized stiffness equals zero, so the critical weight of one palette we calculate from the following relation:

$$k_G = 0 \Rightarrow Q_{cr} = \frac{EI \int_0^L [\Psi''(x)]^2 \, dx}{\int_0^{x_1} [\Psi'(x)]^2 \, dx + \int_0^{x_2} [\Psi'(x)]^2 \, dx + \int_0^{x_3} [\Psi'(x)]^2 \, dx} \,. \tag{16}$$

Taking into account that x_1 = L·6050/8000 = 0,75625·L, x_2 = 0,5125L, x_3 = 0,26875L we calculate the integrals of equation (16). Since we assumed the shape function in the form of (8), the results are as follows:

$$\int_0^L [\Psi''(x)]^2 \, dx = \int_0^L \frac{\pi^4}{4L^4}\left(\cos\frac{\pi x}{L}\right)^2 dx = \frac{\pi^4}{8L^3}$$

$$\int_0^{x_1} [\Psi'(x)]^2 \, dx = \int_0^{0,75625 \cdot L} \frac{\pi^2}{4L^2}\left(\sin\frac{\pi x}{L}\right)^2 dx = 0,45765\frac{\pi^2}{4L}$$

$$\int_0^{x_2} [\Psi'(x)]^2 \, dx = \int_0^{0,5125 \cdot L} \frac{\pi^2}{4L^2}\left(\sin\frac{\pi x}{L}\right)^2 dx = 0,26249\frac{\pi^2}{4L} \tag{17}$$

$$\int_0^{x_3} [\Psi'(x)]^2 \, dx = \int_0^{0,26875 \cdot L} \frac{\pi^2}{4L^2}\left(\sin\frac{\pi x}{L}\right)^2 dx = 0,2134\frac{\pi^2}{4L}$$

Substituting these results into (16) we receive:

$$Q_{cr} = \frac{EI \cdot \pi^4 \cdot 4L}{8L^3 \pi^2 (0{,}45765 + 0{,}26249 + 0{,}2134)} = 6942 \text{ N.} \tag{18}$$

Since the average palette's weight is Q = 7700 N, the critical loading of the bearing column is exceeded. The total critical load of the column is 3Q = 20826 N. If we compare this result with (7), we note that the difference is about 3%. Unfortunately, both methods are approximate. In the case of Rayleigh's method we had to assume a shape function. If the admitted shape function were the true one, the calculated critical buckling force would be the exact one too. Every shape function other than the true one yields greater critical buckling force.

The shape function we admitted would be the true one if the loading was applied on the top of the column. Therefore, we may assume a sufficient correctness of our calculations.

5. Conclusions

The analysed multi-level storing frame was designed with aid of a professional computer program by experienced engineer. Therefore, the most probable cause of buckling of the construction was overloading (fig. 1.).

The buckling of the frame began then the construction was loaded in 80%. This suggests that during the loading of the frame, the telescopic hydraulic stackers could hit any bearing column and cause the local buckling.

Moving the palettes on the higher levels by hydraulic stackers also could produce a bending moment that contributes to the buckling.

References

[1] Seyranian, A., Mailybaev, A., *Multiparameter Stability Theory with Mechanical Applications*, WSPC, Singapore 2003.
[2] Wawczyszyn, Z., Cichori, Cz., Radwańska, M., *Metoda elementów skończonych w stateczności konstrukcji, Arkady*, Warszawa 1990.
[3] Clough, R. W., Penzien, J., *Dynamics of Structures*, Computers & Structures Inc., Berkeley 1995.

INCREASED POWER AND ENERGY LOSSES IN LOW VOLTAGE POWER LINE CAUSED BY LOAD ASYMMETRY

Piotr Kolber

University of Technology and Life Sciences
ul. S.Kaliskiego 7, 85-796 Bydgoszcz, Poland
tel.: 052 3408297, fax: 052 3408495
e-mail: pkolber@utp.edu.pl

Abstract

The paper presents a simulation model enabling determination of load resultant active power and energy losses, with regard to load in rural distribution low voltage power networks supplying the so called scattered consumers. The subject of examinations was a three-phase, four-wire, airborne low-voltage power line. The studied type of line is characteristic to, and most commonly used in, rural areas. The considerations included twenty-four-hour load measurement at representative consumers and at the beginning of the line – in a MV/LV transformer station. On the basis of the developed model, a simulation program enabling calculation of power and energy losses has been elaborated. Also, selected results of examinations concerning increase in active power and energy caused by load asymmetry for power line supplying two types of consumers: residential and production ones, have been presented.

Keywords: *low-voltage line, rural consumers, single-phase receivers, load asymmetry, power and energy losses*

1. Introduction

Load asymmetry in a low-voltage line results in current asymmetry in the line, limitation of power consumption, power asymmetry and increase in active and passive power losses in an inductive line.

However, in reality, in the line fixed operation states, there should be distinguished two kinds of asymmetry [4]:
  a) internal asymmetry of the power line elements (lines and transformers) caused by different self- and inter-impedances and of particular phases,
  b) external asymmetry:
    - supply point, when three-phase voltage in the line power point (MV/LV station) is unsymmetrical,
    - receiving point asymmetry when receptions connected in particular points of the power line are of different power in each phase,
    - receiving spatial when single-phase receptions of the same or different power are connected to the line at different points.

Receiving external asymmetry, including both the point ad the spatial asymmetry, and especially asymmetry occurring in four-wire low voltage power network 3×400/230V is of the biggest practical importance.

The considerations were limited to load power losses in the line as one of the most negative

effects for rural distribution low voltage power lines. Due to the fact that active power losses [1] are most common, the considerations have been focused on them. Asymmetry of the power line is caused by the consumers themselves who use single-phase receivers. It results in non-uniform power distribution in the line. With the line asymmetrical load, active power losses are the sum of losses in particular wires, i.e. phase and neutral ones. The increase in power losses and related energy losses in lines, in case of load asymmetry, in relation to power losses with asymmetrical loads, is caused by transmitting the so called asymmetry power [4, 5]. Load asymmetry occurs mainly in rural low-voltage power networks where lines are relatively long and to which a relatively smaller numbers of consumers using receivers of higher powers and take energy of higher values than in urban power networks are connected. All the consumers receiving energy connected to the line have an influence over the loss values, and therefore, a simulation model enabling determination of active power and energy losses with regard to load asymmetry has been developed.

2. Simulation model for power and energy loss determination in low-voltage power line

Considering a low-voltage power line in terms of power and energy loss determination, it was necessary to define division of the power into phases, at particular consumers. This power division is defined by a load unbalance coefficient:

a) indirect load coefficient

$$k_{1i} = \frac{P_{pi}}{P_{\max i}} \approx \frac{I_{pi}}{I_{\max i}}, \tag{1}$$

b) minimal load coefficient

$$k_{2i} = \frac{P_{\min i}}{P_{\max i}} \approx \frac{I_{\min i}}{I_{\max i}} \tag{2}$$

c) maximal load coefficient

$$w_i = \frac{P_{\max i}}{P_i} \tag{3}$$

where:

$$P_i = P_{\max i} + P_{pi} + P_{\min i} \tag{4}$$

P_{maxi}, I_{maxi}, P_{pi}, I_{pi}, P_{mini}, I_{mini} – power and current of the phase, respectively: the most, medium and the least loaded, in its particular receiving points

Mutual relation between coefficient values is defined by the dependence:

$$w_i = \frac{1}{k_{1i} + k_{2i} + 1} \tag{5}$$

For symmetrical load, these coefficients reach values: $k_{1i} = 1$, $k_{2i} = 1$, $w_i = 1/3$, whereas, in case of extreme asymmetry, when the total power is taken by one phase, their values are as follows: $k_{1i} = 0$, $k_{2i} = 0$, $w_i = 1$.

Permitted value ranges of particular coefficients are defined by dependencies:

$$\frac{1}{3} \le w_i \le 1 \tag{6}$$

$$k_{1i} \ge k_{2i} \tag{7}$$

for $w_i \in <1/3 ; 1/2)$

$$\frac{\frac{1}{w_i} - 1}{2} \le k_{1i} \le 1 \tag{8}$$

$$\frac{1}{w_i} - 2 \le k_{2i} \le \frac{\frac{1}{w_i} - 1}{2} \tag{9}$$

for $w_i \in <1/2 ; 1>$

$$\frac{\frac{1}{w_i} - 1}{2} \le k_{1i} \le \frac{1}{w_i} - 1 \tag{10}$$

$$0 \le k_{2i} \le \frac{\frac{1}{w_i} - 1}{2} \tag{11}$$

Permitted ranges of their values are also presented in Table 1.

Table 1. Permitted value ranges of load asymmetry coefficients

w_i	**0,33**	0,36	0,4	0,44	**0,5**	0,57	0,67	0,8	**1**
k_{1i}	**1**	0,875÷1	0,750÷1	0,625÷1	**0,5÷1**	0,375÷0,75	0,25÷0,5	0,125÷0,25	**0**
k_{2i}	**1**	0,875÷0,75	0,750÷0,5	0,625÷0,25	**0,5÷0**	0,375÷0	0,25÷0	0,125÷0	**0**

On the basis of the performed research, concerning phase loads at representative consumers in rural areas, values of load unbalance coefficients have been demonstrated in Table 2.

Table 2. Values of load unbalance coefficients at rural consumers

Load unbalance coefficients	w_i	k_{1i}	k_{2i}
Arithmetical mean	0,541	0,650	0,287
Standard deviation	0,134	0,233	0,239
Minimum	0,368	0,075	0,002
Maximum	0,928	0,967	0,783

Phase currents, in LV line, in sections between (i-1), and the i-th receiving point for the j-th time moment are determined from dependencies:

$$\underline{I}_{L1ij} = \sum_{i=1}^{n}\sum_{k=i}^{n} \underline{I}_{Akj} \qquad \underline{I}_{L2ij} = \sum_{i=1}^{n}\sum_{k=i}^{n} \underline{I}_{Bkj} \qquad \underline{I}_{L3ij} = \sum_{i=1}^{n}\sum_{k=i}^{n} \underline{I}_{Ckj} \tag{12}$$

where:

$\underline{I}_{Akj}$, $\underline{I}_{Bkj}$, $\underline{I}_{Ckj}$ − combined values of phase powers received at the k-th receiving point for the j-th time moment

$$\underline{I}_{Akj} = I_{Akj}(\cos\varphi_{Akj} + j\sin\varphi_{Akj}) \tag{13a}$$

$$\underline{I}_{Bkj} = I_{Bkj}(\cos\varphi_{Bkj} + j\sin\varphi_{Bkj}) \tag{13b}$$

$$\underline{I}_{Ckj} = I_{Ckj}(\cos\varphi_{Ckj} + j\sin\varphi_{Ckj}) \tag{13c}$$

$$I_{Akj} = \frac{P_{Akj}}{U_{Akj}\cos\varphi_{Akj}} \qquad I_{Bkj} = \frac{P_{Bkj}}{U_{Bkj}\cos\varphi_{Bkj}} \qquad I_{Ckj} = \frac{P_{Ckj}}{U_{Ckj}\cos\varphi_{Ckj}} \tag{14}$$

where:

P_{Akj}, P_{Bkj}, P_{Ckj} − values of phase powers taken in the k-th receiving points for the j-th time moment,
$\cos\varphi_{Akj}$, $\cos\varphi_{Bkj}$, $\cos\varphi_{Ckj}$ − values of power phase coefficients taken in the k-th receiving points for the j-th time moment,
U_{Akj}, U_{Bkj}, U_{Ckj} − values of phase voltages in the k-th receiving points for the j-th time moment.

Asymmetrical current in the line, in the came section, for the same time moment, is determined as the arithmetical mean of phase currents from the line:

$$I_{sij} = \frac{1}{3}(I_{L1ij} + I_{L2ij} + I_{L3ij}) \tag{15}$$

Then, power losses for asymmetrical load in the line supplying n customers for the j-th time moment, can be obtained on the basis of the dependence:

$$\Delta P_{sj} = \sum_{i=1}^{n}\frac{1}{3}(I_{L1ij} + I_{L2ij} + I_{L3ij})^2 R_i \tag{16}$$

where:

R_i − value of the line cable resistance between (i-l) and the i-th receiving point.

However, the power loss value for the j-th time moment in a power line, for n customers, for asymmetrical load, is determined from the dependence:

$$\Delta P_{nsj} = \sum_{i=1}^{n}(I_{L1ij}^{\ 2} + I_{L2ij}^{\ 2} + I_{L3ij}^{\ 2})R_i + \sum_{i=1}^{n}I_{Nij}^{\ 2} R_{Ni} \tag{17}$$

where:

I_{Nij} − value of current in the neutral wire of LV line between (i-l) and i-th receiving point for the j-th time moment,
R_{Ni} − value of the line neutral wire resistance between (i-l) and the i-th receiving point.

Power losses are determined for a given time moment, e.g. maximum load. Whereas, energy

losses can be determined in result of integration of power losses for a given period. This period can be, e.g. twenty four hours a month.

Energy loss increase coefficient caused by load asymmetry can be defined in connection with this:

$$k_E = \frac{\Delta E_{ns}}{\Delta E_s}$$ (18)

where:

ΔE_{ns} - energy loss with asymmetrical load,

ΔE_s - energy loss with symmetrical load.

3. Simulation program for determination of power and energy losses in low-voltage lines

The developed model served for elaboration of simulation program enabling determination of power and energy losses in LV line.

First, the line topology, i.e. for its given length, and a fixed number of receiving points n, their arrangement was generated on the basis of triangular distribution. Acceptance of triangular distribution was dictated by the fact that most of customers are usually located near the MV/LV transformer stations and their number decreases along with the distance. Next, the line phase was defined randomly: the most, medium and the least loaded by the consumers in each *i*-th receiving point.

The investigations covered day and night measurements at representative customers, and at the beginning of the line (in station 15/0,4 kV on LV rails) [2]. For carried out line simulations, values of momentary phase loads concerning the line receiving points, were generated. In each generation point, i.e. time moment, the value was generated from normal distribution with parameters obtained on the basis of measurements, during 14 days and nights, at representative customers. For simulation studies, two types of customers were accepted – individual and business ones. Load division into phases was carried out by generating empirical distributions obtained from load measurements taken at the customers. Momentary values of phase power coefficients - $\cos\varphi_{fi}$ for receiving points were generated on the basis of empirical distributions obtained from measurements at the station of 15/0,4 kV. It seems that these values do not differ much from those obtained from customers. Phase load values and values of power coefficients were the basis for determining currents in the line (in phase and neutral wire) between receiving points. It enabled the calculation of power losses in the power line, for particular time moments. Basing on values of momentary power losses, using the method of numerical integration [3], values of energy losses, for symmetrical and asymmetrical loads, were determined. It allowed the determination of coefficient value being a ratio of losses for load asymmetry to losses for load symmetry.

4. Selected results of simulation investigations

In result of simulation, there was generated, among others, a low voltage line with length of $l = 1048$ m, to which 10 customers are connected, located in the following distances from the line beginning:

$l_1 = 82$ m, $l_2 = 105$ m, $l_3 = 284$ m, $l_4 = 301$ m, $l_5 = 368$ m, $l_6 = 495$ m, $l_7 = 589$ m, $l_8 = 750$ m, $l_9 = 841$ m, $l_{10} = 1048$ m.

Within the conducted research, an airborne power line with flat phase and neutral wire setting whose cross-section values were:

$s = s_n = 35$ mm^2

For the analyzed line, two types of customers were analyzed, i.e. 5 residential and 5 production consumers. Both types of customers are characterized by the following values of installed power:

    a) $P_z = 9$ kW – residential consumers
    b) $P_z = 32$ kW – production consumers

The value of the installed power is understood here as the sum of power of all the receivers owned by a given customer.

It is estimated on the basis of literature, that the level of this power utilization for the top loaded hours is 20-30%.

Table 3 presents simulation results of power losses for day-and-night operation, during top load, in the time of autumn and winter, as well as energy losses during one month (30) days, and 133 days of the same period, for load asymmetry and symmetry. Customer load measurements which served for phase load generation were taken in the autumn-winter time. It is assumed that 365 days of the year are divided into 232 days of spring-summer time and 133 days of the autumn-winter period [5]. The value of power losses for peak load, during 24 hour's time, obtained in result of simulations was consistent with load asymmetry obtained at the beginning of the line which was: $\alpha_{i2} = 0,18$ $<\alpha_{i2} = I_N / (I_{L1}+I_{L2}+I_{L3})>$.

Table 3. Power and energy loss values for LV line

Power and energy losses	Symmetrical load	Asymmetrical load
Power losses for peak load, during operation for 24 hours [kW]	0,873	1,060
Ratio of power loss for peak load	1,22	
Energy losses during one month, in [kWh]	110,81	132,90
Energy losses during 133 days, in [kWh]	488,06	585,34
Ratio of energy losses for load symmetry and asymmetry	1,20	

5. Conclusions

Load asymmetry for the simulation carried out at the beginning of the line, for its peak load, during 24 hours of its operation was $\alpha_{i2}^{*} = \alpha_{i2} \cdot 100\% = 18\%$ (for load symmetry the coefficient assumes value 0%)

On the basis of an analysis of the results obtained from exemplary simulations, it can be said that the increase in power and energy losses in the power line supplying residential and production customers caused by load asymmetry would be about 20% higher in comparison with energy losses for load symmetry, which is a significant value. The maximum loss increase that could be possible for the carried out simulation would be 64%. It would take place if the phases: most, medium and least loaded were assigned simultaneously at all customers, respectively to the line's first, second and third phase, which seems to be unreal with such a number of customers ($n = 10$).

In a given area covered by the power network and consisting of many lines, while making a general power and energy analysis involving determination of values of expected loads, the

value of transmission capacity and additional costs connected with power transmission, it is necessary to take into account additional losses caused by load asymmetry.

References

[1] Horak, J., Gawlak, A., Szkutnik, J., *Sieć elektroenergetyczna jako zbiór elementów*, Wydawnictwo Politechniki Częstochowskiej, Częstochowa 1998.

[2] Kolber, P., *Wpływ wybranych czynników na nierównomierność obciążeń wiejskich elektroenergetycznych sieci niskiego napięcia* (rozprawa doktorska), Uniwersytet Warmińsko-Mazurski, Olsztyn 2006.

[3] Kosma, Z., *Metody numeryczne dla zastosowań inżynierskich*, Wydawnictwo Politechniki Radomskiej, Radom 1999.

[4] Kujszczyk, S., *Elektroenergetyczne sieci rozdzielcze*, Cz.2., PWN, Warszawa 1991.

[5] Matla, R., *Gospodarka elektroenergetyczna*, Wydawnictwo Politechniki Warszawskiej, Warszawa 1988.

RESEARCH ON THE INFLUENCE OF COOLING AND LUBRICATION ON THE SURFACE LAYER SELECTED PROPERTIES

Tadeusz Leppert

University of Technology and Life Sciences
Faculty of Mechanical Engineering
Ul. Ks. Kordeckiego 20, 85-225 Bydgoszcz, Poland
e-mail tleppert@utp.edu.pl

Abstract

The paper presents the structure and selected results of the BW 13/2007 research conducted in the Production Engineering Department. It describes the conditions and application range of dry and MQL cutting, as well as the results of an analysis into the machined surface geometrical structure, cutting forces and residual stresses in the surface layer.

**Keywords**: *turning, dry cutting, minimum quantity lubrication, MQL, surface layer, cutting force, residual stresses*

1. Introduction

Within the BW 13/2007 research program – ECOLOGY-ORIENTED SURFACE SHAPING ENGINEERING FOR SPECIFIC SERVICEABLE FEATURES – the Department of Production Engineering conducts research on the physical nature and conditions of cutting processes and their influence on technological and operational characteristics of the machined surfaces. The predominant field in the ecology-oriented surface shaping is the author's research on the influence of cooling and lubrication in the cutting zone on the machined surface layer properties in turning steel 45 and austenitic stainless steel 00H17N14M2.

2. Conditions and range of application of dry and MQL cutting

The increasing awareness of the negative impacts of production processes has led in many countries to legislative regulations limiting or eliminating some of the manufacturing processes. This has caused an increase in production costs related mainly to the prevention and elimination of the negative effects. The current pro-ecology actions necessitate a search for new solutions to minimize and, eventually, to eliminate the harmful by-products of production processes. It can be achieved by improving the currently employed technologies and elaborating new ones which will conform to rigid environment protection standards. Among the production methods, machining has found its way into many branches of industry. Because of its huge share in manufacturing processes and a negative

impact on the environment, it has also attracted the attention of many scientific and industrial centers. An important factor in the cutting process, which often positively affects the quality of the machined elements, tool life and production costs, is the cutting fluid. Critical as cutting fluids are for machining processes, they also pose a substantial threat to the direct surrounding of the workplace, health and safety of machine operators as well as to the natural environment (air, water, soil) [3, 4]. Hence the effort aimed at eliminating (dry cutting) or limiting (minimum quantity cooling/lubrication – MQC/MQL cutting) their use [1, 2]. Conditions underlying wide interest in eco-friendly manufacture and its resulting advantages are shown in Fig. 1.
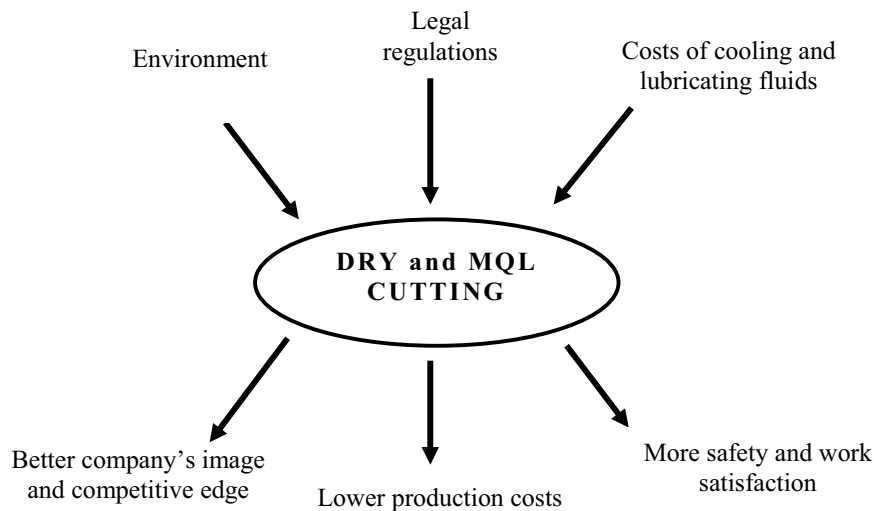
Fig. 1. Conditions and advantages of dry and MQL cutting [3]

The primary objective of cutting fluids in the cutting process is cooling and lubricating the cutting zone, which diminishes friction between the adjoining surfaces and facilitates the removal of chips from the cutting area (fig. 2). The elimination of the cooling and lubricating fluid (CLF) in dry cutting causes that neither cooling nor lubrication or removal of chips from the machine working space is performed. This seems to be the basic drawback of dry cutting, which also leads to undesired changes in cutting conditions. Lack of cooling means a higher cutting temperature, shorter tool life, warped surface texture with greater residual stresses, lesser dimensional and shape accuracy. It also results in degraded surface roughness and difficulty in removing hot chips and measuring the machined object. From the ecological point of view, without the flushing action of the CLF, the air, the machine and its immediate surrounding become polluted with metal dust and chippings. All these come about if there is no CLF, making the dry cutting method difficult for industrial application. As long as there is no substitute for CLFs to effectively perform their functions, dry cutting cannot be successfully implemented [9, 10, 11].

The complete elimination of CLF is also impossible in the case of certain machined materials or machining methods because it leads to degraded quality, lower machining productivity and inferior conditions of chip disposal.
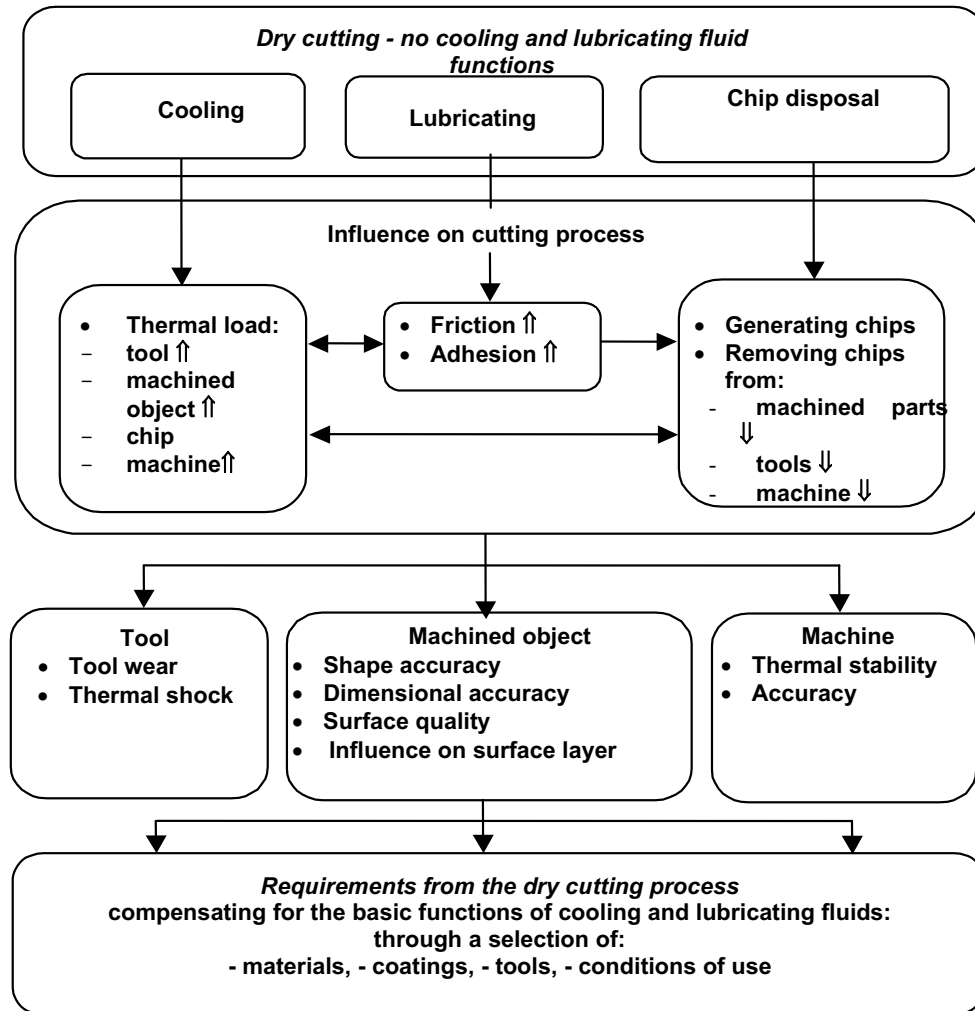
Dry cutting - no cooling and lubricating fluid functions

| Cooling | Lubricating | Chip disposal |

Influence on cutting process

- **Thermal load:**
  - **tool ⇑**
  - **machined object ⇑**
  - **chip**
  - **machine ⇑**

- **Friction ⇑**
- **Adhesion ⇑**

- **Generating chips**
- **Removing chips from:**
  - **machined parts ⇓**
  - **tools ⇓**
  - **machine ⇓**

Tool
- **Tool wear**
- **Thermal shock**

Machined object
- **Shape accuracy**
- **Dimensional accuracy**
- **Surface quality**
- **Influence on surface layer**

Machine
- **Thermal stability**
- **Accuracy**

Requirements from the dry cutting process
compensating for the basic functions of cooling and lubricating fluids:
through a selection of:
- materials, - coatings, - tools, - conditions of use

Fig. 2. Effects and requirements of dry and MQL cutting [9]

When dry cutting is not an option because of its drawbacks and difficult cutting conditions, minimum quantity cooling and lubrication may be an alternative. It helps to decrease production costs by 10 – 50% as well as minimizing environmental and health hazards. Minimum quantity cooling and lubrication (MQL) cutting or minimum quantity fluid (MQF) cutting, also referred to as quasi-dry cutting, can be characterized by a small quantity of cooling and lubricating fluid supplied to the cutting zone – the amount usually does not exceed 50ml/h [2, 11].

Despite the described issues with dry and MQL cutting, they are used especially in high volume and mass production (Table 1).

Tab. 1. Application range of dry and MQL cutting [11]

Material Process	Aluminum		Steel		Cast iron
	Cast alloys	Wrought alloys	High alloyed steel	Construction steel	
drilling	MQL	MQL	MQL	MQL	MQL
reaming	MQL	MQL	MQL	MQL	MQL
tapping	MQL	MQL	MQL	MQL	MQL
deep hole drilling	MQL	MQL	MQL	MQL	MQL
milling	MQL/dry	MQL	dry	dry	dry
turning	MQL/dry	MQL/dry	dry	dry	dry
gear milling			dry	dry	dry dry
sawing	MQL	MQL	MQL	MQL	MQL
broaching			MQL	MQL/dry	dry

3. Research and results

The conducted research into the formation of surface layer in dry and MQL turning covers the areas presented in Fig. 3.

The results of the research into cutting force in turning steel 45 and stainless steel 00H17N14M2 have shown that eliminating or limiting the application of the cutting fluid in the cutting zone does not cause any substantial change in the value of the total cutting force (Fig. 4). However, the cutting force's components: F_c, F_f and F_p are more affected. The influence of the cooling and lubrication mode largely depends on the employed cutting parameters: cutting speed and feed rate [5].

The analyses of the machined surface texture parameters shown in Fig. 5 and 6 have confirmed a major influence of the cooling and lubrication mode on the analyzed surface characteristics of the geometrical structure in turning steel 45 and 00H17N14M2. It also needs to be added that this influence was dependent on the employed cutting parameters [6, 7]. Dry and MQL turning of steel 00H17N14M2 generated smaller surface roughness and waviness than turning with a cutting emulsion supplied to the cutting zone. Depending on the employed cutting parameters, the MQL method gave a smaller roughness and waviness of the machined surface, compared to dry and emulsion cutting. The cooling and lubrication mode in the cutting zone substantially influence the bearing ratio of the roughness profile at slow cutting speeds. The influence diminished at faster speeds. An unfavorable change appeared with the increase of feed rate: the bearing ratio of the roughness profile decreased.
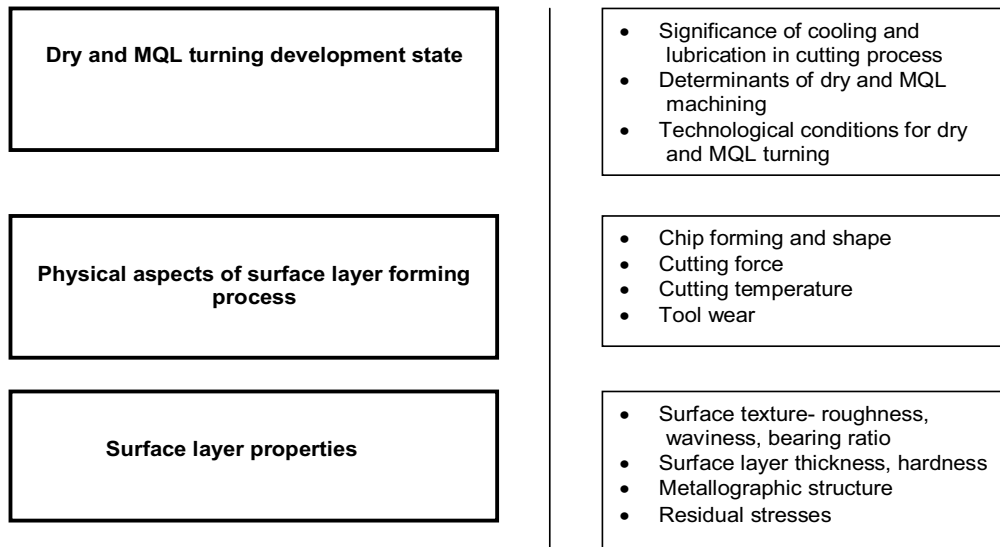
Dry and MQL turning development state	• Significance of cooling and lubrication in cutting process • Determinants of dry and MQL machining • Technological conditions for dry and MQL turning
Physical aspects of surface layer forming process	• Chip forming and shape • Cutting force • Cutting temperature • Tool wear
Surface layer properties	• Surface texture- roughness, waviness, bearing ratio • Surface layer thickness, hardness • Metallographic structure • Residual stresses

Fig. 3. Surface layer research structure
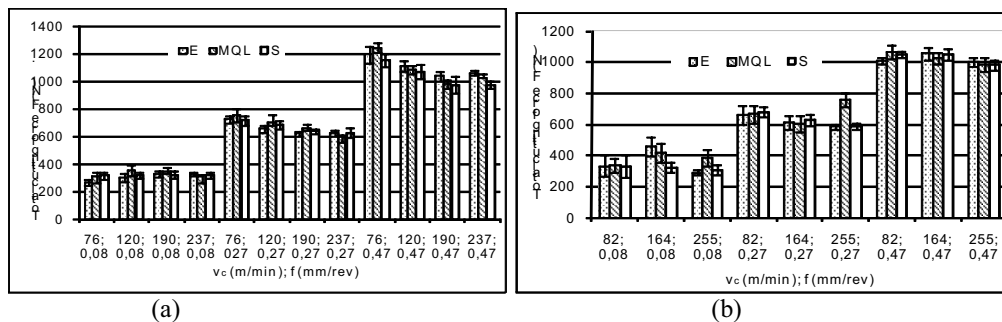

(a)

(b)

Fig. 4. The influence of the cooling and lubrication mode, the cutting speed and feed rate on the total cutting force, a – steel 45, b – steel 00H17N14M2 [5]
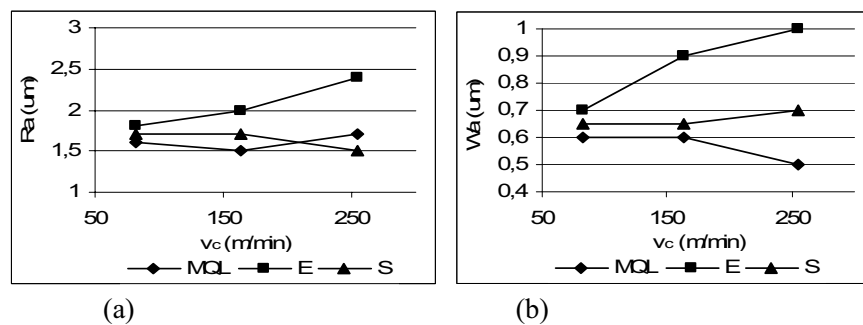

(a)

(b)

Fig. 5. Influence of cooling and lubrication and cutting parameters on surface: roughness R_a -a and waviness W_a -b (steel 00H17N14M2) [6]
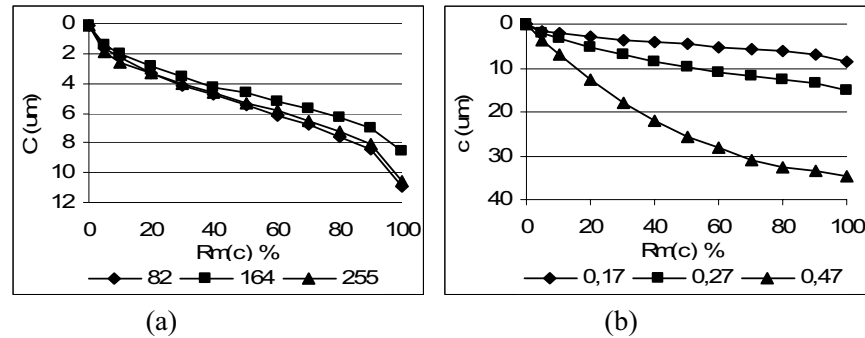
Fig. 6. Influence of cutting speed and feed rate on bearing ratio in turning with MQL: a- f= 0,17mm/rev; b- v_c= 164 mm/min (steel 00H17N14M2) [7]

The research into the influence of the cooling and lubrication mode in the cutting zone on residual stress conducted in association with the Linkoping University in Sweden has shown a considerable influence of dry cutting on residual stress in the surface layer (Fig. 7). The value of tensile stresses both in the hoop and axial direction largely depend on the employed cutting parameters. Depending on the cutting speed, the elimination of cooling and lubricating fluids led to a decrease or increase of hoop stress along with an increase of feed and an increase of axial stress [8].
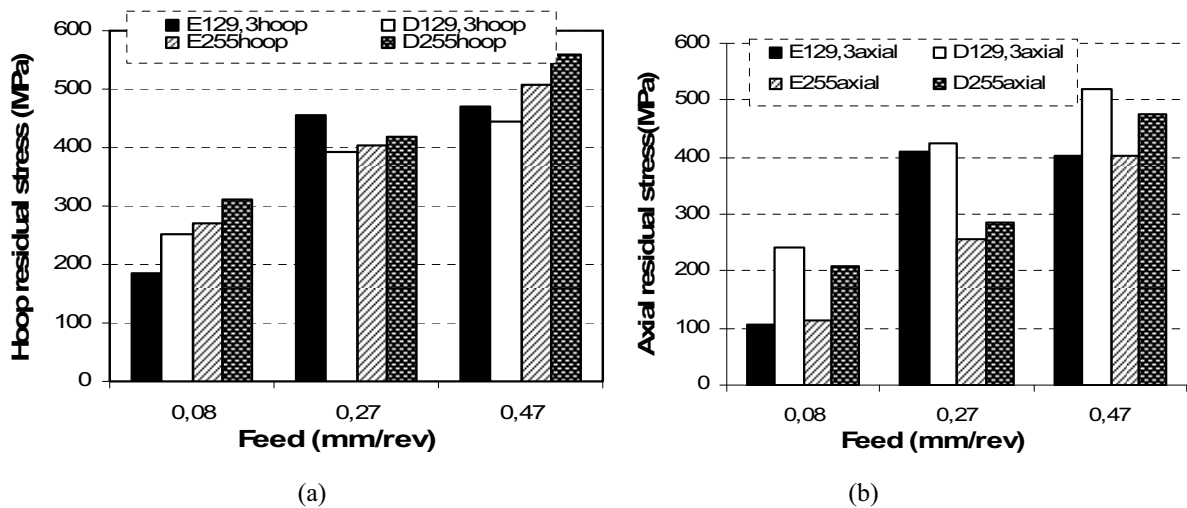

Fig. 7. Hoop (a) and axial (b) residual stresses in surface layer in turning dry and with emulsion (steel 45) [8]

4. Conclusions

The research has shown that with a proper choice of cutting parameters, the values of the analyzed geometrical surface layer parameters as well as its physical properties after dry and MQL turning are comparable to those obtained in turning with a continuous supply of cutting fluids. The results emphasize a possibility of eliminating or limiting the application of cutting fluids while cutting steel 45 and 00H17N14M2.

The current state of knowledge on dry and MQL turning encourages further research on the phenomena in the cutting zone and the characteristics of the surface layer in dry and MQL turning.
This particularly refers to:

- influence of eliminating or limiting the application of CLF on thermal phenomena in the cutting process
- surface geometrical structure, including a relation between the characteristics of the technological and operational surface layer

- physical properties of the surface layer
- air pollution around the workplace
- modeling the characteristics of the surface layer, including the cutting zone cooling and lubricating conditions
- characteristics of the surface layer in other cutting processes: milling, grinding, deep drilling – performed with or without cooling and lubricating fluids

REFERENCES:

[1] Graham, D., Huddle, D., McNamara, D., *Machining dry is worth a try: reducing cutting fluid use offers the chance for considerable cost savings. Tool life may even improve*, Modern Machine Shop, October, 2003.

[2] Klocke, F., Eisenblaetter, G., *Dry Cutting*, CIRP Vol. 46/2, pp. 519 – 526, 1997.

[3] Leppert, T., *Skrawanie na sucho i z minimalnym chłodzeniem i smarowaniem ekologiczną alternatywą w obróbce skrawaniem,* Ekologia i technika nr 6, s. 229-236, 2006.

[4] Leppert, T., *Ekologiczne aspekty obróbki wiórowej,* Ekologia i technika nr3, pp. 87-91, 1998.

[5] Leppert, T., *Badania wpływu chłodzenia i smarowania na siły skrawania podczas toczenia,* (II Szkoła obróbki skrawaniem), s. 368-376, 2008.

[6] Leppert, T., *The influence of cooling and lubrication on surface layer properties and cutting process in turning,* Advances in manufacturing science and technology vol. 31, No. 1, pp. 35-47, 2007.

[7] Leppert, T., *Wpływ chłodzenia i smarowania na wybrane cechy struktury geometrycznej powierzchni po toczeniu stali odpornej na korozję 00H17N14M2,* I Szkoła obróbki skrawaniem, s. 244-253, 2007.

[8] Leppert, T., Peng R.L., *Surface residual stresses in dry turning of 0,45% C steel,* ICRS, Colorado, USA, 2008 artykuł w druku.

[9] Oczoś, K., *Rozwój innowacyjnych technologii ubytkowego kształtowania materiałów. Cz. I Obróbka skrawaniem,* Mechanik 8-9, s. 537-550,2002.

[10] Sokovic, M., Mijanovic, K., *Ecological aspects of the cutting fluids and its influence on quantifiable parameters of the cutting processes,* Journal of Materials Processing Technology 109, pp. 181-189, 2001.

[11] Wienert ,K., Inasaki, I., Sutherland, J.W., Wakabayashi, T., *Dry machining and minimum quantity lubrication,* CIRP vol. 53 (2), pp. 511-537, 2004.

DECARBURISATION OF FERRITE LATHS DURING BAINITE REACTION IN ADI

Zdzisław Ławrynowicz *, Stanisław Dymski

University of Technology and Life Sciences in Bydgoszcz
Department of Materials Science and Engineering
Mechanical Engineering Faculty
Av. Kaliskiego 7, 85-796 Bydgoszcz, Poland
* *E-mail address: lawry@utp.edu.pl*

Abstract

The paper presents an investigation of the time required for the diffusion of carbon out of supersaturated laths of ferrite into the retained austenite. Experimental measurements of volume fraction of bainitic ferrite and volume of the untransformed austenite indicate that there is a necessity of carbides precipitation from austenite. A consequence of the precipitation of cementite from austenite during austempering is that the growth of bainitic ferrite can continue to a larger extent and that the resulting microstructure is not an ausferrite, but is a mixture of bainitic ferrite, retained austenite and carbides. The carbon concentration in retained austenite demonstrates that at the end of bainite reaction the microstructure must consist of not only ausferrite but additionally precipitated carbides.

Key words: *c*arbon diffusion, decarburisation, bainite, ductile iron ADI

1. Introduction

The development of austempered ductile iron (ADI) is a major achievement in cast iron technology. The starting material for the development of ADI is the high quality ductile or nodular cast iron. It is then subjected to an isothermal heat treatment process known as "austempering". The attractive properties of ADI are related to its unique microstructure that consists of ferrite and high carbon austenite. Because of this microstructure, the product of austempering reaction in ductile iron is often referred to as "ausferrite" rather than bainite [1,2].

Ausferrite consists of ferrite and high carbon, stabilised austenite. If ADI is kept for long time periods, the high carbon austenite will eventually undergo transformation into bainite, the two phase ferrite and carbide ($\alpha + Fe_3C$).

During isothermal transformation, the excess carbon in the bainite partitions into the residual austenite, forcing the next plate to grow from carbon enriched austenite. The process finally ceases as the austenite carbon content reaches $T_0{}^*$ value, leading to the so-called 'incomplete reaction

---

* The T_0 temperature can be defined [3] such that stress free austenite and ferrite of the same composition (with respect to both the interstitial and the substitutional alloying elements) are in metastable equilibrium. Thus any displacive transformation involving a full supersaturation of carbon (i.e. bainitic ferrite would then inherit the carbon content of

phenomenon' [4]. This also explains why the degree of transformation to bainite is zero at the bainite start temperature (B_S) and increases with undercooling below B_S.

The purpose of the present paper is to demonstrate how a thermodynamic method can be used for solving a problem of the mechanism of bainite reaction in ADI and determination of the carbon concentration in the retained austenite. This should in principle enable to examine the partitioning of carbon from supersaturated ferrite laths into adjacent austenite and the carbon content in retained austenite using analytical method.

2. Material and methods

The chemical composition of the experimental ductile iron is listed in Table 1. The concentration of alloying elements in the matrix is obtained from the chemical analysis. Ductile iron blocks were produced in a commercial foundry furnace. The melt was poured into a standard Y block sand molds (ASTM A-395), which ensured sound castings. Specimens austenitised at $T_\gamma = 950^{\circ}$C for 60 minutes were rapidly transferred to a salt bath at austempering temperatures 250, 300, 350 and 400°C, held for 15, 30, 60, 120 and 240 minutes, and then water-quenched to room temperature. The microstructure of the as-cast material matrix contains 40% ferrite and 60% pearlite, however graphite nodules in material is 11.5%.

After heat treatment, the samples were prepared for metallographic analysis. The samples were etched using 2% nital. Optical micrographs were taken with a Nikon camera attached to a light microscope.

Tab. 1. Chemical composition of ductile cast iron ADI, wt-%

C	Si	Mn	P	S	Mg	Cr	Ni	Mo
3.21	2.57	0.28	0.06	0.01	0.024	0.036	0.098	0.015

The *X*-ray investigations were performed on the specimens heat treated after a specific time of the isothermal bainite reaction at the given temperature. The total volume fraction of the retained austenite was measured from the integral intensity of the $(111)_\gamma$ and $(011)_\alpha$ peaks. The presence of high silicon content in ADI retards the formation of cementite in ferrite and austenite. The carbon concentration was calculated from measured lattice parameter of the retained austenite. The *2θ* values for austenite peaks were used to calculate the *d* spacing with Bragg's law and then the lattice parameters. The lattice parameter of austenite (a_γ) is related to the known relationship between the parameter and the carbon concentration [5]:

$$a_\gamma \text{ (nm)} = 0.3573 + 0.0033 \, x_\gamma \tag{1}$$

where x_γ is the carbon concentration in austenite, in weight %.

The matrix carbon concentration, x_γ^m, of the ductile iron was also determined experimentally with Dron 1.5 diffractometer using *Co K_α* radiation on specimens austenitised at 950 ^{0}C for 60 minutes and quenched to ambient temperature. It was found that after quenching the calculated carbon content in matrix is $x_\gamma^m = 1.044\%$C and measured carbon content is $x_\gamma^m = 1.05\%$C, thus, the measured values were taken for further calculation.

the parent austenite) can occur only below the appropriate T_0 temperature. Strain energy would have effect of shifting curve to lower carbon concentration, T_0' curve [4].

3. Method of calculation of the decarburisation of supersaturated bainitic ferrite laths

The time t_d needed to decarburise the ferrite is intuitively expected to be at least comparable to that required for a lath to complete its growth. If t_d is small relative to the time required to relieve the carbon supersaturation by the precipitation of carbides within the ferrite, then upper bainite is obtained, otherwise lower bainite forms [4, 6].

Kinsman and Aaronson [7] first considered the kinetics of the partitioning of carbon from bainitic ferrite of the same composition as the parent phase. For a plate of thickness w_α the flux of carbon is defined along with a coordinate z normal to the α/γ interface, with origin at the interface and z being positive in the austenite (Fig. 1).

The method used to calculate the time of decarburising of bainitic ferrite laths is based on the hypothesis that transformation to bainite can only occur in regions of austenite where $x_\gamma \leq x_{T_0}$, where x_γ is the carbon concentration in austenite and x_{T_0} is the carbon concentration corresponding to the T_0 curve. As a lath of bainitic ferrite forms it partitions its excess carbon into the retained austenite. This creates a carbon diffusion field around the lath. Another parallel lath (of the same sheaf) which forms subsequently can only approach the original lath to a point where $x_\gamma \leq x_{T_0}$. The method assumes that the interval between lath formations is larger than the time required to decarburise each lath.
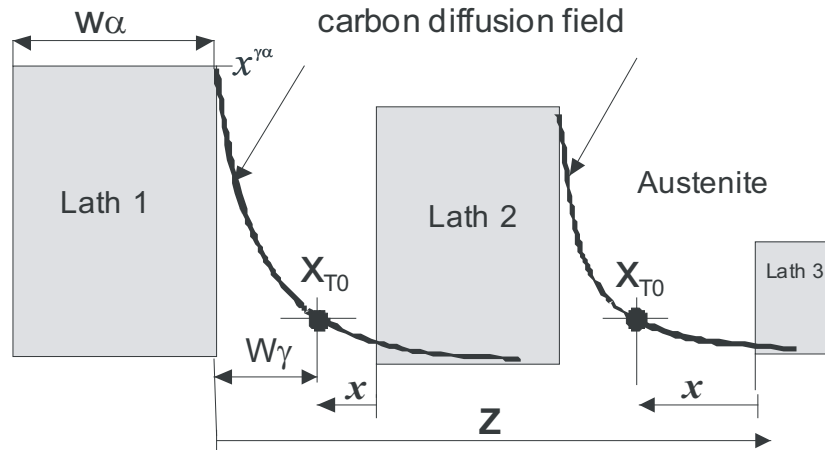

Fig. 1. Schematic diagram of method used in estimating the time of decarburising the bainitic ferrite laths. Lath 1 forms first and lath 2 and 3 and next is allowed to approach it to point where $x_\gamma \leq x_{T_0}$ (distance of this point from lath 1 is denoted w_γ). This is in fact the thickness of the retained austenite film. The mean thickness of the retained austenite films is almost tenfold thinner (0.01-0.02 μm) than the average thickness of the bainitic ferrite laths ($\sim 0.2 \mu m$).

The average carbon diffusion distances also depend on the mean spacing between the graphite nodules. Figure 2 shows a photomicrograph which contains graphite nodules with diverse distance between them, changing from about 150 to 50 μm (marked z_1 and z_2 in Fig. 2). Thus, the average distance among nodules in the examined ADI is assumed about 100 μm.

The problem is the calculation of the sum of the decarburisation times of all bainite laths existing on the coordinate connecting the nearest graphite nodules (Fig. 2).

The time needed to decarburise the ferrite matrix between the adjacent nodules of graphite t_{dz}:

$$t_{dz} = \sum_i t_{di} \qquad (2)$$

where t_{di} is the time required to decarburise individual supersaturated bainitic ferrite lath of specific thickness $w_{\alpha i}$.
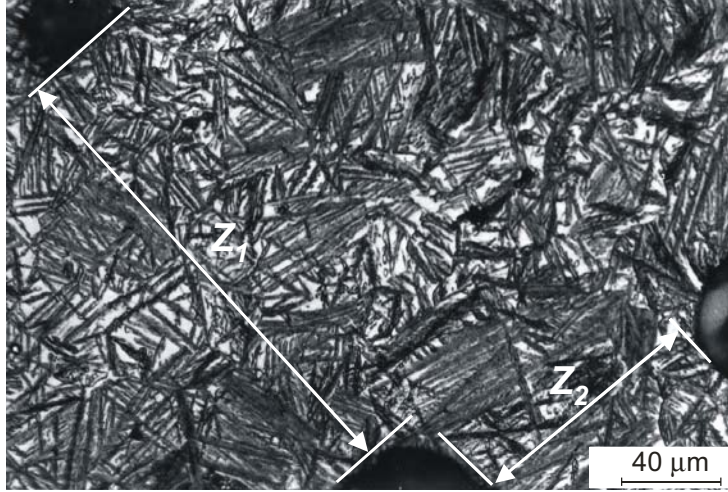

Fig. 2. Microstructure of ADI austenitised at 950 °C and austempered at 350 °C for 240 min. Etched with 2% nital

Because of the inhomogeneous distribution of carbon and other solutes in the matrix after transformation to bainite the retained austenite is enriched to a greater extent in the immediate vicinity to bainite platelets or in the region trapped between the platelets and in the eutectic cell boundary while other region contains relatively poor carbon [5, 6, 8]. The above effect can be exaggerated in ADI, since cast iron is usually extremely segregated. Martensite is usually found to be in the cell boundary which solidified last [9, 10, 11]. It indicates that the austenite in cell boundary is less enriched with carbon, and therefore is thermally unstable. From the mass balance for carbon it follows that [8]:

$$(0.5w_\alpha)(\bar{x} - x^{\alpha\gamma}) = \int_{z=0}^{\infty} [x_\gamma\{z, t_d\} - \bar{x}]dz \qquad (3)$$

where $\bar{x}$ is the average mole fraction of carbon in the alloy and $x^{\alpha\gamma}$ and $x^{\gamma\alpha}$ are the paraequilibrium carbon concentration in ferrite and austenite respectively. Since the diffusion rate of carbon in austenite is slower than in ferrite, the rate of decarburisation will be determined by the diffusivity in the austenite and the concentration of carbon in austenite at the interface remains constant for times $0 < t < t_d$ after which it steadily decreases as the austenite becomes homogeneous in composition. The equation (3) corrects an error in the original treatment, the error had the effect of allowing $t_d \to 0$ as the upper integration limit $\to \infty$. The function x_γ is given by [8]:

$$x_\gamma = \bar{x} + (x^{\gamma\alpha} - \bar{x})erfc\{z / 2(Dt_d)^{0.5}\} \qquad (4)$$

This assumes that for $t < t_d$, the concentration of carbon in the austenite at the interface is given by $x^{\gamma\alpha}$.

The diffusion coefficient of carbon in austenite $D\{x\}$, is very sensitive to the carbon concentration and this has to be taken into account in treating the large concentration gradients that develop in the austenite. It is clearly necessary to know $D\{x\}$ at least over a range $\bar{x} \rightarrow x^{\gamma\alpha}$, although experimental determinations of $D\{x\}$ do not extent beyond $x = 0.06$. The value of D was calculated as discussed in Ref. [12, 13]. The good approximation of the dependent diffusivity of carbon in austenite can be a weighted average diffusivity $\overline{D}$ [14]. Taking into account carbon concentration gradients, it has been demonstrated that for most purposes a weighted average diffusivity $\overline{D}$ can adequately represent the effective diffusivity of carbon [12-15]. Weighted average diffusivity $\overline{D}$ is calculated by considering the carbon concentration profile in front of the moving ferrite interface as given by the following equation [12]:

$$\overline{D} = \int_{\bar{x}}^{x^{\gamma\alpha}} \frac{D dx}{(x^{\gamma\alpha} - \bar{x})} \tag{5}$$

The calculated diffusion coefficients of carbon in austenite are listed in Table 2.

Tab. 2. The calculated diffusion coefficients of carbon in austenite D{x} and a weighted average diffusivity $\overline{D}$ after austenitisation at 950 °C and austempering at 400, 350, 300 and 250 °C.

Diffusion coefficients	Austempering temperature, °C			
	250	300	350	400
D [m²/s]	0.2544 x 10⁻¹⁸	0.4328 x 10⁻¹⁷	0.4688 x 10⁻¹⁶	0.3574 x 10⁻¹⁵
$\overline{D}$ [m²/s]	*	*	0.5013 x 10⁻¹⁵	0.1672 x 10⁻¹⁴

* Diffusion calculation outside of permitted range. Siller-McLellan model fails at high carbon concentrations evaluate $\overline{D}$.

On carrying the integration, the time required to decarburise a supersaturated bainitic ferrite lath of thickness w_α is given by [8]:

$$t_d = \frac{w_\alpha^2 \pi (\bar{x} - x^{\alpha\gamma})^2}{16 \overline{D} (x^{\gamma\alpha} - \bar{x})} \tag{6}$$

where: $\bar{x}$ is the average carbon concentration in the alloy, $x^{\alpha\gamma}$ and $x^{\gamma\alpha}$ are the carbon concentrations in ferrite and austenite respectively, when the two phases are in paraequilibrium.

4. The calculation of decarburisation times

For the investigated ductile cast iron ADI, our calculations show that t_d increases sharply as the thickness of the ferrite laths increases, see Table 3.

Tab. 3. Decarburisation times (t_d) in seconds of distance of 50 μm, consisted of laths with thickness: 0.1 μm; 0.2 μm; 0.5 μm; 1.0 μm; 10 μm; 50 μm.

Ti, °C	Decarburisation times (t_d) in seconds of distance of 50 μm					
	50 μm	5×10 μm	50×1 μm	100×0.5 μm	250×0.2 μm	500×0.1 μm
400	110600	22125	2212	1128	451	225
350	234500	46905	4690	2361	950	470

The calculated times of partitioning are shown in Figure 3 for thickness of bainitic ferrite phase equal 50μm but consisted of laths with different wideness: 0.1μm; 0.2μm; 0.5μm; 1.0μm; 10μm and 50μm.

The decarburisation time t_d as a function of α phase width increases with decreasing austempering temperature, because the diffusion coefficient of carbon also decreases with temperature (Table 2). The decarburisation time also increases as the thickness of the ferrite laths increases (Fig.3).

Furthermore, it is generally observed (Fig. 2) that the width of ferrite laths is highly diverse [6]. This reflect the possibility that cementite can precipitate in thicker bainite laths (when t_d is a long period of time) and in thinner laths has not during isothermal transformation. It is also consistent with the fact that upper and lower bainite often form at the same temperature in a given steel [4, 6, 16, 17, 18].
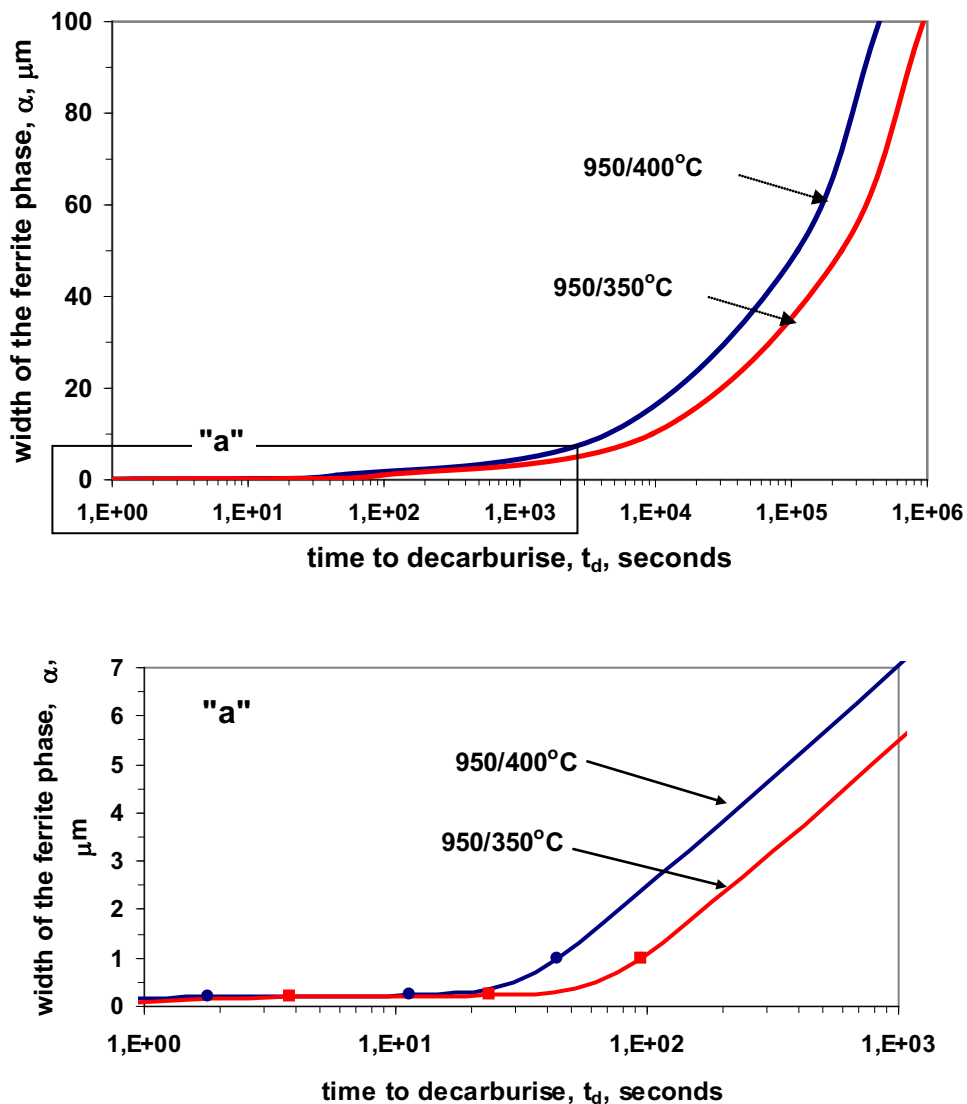

Fig. 3. The calculated times for decarburisation of ferrite phase with width of 50 μm, consisted of laths with thickness: 0.1 μm; 0.2 μm; 0.5 μm; 1.0 μm; 10 μm and 50 μm after austenitisation at 950°C. Enlarged of an area in the bottom part in Fig. 3 corresponds to the marked area "a"

5. Conclusions

The paper presents an investigation of the partitioning of carbon from supersaturated ferrite laths into adjacent austenite in ADI matrix using an analytical method. The following conclusions have been reached:

1. The extent of transformation to bainite in ductile iron, as in steels, decreases when increasing the isothermal transformation temperature towards the bainite start temperature (B_S). This is because the austenite can only transform to bainite if its carbon concentration is less than a value x_{T_o} given by the T_0 curve.

2. The bainite transformation in cast iron is essentially identical to that in steel. In steel, it has been demonstrated that the carbon concentration of the residual austenite reaches the critical value represented by the T_0 curve will render the displacive bainite reaction to cease. Therefore the carbon concentration of austenite can be estimated by the thermodynamics principles described here. Since cast iron is extremely segregated, x_γ determined by X-ray diffraction is richer than that corresponds to the T_0 curve in ADI.

3. The carbon concentration of the residual austenite increases during bainitic transformation as a consequence of the increasing volume fraction of bainitic ferrite.

4. Analytical calculations of the time required for the diffusion of carbon out of supersaturated laths of ferrite into the retained austenite indicate that there is a necessity of carbides precipitation from ferrite.

5. A consequence of the precipitation of cementite from ferrite or/and austenite during austempering is that the growth of bainitic ferrite can continue to larger extent and that the resulting microstructure is not a pure ausferrite but is a mixture of bainitic ferrite, retained austenite and carbides.

References

[1] Chang, L. C., *Carbon content of austenite in austempered ductile iron,* pp. 35-38, Scripta Materialia 39 1998.

[2] Pietrowski, S., *Nodular cast iron of bainitic ferrite structure with austenite or bainitic structure,* pp. 253-273, Archives of Materials Science 18 1997.

[3] Christian, J.W., *Theory of transformations in metals and alloys,* p. 778, Oxford, Pergamon Press, 1965.

[4] Bhadeshia ,H.K.D.H., *Bainite in Steels,* pp. 1-458, Institute of Materials London 1992.

[5] Ławrynowicz, Z., Dymski, S., *Mechanism of bainite transformation in ductile iron ADI,* Archives of Foundry Engineering 6, pp. 171-176 2006.

[6] Ławrynowicz, Z., *Transition from upper to lower bainite in Fe-Cr-C steel,* Materials Science and Technology 20, pp. 1447-1454 2004.

[7] Kinsman, K. R., Aaronson, H.I., *The transformation and hardenability in steels,* Climax Molybdenum Company, Ann Arbor, MI, p.39, 1967.

[8] Bhadeshia, H.K.D.H., Christian, J.W., *Bainite in Steels,* Metallurgical Transactions 21A, pp. 767-797 1990.

[9] Guzik, S. E., *Austempered cast iron as a modern constructional material,* Inżynieria Materiałowa 6, pp. 677-680 2003).

[10] Ławrynowicz, Z., Dymski S., *Application of the mechanism of bainite transformation to modelling of processing window in ductile iron ADI,* Archives of Foundry Engineering 6, pp. 177-182 2006.

[11] Kutsov, A., at al., *Formation of bainite in ductile iron,* Materials Science and Engineering A273-275, pp. 480-484 1999.

[12] Bhadeshia, H.K.D.H., *Diffusion of carbon in austenite,* Metal Science 15, pp. 477-479 1981.

[13] Ławrynowicz, Z., *Criticism of selected methods for diffusivity estimation of carbon in austenite,* Zeszyty Naukowe ATR nr 216, Mechanika 43, pp. 283-287 1998.

[14] Siller, R.H., McLelan, R.B., *The Application of First Order Mixing Statistics to the Variation of the Diffusivity of Carbon in Austenite,* Metallurgical Transactions 1, pp. 985-988 1970.

[15] Ławrynowicz, Z., *Bainitic transformation: estimation of carbon diffusivity in austenite on the basis of measured austenite film thickness,* Zeszyty Naukowe ATR nr 216, Mechanika 43, pp. 289-297 1998.

[16] Takahashi, M., Bhadeshia, H.K.D.H., *A Model for the Microstructure of Some Advanced Bainitic   Steels,* Materials Transaction, JIM, 32, pp. 689-696 1991.

[17] Ławrynowicz, Z.,*Carbon partitioning during bainite transformations in low alloy steels,* Materials Science and Technollogy 18, pp. 1322-1324 2002.

[18] Ławrynowicz, Z., Barbacki, A., Analiza mechanizmu izotermicznej przemiany bainitycznej w stali Cr-Mn-Si. Archiwum Nauki o Materiałach 17, pp. 127-147 1996.

RELATIONS BETWEEN BMD DENSITY AND VOLUMETRIC AND FRACTAL INDICATORS OF HUMAN TRABECULAR BONE

Adam Mazurkiewicz, Tomasz Topoliński

University of Technology and Life Sciences
Kaliskiego 7 Av., 85-789 Bydgoszcz, Poland
Tel.: +48 52 3408446
e-mail: adam.mazurkiewicz@utp.edu.pl

Abstract

BMD density, fractal dimension and volume tissue in volume of sample can be used to estimate the strength of trabecular bone. In the paper, presented is the comparison relations between the indicators for two groups of human trabecular bones – osteoporotic and coxarthrotic. Dependencies between the indicators were described with the determination coefficient R^2. Achieved values of the coefficient are contained in range 0,2÷0,56.

Keywords: *trabecular bone, BMD, fractal dimension*

1. Introduction

For the estimation of bone quality and risk of fracture, densitometric techniques are widely used, such as quantitative computed tomography (QCT) or dual energy x-ray absorptiometry (DEXA). The result of the measurement is the value of density of selected bone parts. The limitation of this methods is a lack of possibilities to explain individual differences in trabecular bone architecture [1-2]. Obtained density is a mean value which isn't allowed for local differences in subvolumes of trabecular bone. For example, one of the results of DEXA measurement is the value of BMD density.

Fractal dimension (Df) is also one of indicators used to describe a complex porous structure in medicine, e.g. trabecular bone architecture [3-5]. The dimension can be calculated for the structure of all samples of trabeculaes or subvolumes. The other indicator used to describe trabecular bones is the volume of tissue (V). The volume can be also calculated for all sample or subvolumes.

BDM, Df and V can be used to describe the strength of trabecular bone. The aim of this study is the estimation of relations between BMD density, fractal dimension and volume of tissue for trabecular bone.

2. Experimental methods

Material for the investigation were samples of human trabecular bone. Samples were collected from 21 osteoporotic (Ost) and 21 coxarthrotic (Cox) femoral heads gained in result of hip arthroplasty. Coxarthrosis is one of bone diseases. One of the results is hyperthrophy articular cartilage in volume and surface femoral head. Because authors didn't have possibilities to use as a reference group similar numbers of samples collected with bones without any bone diseases, they

assumed as reference group a set of coxarthrosis samples. Because coxarthrotic bones similarly as healthy bones are subject to fracutre very seldom, they assumed that mechanical strength of the bones is not less than that of bones without any bone diseaes [6].

The samples used for investigation have cylindrical shape with diameter of about 10 and height of 8,5mm. The manner of collecting samples is presented in Fig. 1.
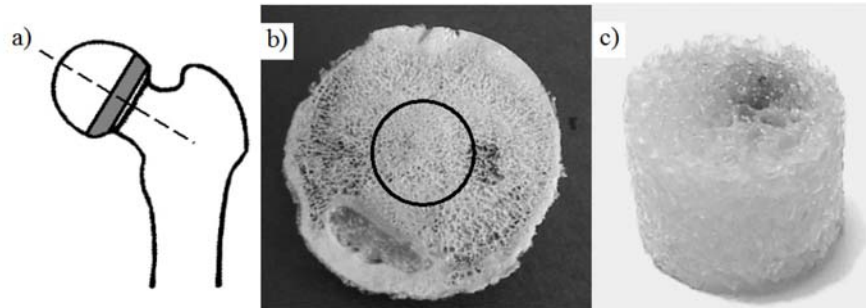

Fig. 1. Manner of collecting samples: cutting slice a), cutting sample b), sample c)

BMD density of samples was performed with scanner Lunar Expert, General Electric Company. Samples were also examined at microCT device (μCT80) with resolution of 36μm. In result of the investigation, sequential images slices perpendicular to the axis of the sample were obtained. On the basis of the images, geometrical models of samples were created. These were divided into subvolumes in shape of layer of height of about 36μm. The layers were created as following: images of two neighbouring slices were compared. When on the same coordinate in both image, colored pixels represented the bone, voxels of layer of bone between the images were created. The size of voxels was the same as of the pixels at images, i.e. 36μm.

The volume (V) of all layers for every sample was examined. On that basis, found were the mean (V_m), minimal (V_{min}) and maximal (V_{max}) volumes of layer for every sample.

For the same layers, the fractal dimension (Df) was calculated and then the mean (Df_m), minimal (Df_{min}), maximal (Df_{max}) value of this dimension for every sample was determined. For the purpose of defining the fractal dimension, the definition of 'box' dimension (Minikowski – Bouligand) was used.

Experimental results

In Tab. 1, presented are the values of detemination coefficient R^2 obtained for relations between BMD and mean, minimal and maximal volume of tissue for layers of sample. In Tab. 2, presented are the values of determination coefficient obtained for relations between BMD and mean, minimal and maximal fractal dimensions. In the tables, maximal values of R^2 are presented for the study of the description of power, logarithmic and numerical functions.

Tab. 1. Value of determination coefficient R^2 for the relationship of BMD with volume of tissue

Samples	Ref		V_m	V_{min}	V_{max}
		1	2	3	4
Ost	1	BMD	0,41	0,40	0,34
Cox	2	BMD	0,35	0,48	0,20

Tab. 2. Value of determination coefficient R^2 for the relationship of BMD with fractal dimension

Sample	Ref		Df_m	Df_{min}	Df_{max}
		1	3	4	5
Ost	1	BMD	0,42	0,37	0,34
Cox	2	BMD	0,44	0,56	0,23

Generally obtained values R^2 weren't to high and contained within the range (0,2÷0,56). In case of osteoporotic samples, better relations have been obtained for mean values V_m and Df_m. In case of coxarthrotic samples, better relations have been obtained for minimal values V_{min} and Df_{min}. Authors, on the basis of the analysis of topic literature, aren't able explain this fact. However, it indicates significant differences in the structure of both groups of samples.

The values R^2 pointed out that relations between BMD and V or Df aren't described with strong dependences. In result, for few samples of the same value of BMD we probably get different values of tissue volume and fractal dimension. It confirms the fact that the use of BMD can't find local differences in the structure of trabecular bone, thus finding places where risk of fracture is the greatest is impossible.

A further stage of the investigation will be mechanical uniaxial compression test of samples and finding description compression strength with the use of indicators. Obtained values R^2 point out that probably different exactitude of description of strength will be obtained using a different indicator.

Perhaps double combination of BMD and any indicator of trabecular architecture, e.g. fractal dimension or tissue volume, would probably get better results than the predicted strength of bone using only BMD density,V or Df .

Acknowledgements

References

[1] Bauer, J. S., Kohlmann, S., Eckstein, F., Mueller, D., Lochmüller, E. M., Link, T. M., *Structural analysis of trabecular bone of the proximal femur using multislice computed tomography: a comparison with dual X-ray absorptiometry for predicting biomechanical strength in vitro*, Calcif Tissue Int., Vol. 78 (2006), pp. 78-89.

[2] Lochmüller, E. M., Bürklein, D., Kuhn, V., Glaser, C., Müller, R., Glüer, C. C., Eckstein, F., *Mechanical strength of the thoracolumbar spine in the elderly: prediction from in situ dual-energy X-ray absorptiometry, quantitative computed tomography (QCT), upper and lower limb peripheral QCT, and quantitative ultrasound*, Bone, Vol. 31 (2002), pp. 77-84.

[3] Feltrin, G. P., Macchi, V., Saccavini, C., Tosi, E., Dus, C., Fassina, A., Parenti, A., De Caro R., *Fractal analysis of lumbar vertebral cancellous bone architecture*, Clin Anat., Vol. 14 (2001), pp. 414-417.

[4] Benhamou, C. L., Poupon, S., ,Lespessailles, E., Loiseau, S., Jennane, R., Siroux, V., Ohley, W., Pothuaud, L., *Fractal analysis of radiographic trabecular bone texture and bone mineral density: two complementary parameters related to osteoporotic fractures*, J Bone Miner Res., Vol. 16 (2001), pp. 697-704.

[5] Majumdar, S., Link, T. M., Millard, J., Lin, J. C., Augat, P., Newitt, D., Lane, N., Genant, H. K., *In vivo assessment of trabecular bone structure using fractal analysis of distal radius radiographs*, Med Phys., Vol. 27 (2000), pp. 2594-2599.

[6] Ostrowska, A., Mazurkiewicz, A., Będziński, R., Ścigała, K., *The Investigations of Mechanical and Histomorphometric Properties of Human Femur Cancellous Bone*, Biomaterials Engineering, vol. 47-53 (2005), pp. 78-80.

ENERGY CUMULATION UNDER CONSTANT – AMPLITUDE AND PROGRAMMED LOADINGS

Stanisław Mroziński

*University of Technology and Life Sciences in Bydgoszcz, Faculty of Mechanical
Engineering, Al. Prof. S. Kaliskiego 7, 85-789 Bydgoszcz,
tel.: 48 52 340-82-64, fax: 48 52 340-82-71, e-mail: mrozinski.stanislaw@utp.edu.pl*

Abstract

In the paper there were presented test results of energy cumulation of plastic strain ΔW_{pl} in the specimen made of PA7 alluminium alloy under constant - amplitude and programmed loadings. During the tests it was found that the courses of changes of ΔW_{pl} energy on the same strain levels both under constant- amplitude and programmed loading were similar. It was shown that value of $\Sigma \Delta W_{pl}$ energy cumulated in the material till the fatigue failure is not constans and decreases with the increase of fatigue life.

Keywords: cyclic properties, fatigue life

1. Introduction

The base of fatigue life calculation effectiveness of construction elements is the insensitiveness of the standard value used during calculations to the changes of cyclic properties. It has been accepted that an energy description of the fatigue is less sensitive to changes of cyclic properties than stress or strain description. Among energy criteria of the fatigue process description various approaches can be distinguished. In one of them plastic strain energy $\Sigma \Delta W_{pl}$ [1] cumulated in the complete fatigue trial is accepted as the standard value. $\Sigma \Delta W_{pl}$ energy is the sum of plastic strain energies ΔW_{pl} from individual variable loading cycles till failure. The measure of the plastic strain energy ΔW_{pl} in the single loading cycle is the hysteresis loop area.
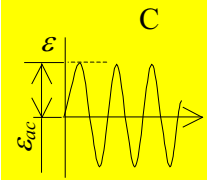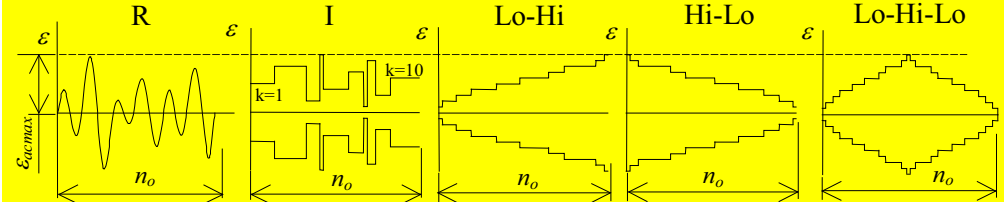
Available literature data concerning description of the course of energy cumulation mostly deal with constant - amplitude loadings or with simple (two step) programmed loadings. The course of operating loadings is most often very complex and is characterized by the variability of many of its parameters (amplitude, mean value, frequency, etc.). The research problem undertaken in this paper is the valuation of the influence of the kind and form of loading program and its parameters on the course of plastic strain energy cumulation during variable loading.

2. Tests description

Specimen for the tests were made of aluminium alloy PA7, which undergoes the strong hardening process during cyclic loading. Specimen were made according to the standard [2]. During the tests there were applied constant – amplitude (C), programmed (I) and random (R) loadings. In order to valuate the influence of the step sequence in the loading program on the course of energy cumulation there were applied diversified loading programs. Among them there

were following loadings: gradually increasing *Lo-Hi*, gradually decreasing *Hi-Lo* and gradually increasing and then decreasing *Lo-Hi-Lo*. Common characteristics of these programs were the same values of maximum strain in the program ε_{acmax}, coefficient of spectrum density ζ and block capacity n_0. Loading programs consisted of the oscillatory cycles (R=-1), and as the steering value the amplitude of total strain was accepted. The schemes of the loading programs and their parameters are presented in Table 1.

Table 1 Loading programs parameters

Constant-amplitude	Programmed loading				
ε_{ac}=0,35%; ε_{ac}=0,8% ε_{ac}=0,5%; ε_{ac}=1,0% ε_{ac}=0,65%	ζ=0,34, ζ=0,56, ζ=0,77, n_o=100, k=10 ε_{acmax}=0,35%; ε_{acmax}=0,5%; ε_{acmax}=0,8 %;				

3. Tests results and their analysis

3.1. ΔW_{pl} energy changes and its cumulation during constant-amplitude loading

ΔW_{pl} energy values for individual cycles of constant – amplitude loading were determined with the use of momentary values of the loading force and specimen strains which were registered during the test. Momentary σ stress values were calculated dividing momentary value of the loading force by the initial cross - section area of specimen measurement point. The scheme illustrating process of ΔW_{pl} energy calculations and relation being used was presented in Fig. 2.
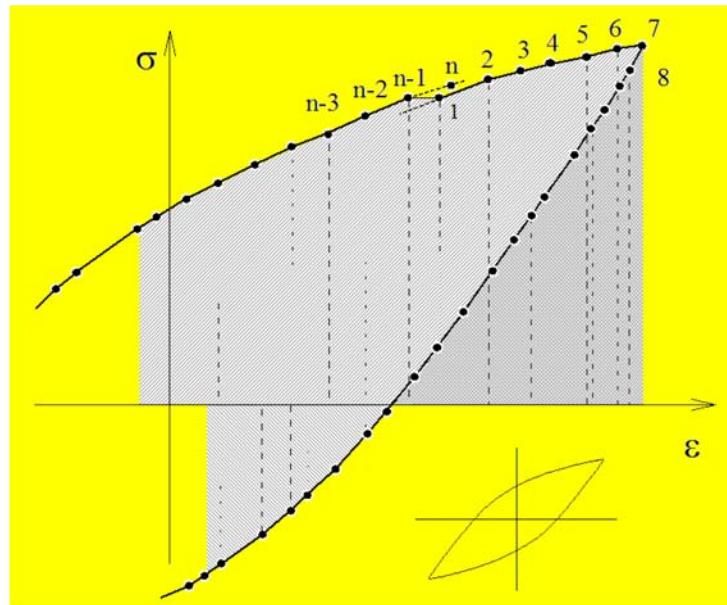

Fig. 2. Scheme for calculations of plastic strain energy ΔW_{pl}

By using the specimen momentary values of stress σ_i and strain ε_i, the energy ΔW_{pl} for individual loading cycle was calculated from the relation (1):

$$\Delta W_{pl} = [\sum_{i=1}^{n-1} \frac{1}{2}(\sigma_i + \sigma_{i+1})(\varepsilon_{i+1} - \varepsilon_i)] + (\sigma_n + \sigma_1)(\varepsilon_1 - \varepsilon_n) \qquad (1)$$

where: n – records number of momentary values of the force and strain taken during one loading cycle (n=200 points).

Cyclic hardening of the alloy, which appeared during constant – amplitude loading, was visible in ΔW_{pl} energy courses at five strain ε_{ac} levels. An example diagrams of ΔW_{pl} energy changes at these levels in double logarithmic coordinate system were shown in Fig. 3a.

a)   b)
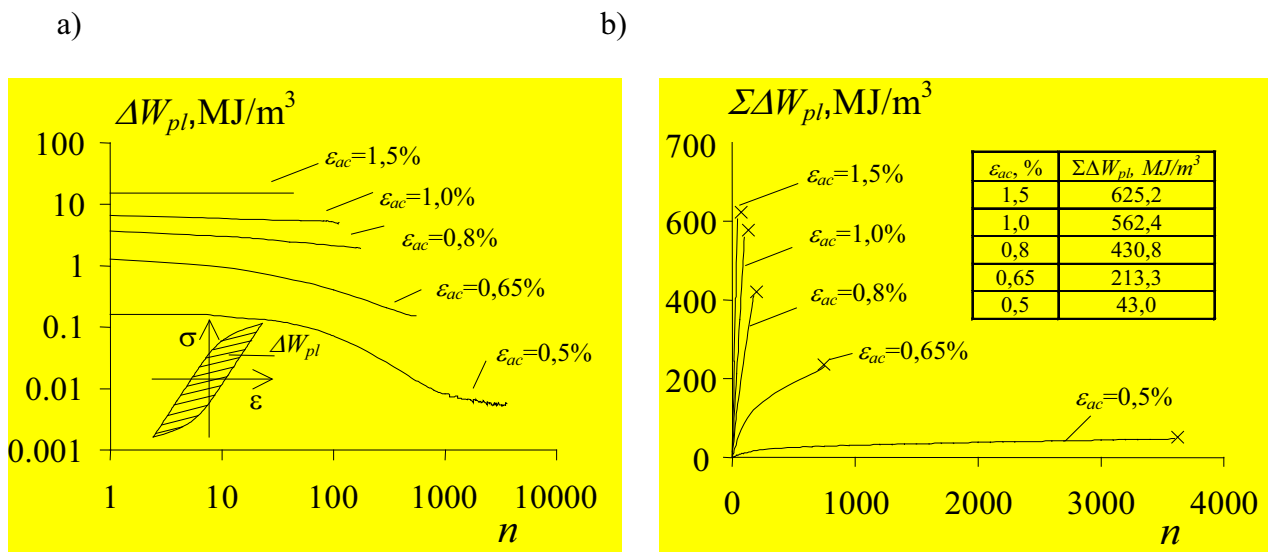
Fig. 3. ΔW_{pl} energy at five strain levels (a) and its cumulation (b)
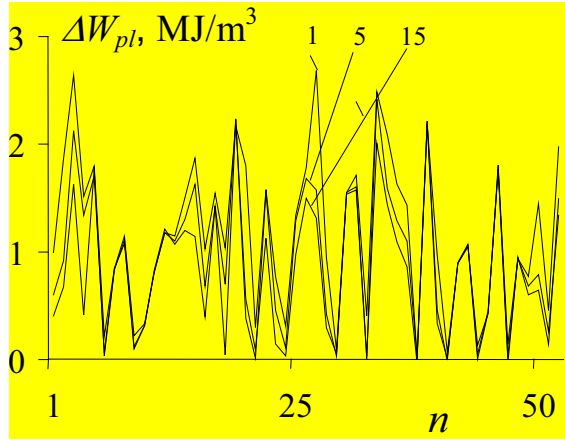
Basing on the diagrams of energy ΔW_{pl} it can be stated that magnitude of the changes of cyclic properties (degree of the material hardening) increases with the decreasing of strain level ε_{ac}. Hardening of PA7 alloy is also visible in the energy cumulation diagrams (Fig. 3b). For the highest strain ε_{ac} levels energy $\Sigma\Delta W_{pl}$ cumulated in the material increases proportionally with the number of loading cycles, at the lowest levels, however, cumulation diagrams are characterized by distinct nonlinearity. The highest value of energy $\Sigma\Delta W_{pl}$ cumulated until specimen failure under constant – amplitude loadings was obtained for the strain level ε_{ac}=1,5% and the lowest one for the strain level ε_{ac}=0,5 %.

3.2. Energy changes during irregular loadings

For every sequence of programmed and random loadings there was observed similar quality of the energy ΔW_{pl} courses in the block of program. In order to visualize them, in Fig. 4 there were shown example diagrams of energy ΔW_{pl} in blocks of random and programmed loading registered in various periods of life. In the figures there were marked the numbers of the block repetitions for which the diagram was made. To make diagrams obtained under random loadings more legible (Fig. 4a) they were limited to the half volume in the block of the loading program ($0,5n_o$=50 cycles).
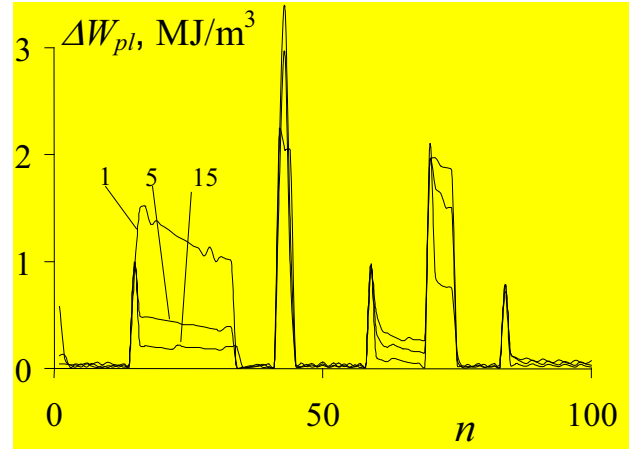
a)   b)

Fig. 4. Energy ΔW$_{pl}$ in the block of loading program of various form a) „R", b) „I", (ε$_{acmax}$=0,8 %, ζ=0,56)

Basing on the analysis of ΔW_{pl} energy diagrams shown in Fig. 4 it can be stated that under random and programmed loading, similarly like during constant- amplitude loading, tested material is characterized by changes of cyclic properties and by absence of distinct period of stabilization. It is proved by diversified location of ΔW_{pl} energy diagrams for individual cycles (random loading) and steps of loading programs (programmed loading) which were realized in various periods of life. Succeeding ΔW_{pl} energy diagrams in the block are located below the diagrams obtained for the blocks of loading realized earlier. Such a location is the proof of cyclic hardening of the material which is also observed during constant – amplitude loading (Fig. 3a). In the paper there were analysed the courses of ΔW_{pl} energy changes for the cycles from individual steps of loading programs. In Fig. 5 there were shown the examples of energy changes on one step (ε$_{ac}$=0,65%) in succeeding repetitions of *Lo-Hi* and *I* programs. In diagrams there were marked the numbers of the block repetitions.
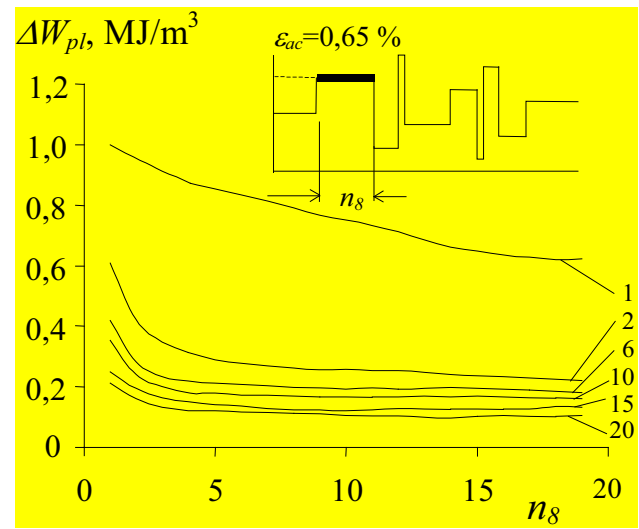
a)   b)
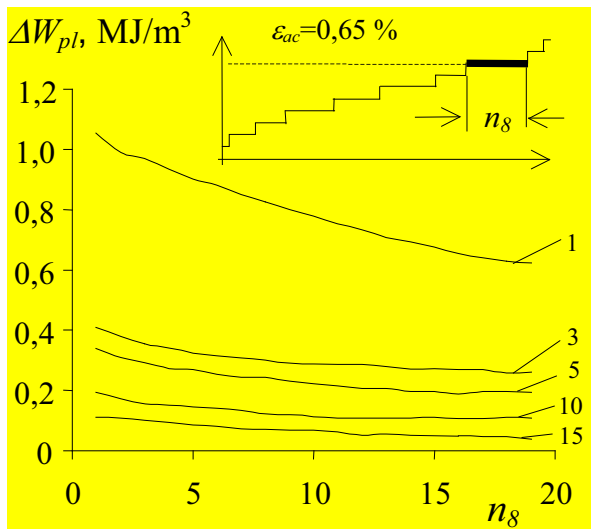
Fig. 5. Changes of ΔW$_{pl}$ on the step with amplitude ε$_{ac}$=0,65 % carried out under loading with various sequence of steps in the block: a) Lo-Hi, b) I

Comparative analysis of ΔW_{pl} energy diagrams on the steps with the same strain amplitude realized for various program sequences allows to conclude that all loading programs result in the similar course of this energy. Its characteristic feature are lower and lower energy levels on the steps in the succeeding repetitions of the program block. Moreover the energy courses on the same levels of strain, which was realized under programmed loading, are qualitatively and quantitatively very similar to the value of ΔW_{pl} energy obtained under constant-amplitude loading. This was presented in Fig. 6 in the form of example ΔW_{pl} energy diagrams in the function of relative life n/N for constant-amplitude loading and selected sequences of random and programmed loading (ε_{ac}=0,65 %, ζ=0,56).
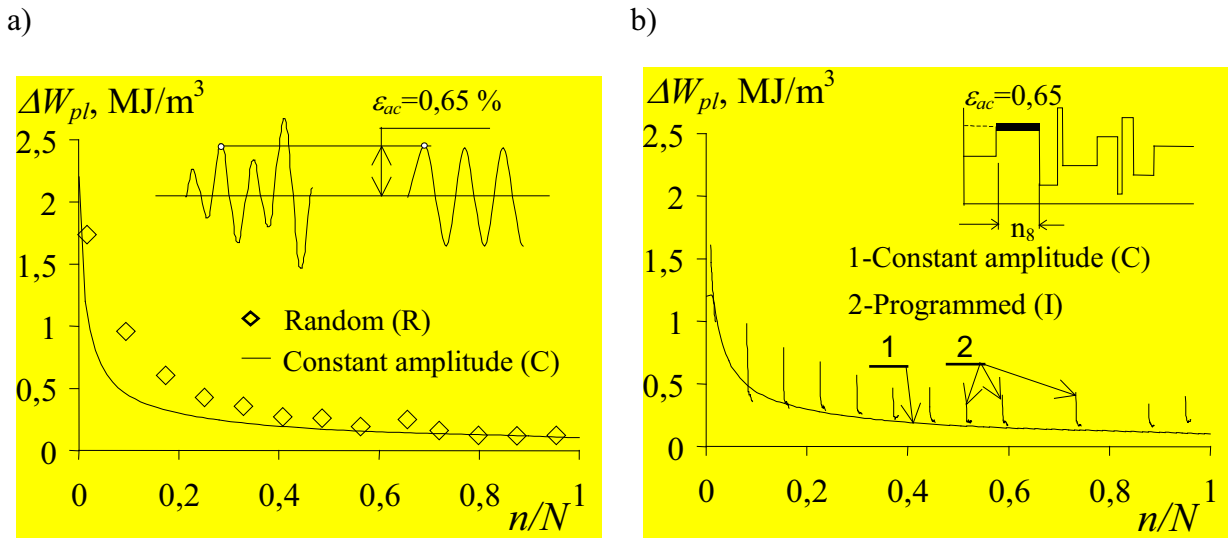

Fig. 6. Energy ΔW_{pl} under diversified loading with ε_{ac}=0,65 %: a) random and constant-amplitude, b) programmed and constant-amplitude

Basing on the mutual position of ΔW_{pl} energy diagrams in the succeeding repetitions of program block it can be concluded that despite the stabilization disturbances resulting from level changes of strain amplitude, material seems to "remember" the energy course which is typical for a given strain level. The tendency of these changes is clearly visible in ΔW_{pl} energy diagrams obtained under loadings with diversified steps sequence. Energy values obtained in the terminal cycles of the individual steps of programmed loading tend toward the level obtained during constant –amplitude loading.

In order to formulate some kind of genaral conclusions there was carried out the comparative analysis of ΔW_{pl} energy values for every strain level and every form of loading program. The comparison of ΔW_{pl} energy was carried out for the same periods of relative life n/N. In the case of programmed loadings with diversified sequence of steps (I, Lo-Hi, Hi-Lo, Lo-Hi-Lo) in the comparative analysis there were used ΔW_{pl} energy values defined for the last cycle of individual program steps. On every strain level there were obtained results supporting earlier observations which concerned the absence of the visible influence of the program form on the course of energy changes on the analysed strain level. An example results presenting these observations were shown in Fig. 7 on the diagrams of energy changes for two strain levels (ε_{ac}=0,65% and ε_{ac}=0,8%). To make these diagrams more legible there were ploted only the results obtained during one of the three trials realized for each sequence of loading program and the course of ΔW_{pl} energy obtained under constant-amplitude loading.
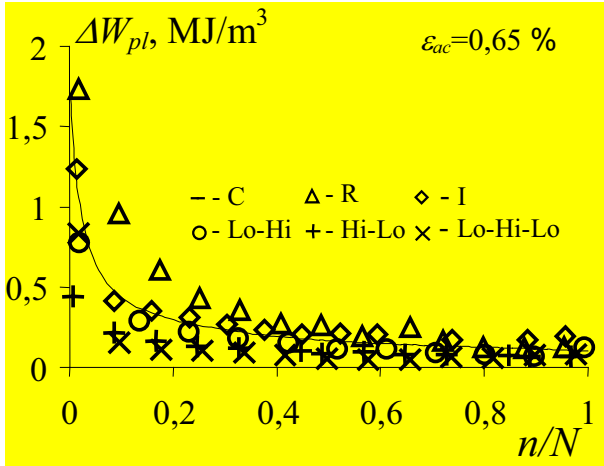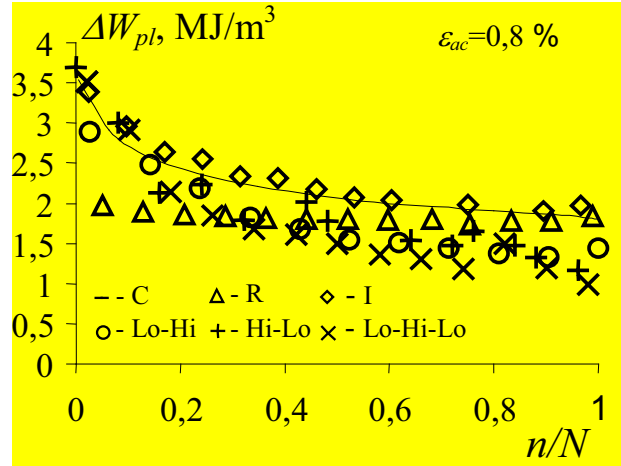
Fig. 7. Energy ΔW_{pl} under constant-amplitude and programmed loadings on two strain levels: a) $\varepsilon_{ac}=0,65$ %, b) $\varepsilon_{ac}=0,8$ %

Comparative analysis of ΔW_{pl} energy diagrams obtained for two strain levels realized in the programs of diversified form allows to conclude that they are locating themselves very closely to the diagrams presenting the courses of ΔW_{pl} energy changes obtained under constant-amplitude loading.

3.3. ENERGY CUMULATION UNDER IRREGULAR LOADING

As it was expected, steps sequence in the loading program influences the course of $\Delta W_{pl(i)}$ energy cumulation in one block of the program. In order to present the above observation, in Fig. 8a there were shown an example courses of ΔW_{pl} energy cumulation in the first block of random and programmed loading with diversified sequence of the steps in the program.
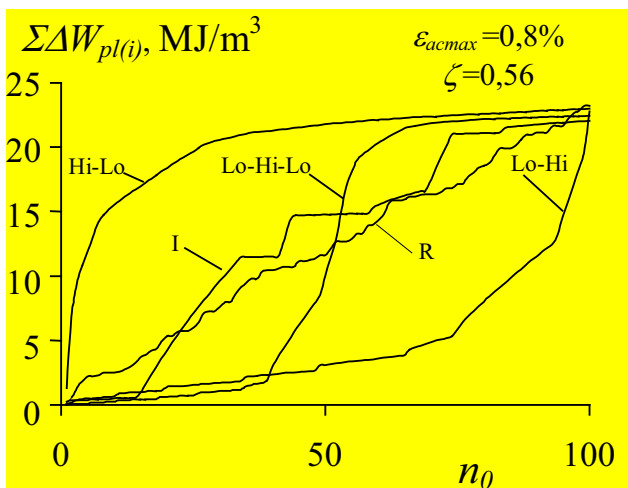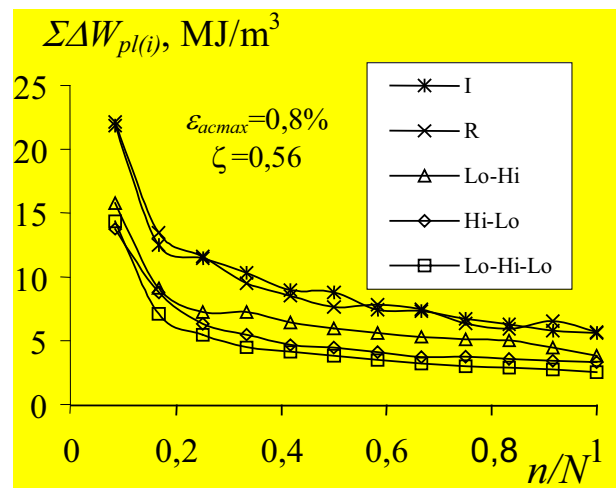

Fig. 8. The course of energy cumulation $\Sigma\Delta W_{pl(1)}$ in one block of the program with various sequence of steps (a), energy $\Sigma\Delta W_{pl(i)}$ in blocks from various periods of life (b)

82

Basing on the mutual position of energy cumulation diagrams in the first block, it can be concluded that the least differences are visible in the case of diagrams obtained during realization of the loading program with random succession of cycles (R) and irregular succession of steps (I). Despite the diversified course of $\Delta W_{pl(i)}$ energy cumulation in one block, the value of the energy cumulated $\Sigma\Delta W_{pl(i)}$ in the first and in succeeding blocks was very similar. In Fig. 8b there were shown an example calculation results of $\Sigma\Delta W_{pl(i)}$ energy cumulated in the blocks of loading realized in various periods of life. Dependence of the level of $\Sigma\Delta W_{pl(k)}$ energy cumulated in one block of loading from the period of life is the confirmation of ΔW_{pl} energy changes observed in Fig. 4 for individual cycles and steps of programmed loading.

Comparative analysis of $\Sigma\Delta W_{pl}$ energy cumulated in the entire fatigue trial for various sequences of loading program showed that its value is not influenced by the sequence of the steps in the loading program, too. In Fig. 9 there was shown schematically the course of energy cumulation during fatigue test for diversified step sequences of the loading program.

Despite the diversified course of energy cumulation in the block of loading program the value of energy cumulated in the entire fatigue test for various step sequences in the block is always very similar. The level of energy cumulated in the entire fatigue test is influenced significantly by the loading program parameters, i.e. ε_{acmax} and ζ (Fig. 9b). The highest values of $\Sigma\Delta W_{pl}$ energy cumulated until fatigue failure were obtained for the highest levels of maximal strain and coefficient of spectrum density ζ.

a)   b)

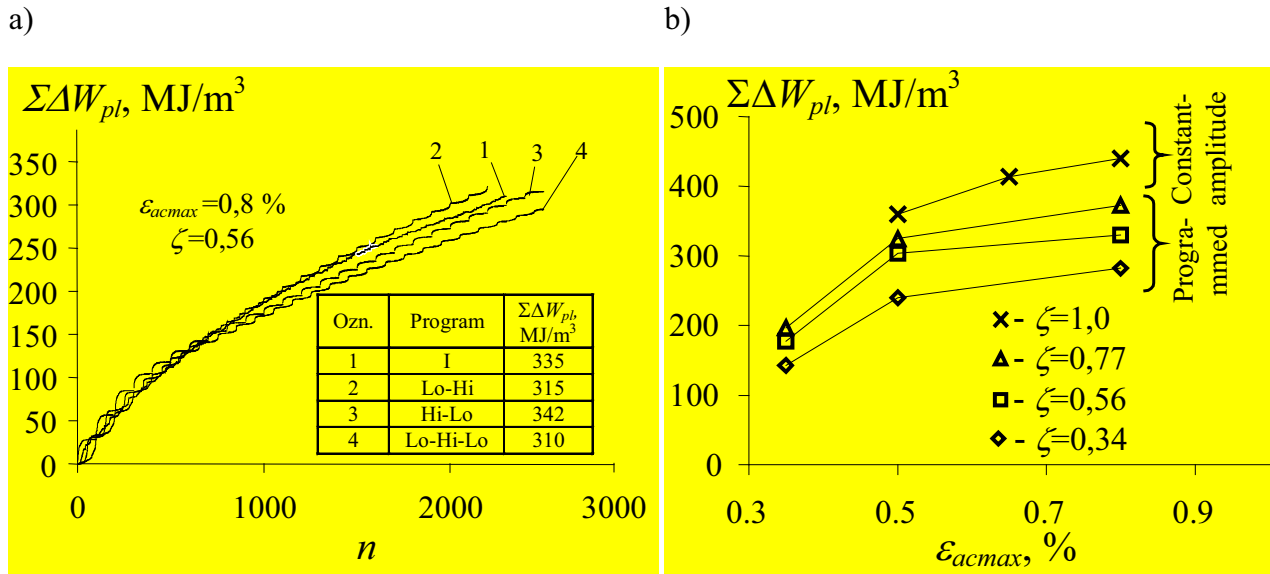| Ozn.	Program	$\Sigma\Delta W_{pl}$, MJ/m³
1	I	335
2	Lo-Hi	315
3	Hi-Lo	342
4	Lo-Hi-Lo	310

Fig. 9. The course of energy cumulation ΔW_{pl} under diversified loadings (a) and energy cumulated in relation to ε_{acmax} and ζ (b)

4. Summary

Plastic strain energy ΔW_{pl}, just like strain or stress, is sensitive to the changes of cyclic properties. The courses of ΔW_{pl} energy changes on the individual strain levels are very little influenced by the form and parameters of variable loading program. The quality of these courses, independently from the form and parameters of the loading program, is very similar, which is the proof of the cyclic hardening of the material. The volume of PA7 alloy hardening depends as in the case of the course of energy changes on the strain level.

For every form and sequence of loading program there was observed similar course of energy cumulation ΔW_{pl}. The characteristic feature of the tests results under random and programmed loading and also under constant- amplitude loading is that the energy cumulated in the material

$\Sigma \Delta W_{pl}$ until the fatigue failure is not constant value. Its level depend on the parameters of loading program (ε_{ac}, ε_{acmax}, ζ) and it decreases with the increase of fatigue life. Obtained test results do not support in this respect the energy criterion of fatigue failure appearance, in which it is accepted that failure is determined by the critical value of energy cumulated of plastic strain [3].

The use of plastic strain energy ΔW_{pl} as the criterion measure during fatigue life calculations of the construction elements made of cyclically unstable materials may lead to the discrepancy of calculations and tests results.

References

1. Ellyin F, Kujawski D.: Plastic strain energy in fatigue failure. J. Pressure Vessel Technology. Trans. ASME, Vol. 106, 1984, pp.342-347.
2. PN-84/H-04334 Badania niskocyklowego zmęczenia metali.
3. Feltner C.E., Morrow J.D., 1961. Microplastic strain hysteresis energy as a criterion for fatigue fracture. Journal Basic Engineering ASSME, March, 15-22.

POWER CONSUMPTION INVESTIGATION IN DISC REFINER AT WASTE PAPER TREATMENT

Adam Mroziński

Department of Special Machines and Environment Protection
Faculty of Mechanical Engineering, University of Technology and Life Science in Bydgoszcz
adammroz@utp.edu.pl, PL 85-763 Bydgoszcz, Al. Prof. S. Kaliskiego 7 Street

Abstract

In the paper there was presented investigation methodology of power consumption by disc refiner which worked on an industrial scale. In the article there was presented the structure of qualitative and energetic model, which described beating process of waste-paper stock in disc refiner. The author has chosen the basic parameters of this process, which can be obtained during investigations on an industrial scale.

Keywords: disc refiner, beating process, waste paper

1. Introduction

In the production of paper, the beating of waste paper stock is the most important process. The most typical refiners in papermaking are the conventional double disc refiners [1, 2, 4]. Working idea of these devices was presented on the Fig. 1. On the scheme, there was presented working knife disc of the refiner and flow system of stock by refiner.
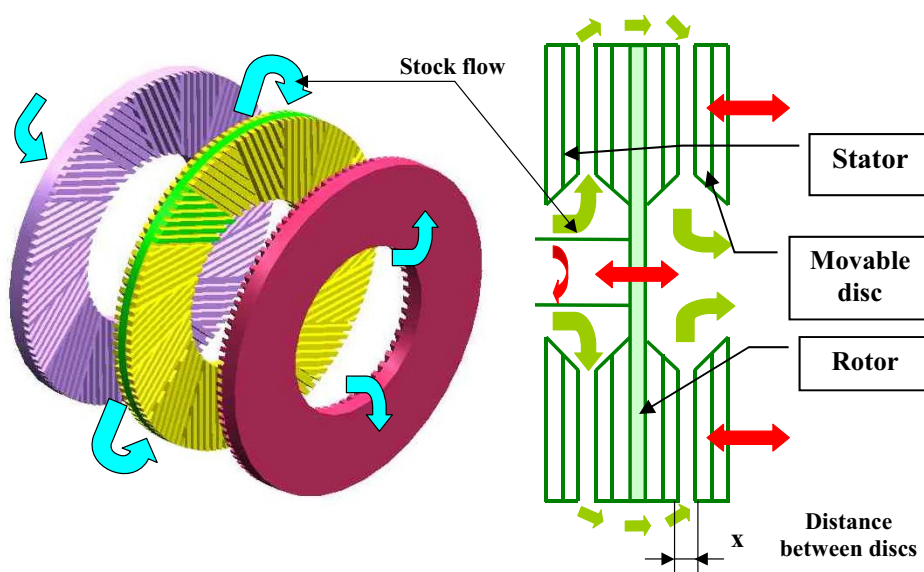

Fig. 1. Typical dimensions of the refining zone [3]

Modern industrial disc refiners are based mainly on a narrow gape treatment of the paper making fibers. In order to achieve the desirable refining effects in waste paper refining the gape between the rotor and stator bars varies in the range 10-400 μm (fig. 2). The average gape of 100 μm corresponds to the thickness of 2-5 swollen fibers or 10-20 collapsed fibers.
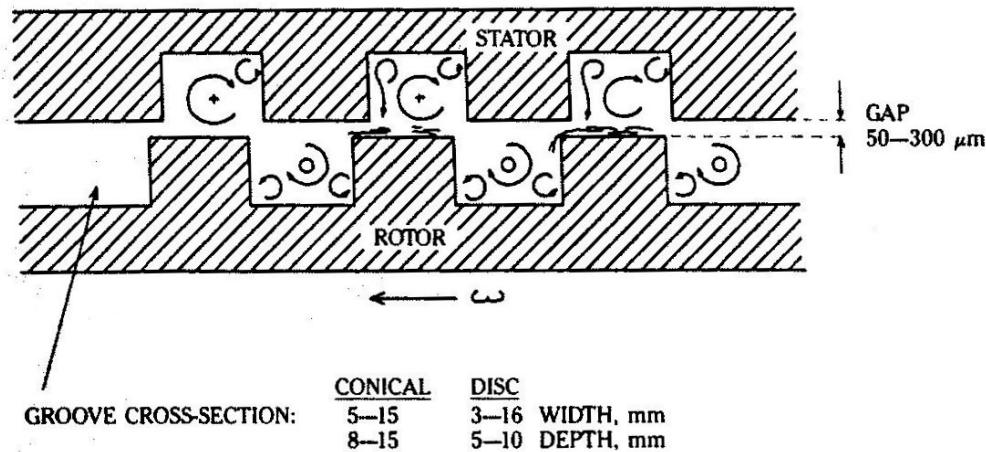

Fig. 2. Typical dimensions of the refining zone [1, 2]

Beating process, like in any other complex technological process, depends on many factors which we can divide into construction and system factors (connected with beating system and with its equipment) and technological factors. To the first group of factors belong: using refining system (periodic, continuous), number of refining devices and their division into units (refining, proper beating, post refining), system of refiners connections and chests and characteristics of the used devices (kind, type, rotary speed, refining elements etc). We cannot change these factors during the exploitation of refiner or these changes would be complicated in practical realization.

Into the most essential parameters of the second group (technological) we can accept [1, 3, 6]:
- properties of waste paper stock before refining,
- flow intensity by refiner,
- distance between disc,
- stock consistency,
- stock temperature.

In this article, technological factors connected with the work of single disc refiner were described. The author undertook an attempt to build a qualitative and energetic model. This model will describe the treatment of waste paper stock in a disc refiner. Below there is presented the description of most factors affecting the refining process.

2. Identification of beating process parameters

The beating of waste paper stock is a complex process. The most important variables were shown diagrammatically in Fig. 3. In this scheme there are presented factors, which influence the beating process in disc refiners. As one can see, it is necessary to introduce indispensable simplifications to the practical description of qualitative and energetic model of beating process.

In Fig. 4 there were specified only these variables which most often change during waste paper treatment in disc refiners. Additional reductions result from stand test in an industrial scale.
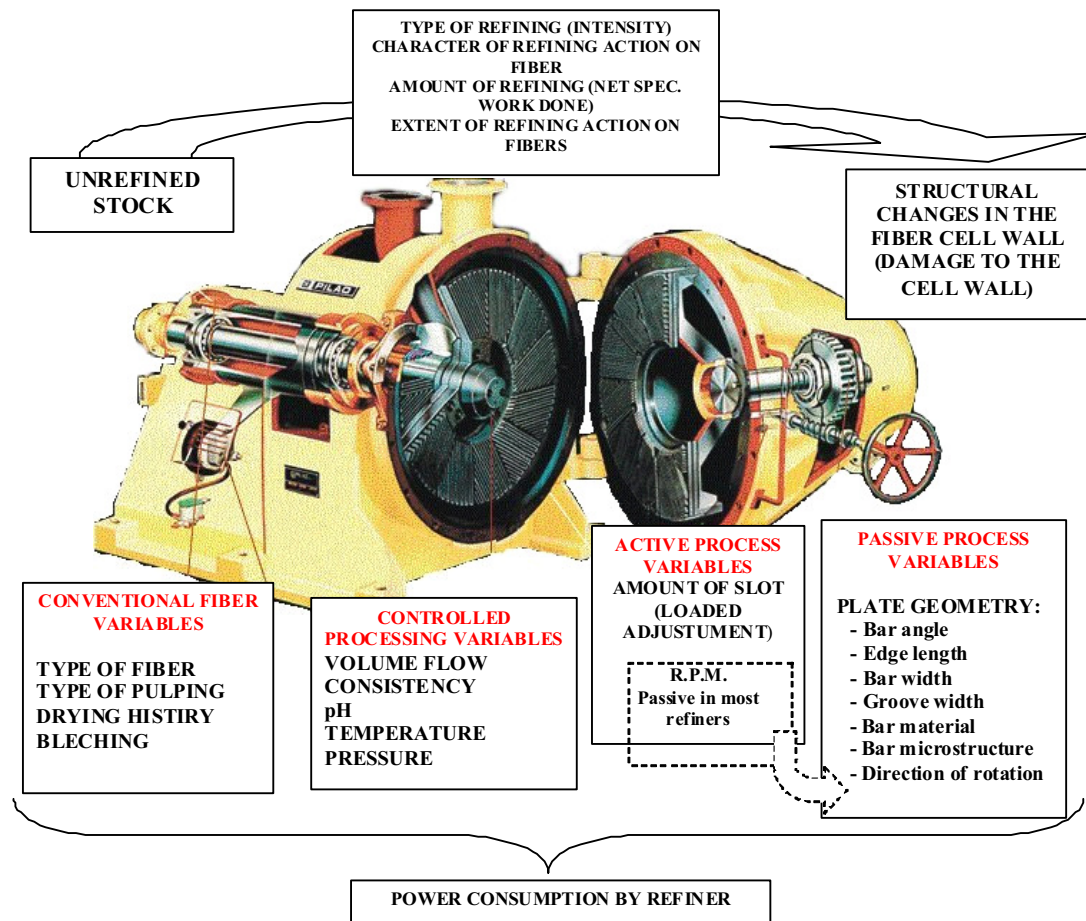
Fig. 3. Qualitative model for the refining process - The most important variables [1, 2, 3]
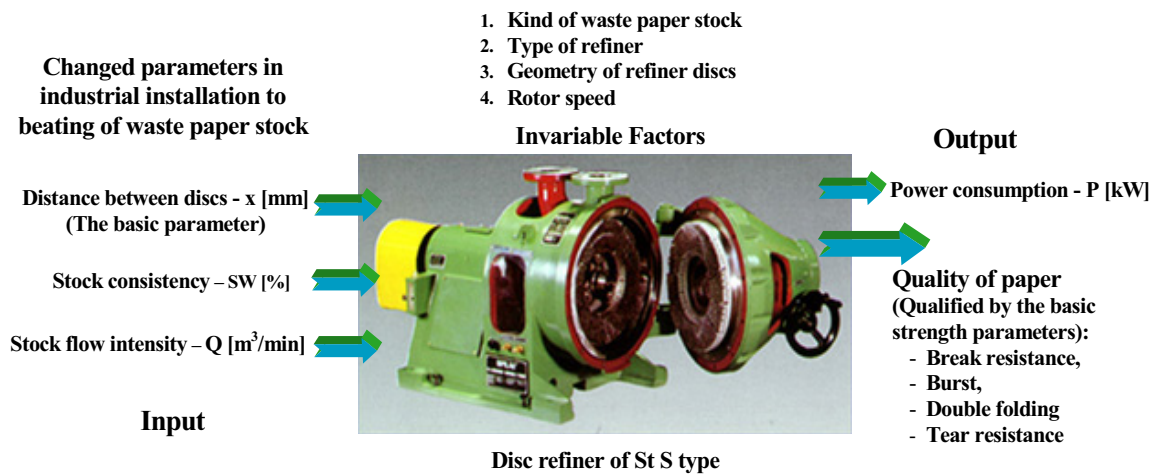

Fig 4. Investigated disc refiner with fundamental variables [3, 6, 7]

3. Description of machine model – disc refiner as paper stock treatment system and distribution of total power

In Fig. 5 there was presented the model of machine identification as treatment system of waste paper stock and energy. In this scheme the machine was presented as the object of investigations. In this figure there are two inputs: 1) delivered total energy N_c, volume of which depends in this

system on slot-gape size; 2) waste paper stock, which has definite properties. At the exit there are symptoms in the form of obtained efficiency of the process, quality of obtained stock and energy consumed on the processes connected with refining. Additionally, in this scheme there were illustrated thermal losses and other processes which we can observe in the refiner: vibrations and noise. The other processes will be used during the verification of the phenomena and changes which take place during refining (slot size correlation with noise and strength properties).

Description of parameters which we can see on the Fig 5:

x - Gape (slot size) - variable - distance between discs;

M_w - Semi-finished product: waste paper stock led to the refiner (its parameters: flow intensity and quality are constants);

M_{wy} - Stock which had specified characterization (parameters before the refiner) transformed in the refiner. Parameters before the refiner affecting the received paper - quality J;

S_c - Losses of refining thermal process - negligibly small;

J - Quality of paper which is verified by selected strength parameters of the received paper.
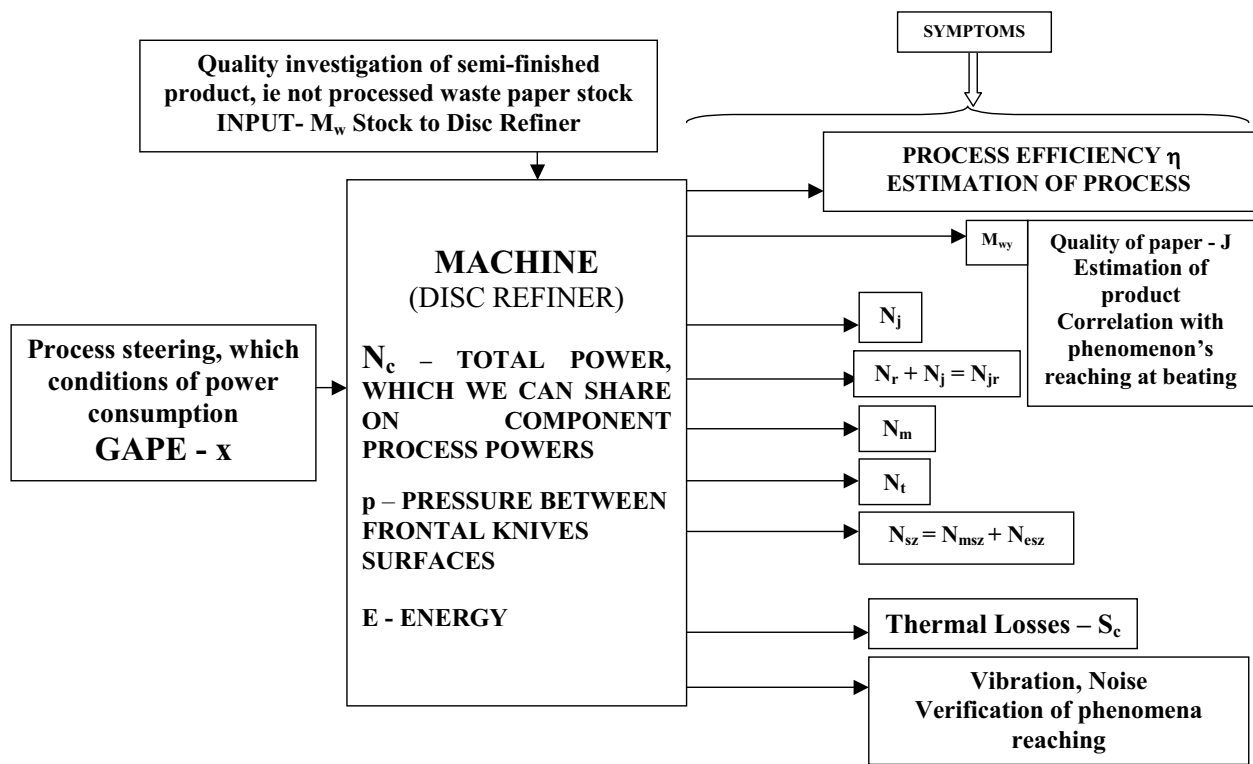

Fig. 5. Model of machine identification as treatment system of waste paper stock and energy [3, 4]

Process powers were qualified by theoretical analyses of the refining process [4, 5]. These powers are as follows:

N_c - Total power consumption which depends on x – distance between disc, refiner construction and stock kind. This power is measured on engine shaft which drives the refiner;

N_j - Power consumed on idle run without stock, for slot size greater than 0.2 mm;

$N_{jr} = N_j + N_r$ - Power consumed on refining with power consumed on idle run (with stock), for slot size $x > 0.2$ mm;

$N_r = (N_j + N_r)$-N_j - Power consumed on refining, N_{jr} - $N_j = N_r$;

N_m - Power consumed on beating;

N_t - Power consumed on fibers cutting;

N_e - Power consumed on metallic friction (friction between frontal surfaces of knives);

N_{sz} - Power consumed on mixed friction (mixed friction consist of metallic friction and friction which is connected with beating process): $N_{sz} = N_{msz} + N_{esz}$;

N_{msz} - Power consumed on beating which is a part of power consumed on mixed friction;

N_{esz} - Power consumed on metallic friction which is a part of power consumed on mixed friction.

Accepted distribution of process powers in relation to the slot size x was presented in Fig. 6. This figure is an example chart obtained during investigations. On the base of investigations, there were obtained curves A-B-C-D-E (for different dryness). The other curves (refining, proper beating, cutting, metallic and mixed friction) were obtained on the basis of mathematical analysis. The character of these powers' changes was described in earlier works [3, 4, 5, 6].
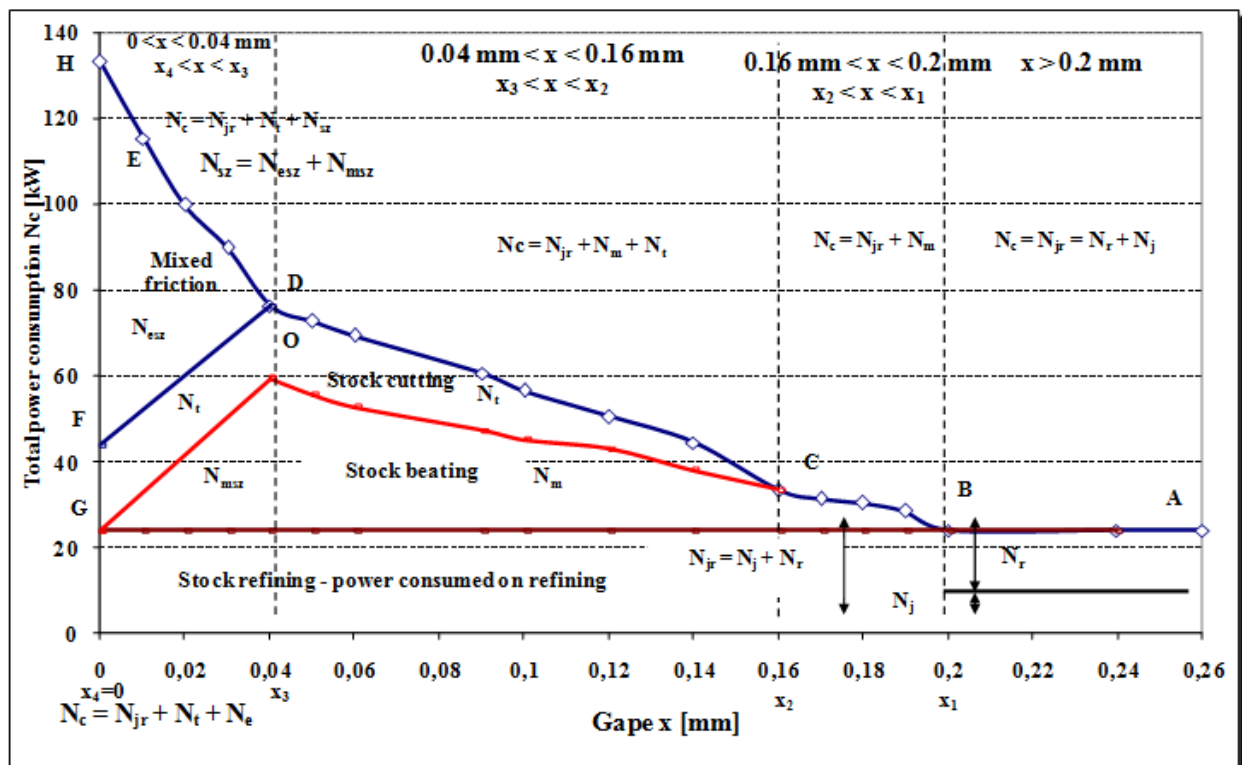

Fig. 6. Chart of total power consumption (A-B-C-D-E-H) in function of distance between discs for disc refiner with regard of proposed composition process powers distribution

4. Conclusion

This paper is an attempt to build qualitative and energetic model of disc refiner work for the distance between discs as a main variable. In the paper there was described the procedure of determining the methodology of investigations. Adjustment gape is most essential from the point of view of quality of obtained paper stock and volume of power consumption by the refiner. In the gape function there was also carried out the description and analysis of process powers which can be defined during the beating of waste paper stock.

References

[1] Hietanen S., Ebeling K., *Fundamental aspects of the refining process*, Paperi ja Puu – Paper and Timber, Vol. 72, No 2, 1990, p. 158-170.

[2] Lumiainen J.J., *Comparison of the mode of operations between conical and disc refiners*, Paper Technology, No 2, 1997, p. 53-58.

[3] Mroziński A.: *Badanie poboru mocy przez zespół rozdrabniający makulaturową masę włóknistą w warunkach zmiennej szczeliny roboczej młyna tarczowego*, Rozprawa doktorska, ATR Bydgoszcz, Wydział Mechaniczny, 25 styczeń 2005.

[4] Mroziński A., Kikiewicz Z., *Modelowanie i symulacja przetwarzania mas papierniczo-makulaturowych*. Inżynieria i Aparatura Chemiczna, Nr 1/2007, Vol. 46 (38), str. 97-99.

[5] Mroziński A., Kikiewicz Z., *Beating of waste paper stock at different slot size between refiner discs*, International Conference on Practical Aspects of Particle Technology, HUN-Pra-PARTEC 2001, Budapest, Hungary, 21-24 August 2001, p. 385-389.

[6] Kikiewicz Z., Mroziński A., *Investigation of disc refiner ST300S to processing of paper stock*, 14th International Congress of Chemical and Process Engineering, CHISA `00, Prague, Czech Republic, 27-31 August 2000, p. 173.

[7] Kikiewicz Z., Mroziński A.: *Wpływ procesu mielenia masy makulaturowej w młynie tarczowym ST300S na właściwości wytrzymałościowe papieru w układzie recyrkulacji*, Zeszyty Naukowe ATR nr 231, Mechanika 49-2000. Bydgoszcz 2000, str. 61-74.

RECIRCULATION OF BEVERAGE CARTONS

Adam Mroziński

Department of Special Machines and Environment Protection
Faculty of Mechanical Engineering, University of Technology and Life Science in Bydgoszcz
adammroz@utp.edu.pl, PL 85-763 Bydgoszcz, Al. Prof. S. Kaliskiego 7 Street

Abstract
In many countries collecting and sorting used packages for recycling have become a part of daily life. Various paper and board packages differ however in their potential use in recycling. Serious problems are caused by so called "combined packages". These are made of different materials (not only paper) or materials joined in layers. Materials of this kind bring about a lot of problems in processing and cause environmental burden to increase. In this paper, recycling and recovery methods for beverage cartons were presented. Beverage cartons are a typical example of combined packages (material in layers).

Keywords: recycling, beverage cartons, recovery of paper, recovery of aluminium foil

1. Introduction

With growing production of material goods increases environmental burden with used packages. It is estimated that packages contribution in total amount of municipal waste equals approximately 50% of its mass, or in respect of volume 70%. In the amount of used packages in turn, the most considerable position is paper and cardboard. Their contribution is calculated to be approximately 34% in respect of mass and 44% of volume. The result of this is that about 100÷200 kg a year of used packages falls to one single inhabitant in individual countries, in this from 34 to 70 kg of paper and board packages [6].

In order to limit the impact of the waste on natural environment it is necessary to introduce suitable legal regulations and acts: they should include the following criteria (four Re criteria) [4, 6]:

Reduction at source - Minimize packaging by weight and volume.

Reuse - The development of reusable packaging.

Recycling - The overall target is to recycle 25% to 45% of all packaging waste, by weigh. For individual materials, the minimum recycling level is 15%. Mills and converts must take into account materials and substances that are liable to create problems in:

- the recycling process,
- the collecting and sorting process,
- those which could have a negative influence on the quality of recycled material.

Recovery - The directive sets targets for 50% to 65% recovery of packaging waste by weight. Recovery includes energy recovery and composting and will be supported by two general standards. These will affect the manufactures and converts of packaging, who must take into account substances or materials, which have a negative impact on energy recovery or biodegradation.

The first two of above activity directions have very restricted use in the case of paper and board packages. Because of hygienic and sanitary reasons and some advertising and marketing aspects and also because it is necessary to insure the quality and durability of products we won`t get away from the packages [1, 10]. Moreover, paper and board are single use packages.

In this situation the most effective ways to limit environmental burden by packages are recycling and recovery. Most of paper and board packages are suitable for recycling. Their use as the waste paper grows up presently in many European countries. For example in Netherlands contribution of package wastepaper in paper and board production equals 70%. Not contaminated paper and board are very attractive materials for recycling. Through the use of wastepaper it is possible to save energy, raw materials and reduce environmental burden [2].

In many countries collecting and sorting of used packaging for recycling have become a part of daily routine. Various paper and board packages differ however in their potential use in recycling. Serious problems are caused by so called combined packages. These are made of different materials (not only of paper) or materials joined in layers. Materials of this kind bring about a lot of problems in processing and cause the environmental burden to increase.

In this paper full recycling and recovery model for beverage cartons is presented. Beverage cartons are typical example of combined packages (materials in layers).

2. Beverage carton packages

The most popular carton today, Tetra Brick Aseptic in the shape of brick, is an example of beverage package. Package material is made of laminate consisting of six layers [8, 10] (Fig. 1). The main component among them is paper which contributes to 75% of package mass. Board forms package frame giving it its rigidness and durability. Polyethylene composing 20% of package mass protects package wall against moisture penetration and also enables to close the package by sealing its walls with each other. Aluminium foil (5% of package mass) is additional barrier for light and oxygen (asepsis).
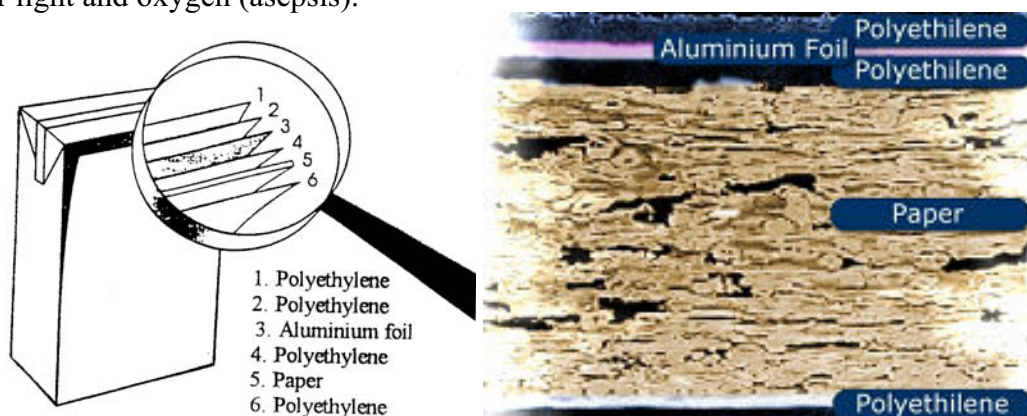

1. Polyethylene
2. Polyethylene
3. Aluminium foil
4. Polyethylene
5. Paper
6. Polyethylene

Fig. 1. Typical beverage carton configurations [8, 10]

Aseptic package market increases by 6% to 8% a year. Into such packages more and more liquid food is packed (in Europe about 70 mln liters of liquid food a day) [7]. That's why it is necessary to manage rationally this kind of package waste.

3. Aseptic packages recycling

We come across quite a few problems while recovering raw materials from aseptic packages. Laminate doesn't easily undergo the process as the secondary raw material [9]. It is necessary to sort out individual components (paper, aluminium foil, polyethylene). Another problem, which arises here, is the fact that used packages are mixed during collecting and delivery to the waste

dump. Therefore before processing these wastes must be sorted. So there should be introduced paper waste collecting infrastructure. It is estimated that amount of such sorted package wastes surpasses 200000 tons worldwide [3].

There are possible various alternative ways of aseptic packages recycling which was shown at the diagram in Fig. 2.
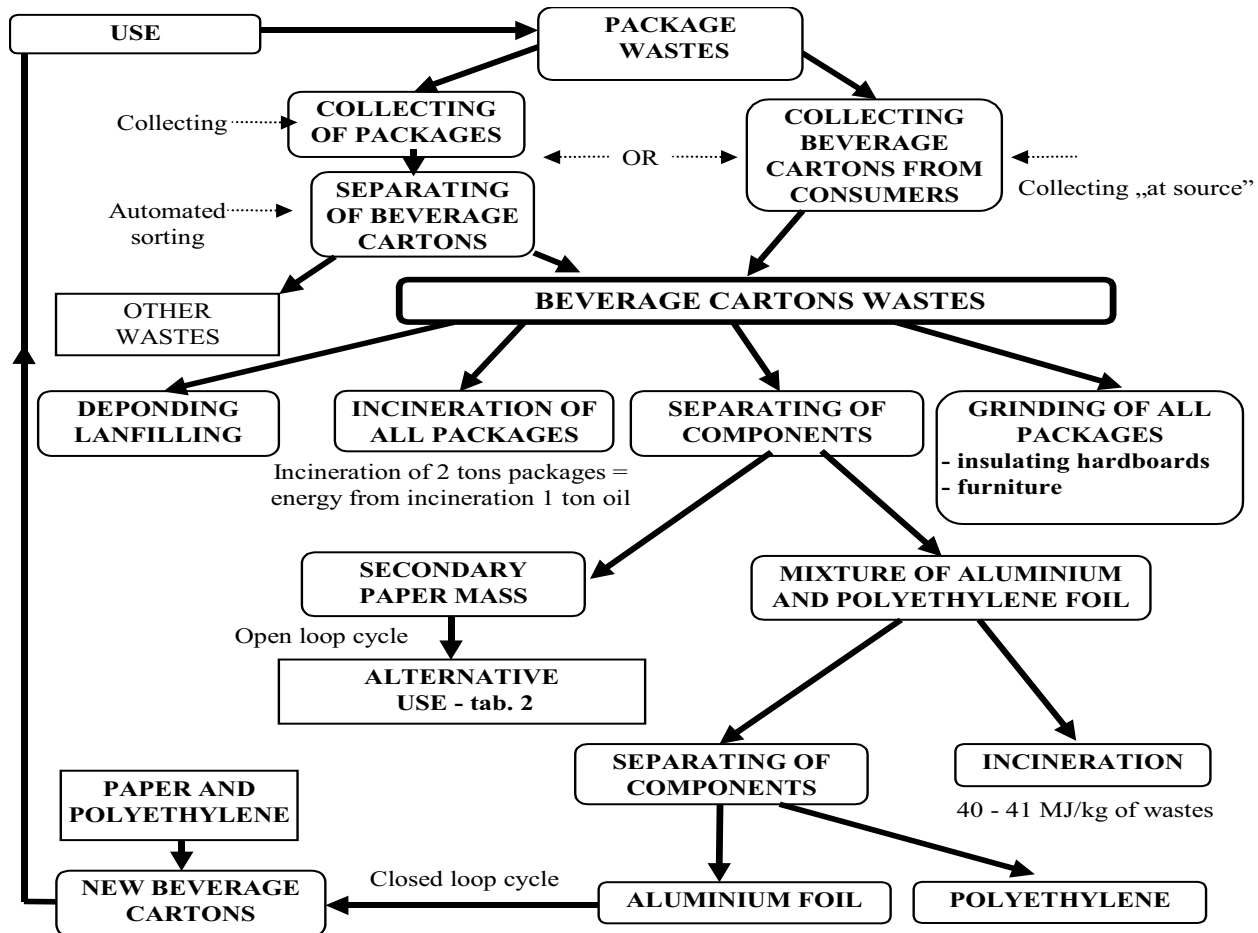

Fig. 2. Various alternative ways of aseptic packages recycling

3.1. Separating and recovery of components

Packages can be utilized as the whole (incineration) or with the separation of individual components. An example here can be Nesa paper mill in Spain where 80000 tons of cartons a year is processed in profitable way [8]. In the process hard pulp fibre is recovered which is suitable for production of sacks and paper bags needed for packing industrial products.

In German factory at Diez in 1990 manufacturing of water-resistant hardboard has began [8]. These boards possess very good mechanical, thermal, acoustic and insulating properties. They can be employed as parquet floor and for production of high quality furniture. They are formed in the heat press moulding of ground packages [3, 8].

For separating paper fiber there can't be used typical hydropulper where grinding takes place. There are used machines which separate paper fiber by washing it out (Regenex system, FiberFlow system) [9, 11]. Aluminium and polyethylene foil are not crumbled in the process of separating paper fiber. They make so called reject.

Regenex system provides high-dilution fiber washing for deinking. It can also separate fiber from polyester film used in milk cartons, drink boxes, poly-coated cups, and similar items.
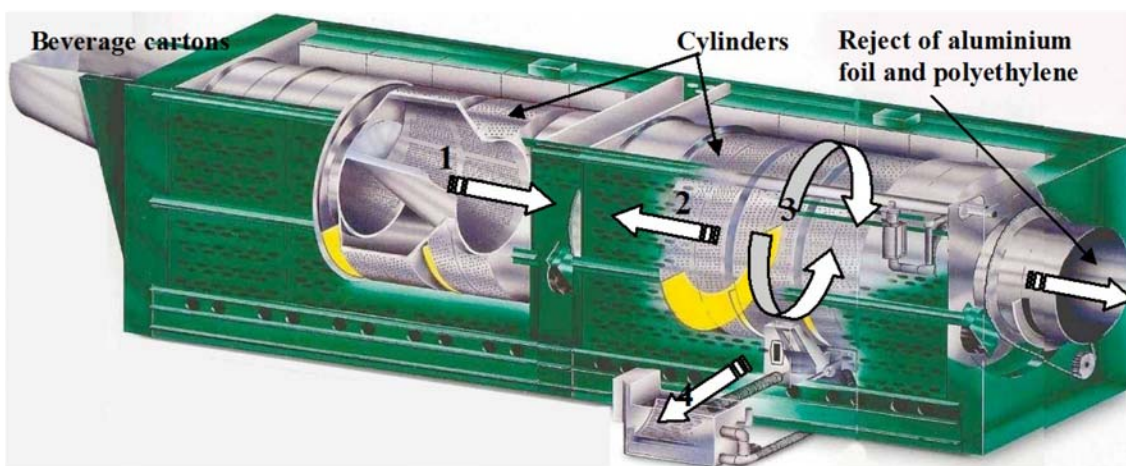
Fig. 3. Single module of Regenex system: 1 - stream of beverage carton mass (integrated perforated transfer scoop), 2 - stream of water (about 4 l/min), 3 - revolutions in both directions of perforated drums, 4 - paper fiber for continued treatment (washing, bleaching, dewatering) [11]

The outer shell of the Regenex system and its inner cylinder enable the machine to create two distinct material transfer paths: one for rejected poly film and the other for cleaned secondary fiber. Thus, the system solves one of the most difficult problems in processing poly-coated materials: separating poly film from fiber and breakdown wet-strength resins. Rejected poly film is removed in sheets or large pieces. The Regenex recovery system is modular. On the Fig. 3 single module of Regenex system was presented.

Pulping and washing processes occur in multiple, connected cylinders, which rotate in synchronization. As the cylinder rotates, stock is lifted from the process water and dropped back into the solution. The resulting mechanical action enhances contaminant separation. Each "batch" moves from module to module by an integrated transfer scoop. On the Fig. 4, an example of all systems of paper fibre separated was presented.

Recovered fiber is not used for production of aseptic packages again because in their production in 80% primary fibre is used [7, 8]. Therefore in case of paper mass we can activate only open loop recycling, where recycled fibres serves as the component for production of the products different from input products. Alternative uses of recycled fibres outside the paper and paperboard industry are presented in Table 2.

Separated foil can be incinerated with energy recovery. Energy value of aluminium foil is the same as burning of coal and energy value of polyethylene is even higher [3].
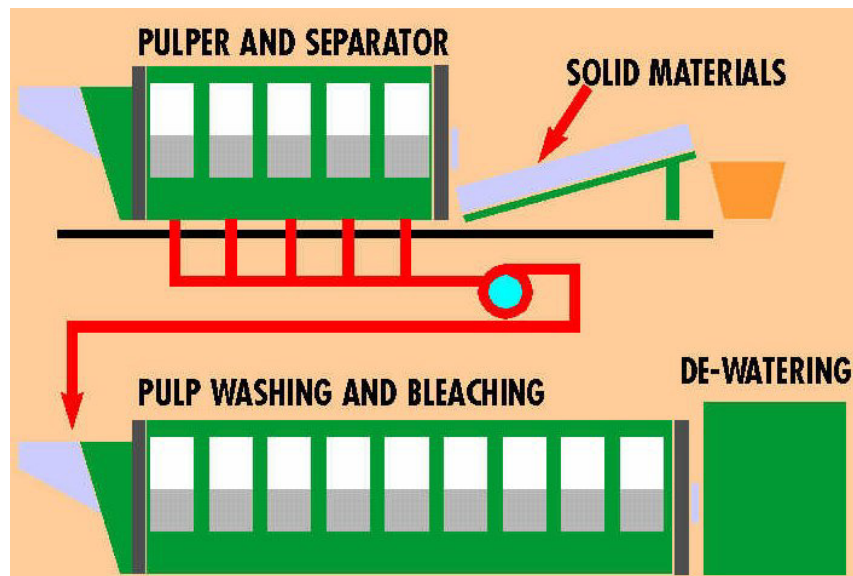
Fig. 4. Example of all systems for paper fibers separated

Tab.1. Examples of alternative uses of paper recycled fibres

ALTERNATIVE USES OF RECYCLED PAPER FIBRE OUTSIDE THE PAPER AND PAPERBOARD INDUSTRY

• MOULDED PULP AND WET-LAID PRODUCTS - egg cartons, fruit trays etc.
• INSULATION
  - cellulose insulation blown into ceilings + additives, moistened fibres (water/glues)
  - building boards
• ASPHALT/FIBRE ROOFING FELT AND GIPSUM WALLBOARD
• FILLER - paints, mastics etc.
• LOOSE FILL FOR INTERIOR PACKAGING - cushioning and void filling
• GROUND COVER, FARMING - boards, shredded
• ANIMAL FODDER
• CHEMICAL DERIVATIVES
  - complex carbonhydrate fraction, single carbonhydrate fraction, lignin fraction
• COMPOSTING
• HOME & SMALL BUSINESS USE
  - making fire, wrapping & packaging, hobby uses, covering
• OTHER SPECIAL USES - pencils, art works etc.

Separating both kinds of foil from the mixture is an alternative for incineration (joint development programme Gränges Eurofoil and Tetra Pak) [3]. In this way it is possible to realize the closed loop recycling for aluminium foil. In the process of aluminium foil recovering processed mixture is sorted gravitationally and magnetically after the separation of paper fiber (Fig. 5) [3, 8].
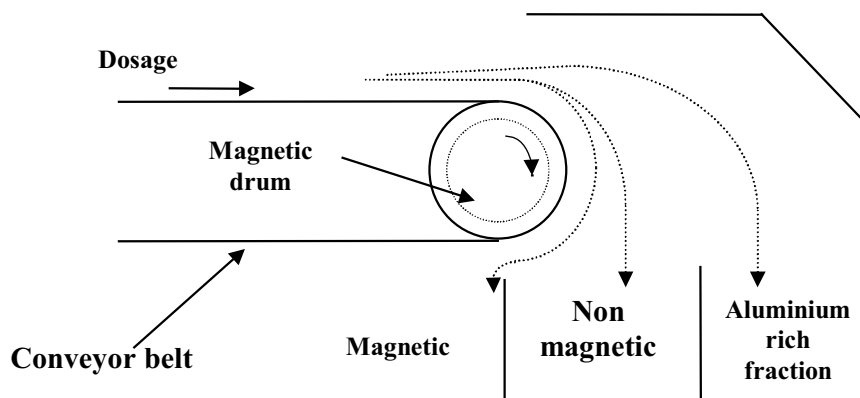
Fig. 5. Eddy current separation

What follows next is thermal separation of aluminium. In the process, the remaining components are incinerated. Obtained aluminium is used for production of foil, which can be used for manufacturing of new beverage cartons. Recovery efficiency of the process is considerable because it reaches to 30 – 35% of foil mass input (In a single one-litre beverage package there are 7g of aluminium foil).

3.2. Incineration with energy recovery

The most popular way of beverage packages recycling is incineration with energy recovery. One typical package weighs 25g. Incineration of 2 tons of used packages brings as much energy as 1 ton of oil [8]. Incineration of the waste, which is left after separation of paper fiber, has also very high energy value, about 40 - 41 MJ per kilogram of wastes. Incineration energy can be applied to many purposes and in this way mineral fuel can be saved.

Incineration process of package waste must take place in strictly defined conditions because of limits of poisonous substances, which can be emitted. European Union recommended the following incineration parameters [1, 2]:
- incineration temperature - higher than 850 ^{0}C,
- incineration time - longer than 2 sec.,
- minimal amount of oxygen - over 6% in the relation to incinerated mass.

Obeying this rules enables to limit emission of pollution (poisonous gasses). Under existing strict requirements defining the highest permissible concentration of poisonous substances in gasses it is necessary to incinerate segregated wastes. The point is to sort out the goods that contain substances which, when incinerated, cause highly poisonous emissions. These are mainly the goods made of polyvinyl chloride, the goods containing compounds of chlorine and also containing lead and mercury. In the case of beverage packages we can state that there doesn't occur high emission of poisonous substances.

In Table 3, there are presented ways of utilizing packages in individual countries of Western Europe. Presented data show that there is considerable contribution of wastes stored at waste dumps. Yet one should notice that there also takes place development of alternative methods of waste utilization (close to 40% of waste mass) [6, 7].

Tab.2. Ways of utilization of packages in individual countries of Western Europe [2, 3, 6]

Country	Mass of wastes in tons	Incineration	Deponding	Composting	Recycling
		%			
Austria	2800	11	65	18	6
Belgium	3500	54	43	0	3
Switzerland	3700	59	12	7	22
Germany	25000	36	46	2	16
Denmark	2600	48	29	4	19
Spain	13300	6	65	17	13
France	20000	42	45	10	3
Italy	17500	16	74	7	3
Norway	2000	22	67	5	6
Holand	7700	35	45	5	15
Sweden	3200	47	34	3	16
England	30000	8	90	0	2
West Europe	1400880	24	63	5	8

4. Summary

Collecting and sorting of used packages has been nearly a daily experience in many countries. Specialists estimate that in 2008 about 25% of beverage packages were recycled. It is significant because of the technological problems, which arise during their sorting and utilization [5, 6].

In the process of beverage cartons recycling it is possible to follow different ways of processing and to choose the optimal one it is necessary to do economic and ecological analyses. An optimal solution will be always the one with minimal financial outlays and maximal limitation of environmental burden. Economic profitability of chosen recycling method will depend on the possible market of recovered materials and on organization of collecting of used packages.

An important requirement for any method of utilization is necessity to sort wastes. One should take into consideration selective collecting of packages "at source" (at customer's house) or sorting after the collecting stage.

References

[1] Jankowski J., *Czy można spalać zużyte opakowania?* Przegląd Papierniczy. No 3/1995, Vol. 51, str. 127.

[2] Kikiewicz Z., Mroziński A., *Model recyklingu opakowań po napojach*. Ekologia i technika. Nr 2, Vol. VI, str. 40-43, Bydgoszcz 1998.

[3] Knutsson L., Nyström T., *Closed loop recycling of aluminium foil in beverage cartons - now technically realized*, R`97 International Congress, Recovery Recycling Re-integration, Geneva, Switzerland, 4 - 7 February 1997.

[4] Mroziński A., Full recycling and recovery model for beverage cartons. 20 Fachtung über Verarbeitung und Anwendung von Polymeren, University of Chemnitz, Chemnitz 15-17.10.2007, p. 97.

[5] Mroziński A., *Ekologiczne cykle opakowań*, Inżynieria i Aparatura Chemiczna, Nr 1-2/2005, Vol. 44(36), str. 71-72.

[6] Mroziński A., Kikiewicz Z., *Aspekty recyrkulacji makulatury w Polsce*, Inżynieria i Aparatura Chemiczna, Nr 4/2008, Vol. 47 (39), str. 57-58.

[7]   Mroziński A., Flizikowski J., Dziadosz K., *Przetwarzanie opakowań wielotworzywowych*, V-ta Międzynarodowa Konferencja Naukowo-Techniczna, Problemy Recyklingu, Warszawa, 26-27 wrzesień 2007, str. 272-279.

[8]   Mälkki H., *Role of recycling in environmental impacts of finish beverage packaging systems*, R`97 International Congress, Recovery Recycling Re-integration. Geneva, Switzerland, 4 - 7 February 1997.

[9]   Wciślik J., Pawelczyk I., *Ekologiczne spojrzenie na produkcję opakowań*, Przegląd Papierniczy, No 4/1996, Vol. 52, str. 169.

[10]   Wendelt P., *Krótka historia wielkiego imperium opakowaniowego*, Przegląd Papierniczy, No 9/1996, Vol. 52, str. 436.

[11]   Wendelt P., *Przerób nieprzerabialnego, czyli nowy system przerobu papierów laminowanych*, Przegląd Papierniczy. No 11/1996, Vol. 52, str. 579.

POLYFLOW SOFTWARE USE TO OPTIMIZE THE PARISON THICKNESS IN BLOWING EXTRUSION

Karol Pepliński, Marek Bieliński

Bydgoszcz University of Agriculture and Technology
al. Prof. S. Kaliskiego 7, 85-789 Bydgoszcz, Poland
tel.: +48 52 3408226, fax: +48 52 3408222
e-mail: karolpep@utp.edu.pl

Abstract

The blowing extrusion is one of the most widely used techniques for the production of hollow plastic products. In order to improve the efficiency of designing plastics processing the blow products from thermoplastic materials used in Computer Aided Engineering software. This paper presents the blowing container simulation with high-density polyethylene (Borealis, BS 2541), using Polyflow software. In the present work was showed the impact of the initial parison geometry distribution onto final wall thickness in the sample container. Two cases of blowing parison were considered. In the first, pre-approved on the basis of a constant parison thickness (g = 2 mm) examined the distribution of the container wall thickness. There has been excessive thinning (between 0,2÷0,3 mm) in the container corners after blowing. On this basis, was made optimization of the parison profile thickness to remove excessive thinning. Noted was a significant effect of the initial extruded parison geometry on the final wall thickness distribution in the considered container. Optimizing the parison profile thickness allowed to eliminate excessive thinning in the corners of container walls. The minimum wall thickness was only 0,9 mm, assuming the final wall thickness of the container to obtain the order of 1mm.

Keywords: blowing extrusion, optimization of the parison profile thickness, Polyflow simulation, container, HDPE

1. Introduction

Predominant increase in the use of packaging primarily from polymer materials in terms of beverages, cosmetics, chemical products, pharmaceuticals, etc. are related, on the one hand, to the replacement of traditional materials (metal, paper, glass), and on the other hand, creating new applications such as multilayer containers, significant primarily for these materials. Already in 2000, the number of blow molding bottles for beverages in the world has exceeded 10 billion units. Nowadays, this number is much higher [2,5,10]. In 2007, Western Europe processed 52,5 million tones of plastics, including up to 37% in the production of packaging [16]. This justifies the expansion of the claim that the manufacturing of packaging technology, especially the extrusion blow molding process, is an important trend in plastics processing.

There are higher and higher requirements for blowing plastics processors to comply with the import of expensive processing tools, and they tend to increase the intensive use of computer-aided manufacturing techniques in order to minimize financial losses resulting from incorrectly designed tools such as blow molds. This be connected inter alia with complex processing properties of polymers in blowing extrusion which hinder the development of accurate prediction of material shape in blow molds and produced final geometry [10,13]. In this direction were taken numerous

experimental studies in the world [1,3,11]. There is, however, a small number of Polish publications dedicated to blow molding simulation of plastics [4,6,7,8,9,12,14], such an important point of view of making good use values such as packaging. One measure to be applied is Polyflow simulation software [15] which can effectively prevent possible errors and optimize the structure of the initial parison geometry. Obtaining a uniform thickness of the wall container at the final stage of designing, the processor does not compromise on the additional costs and shorter design time while improving the properties and provides utility package.

2. Research aims

On the basis of the information contained in the literature [1,10] shows that it is not possible to obtain blowing products with a homogeneous distribution of wall thickness on the basis of parison with constant thickness, especially for products with a more complex structure. In this case, the wall thickness distribution was to be the most equitable form, one should pre-determine differential parison thickness. It is difficult to do it intuitively. This can be done with available simulation programs such as Polyflow.

The aim of this work is to evaluate the distribution of wall thickness in the sample bottle, adopted on the basis of pre-extruded parison, and determine the geometry of parison, which will improve the distribution of container wall thickness. This task has been achieved through the use of Polyflow software 3.12.2.

3. Assumptions

The simulations in the environment of Polyflow 3.12.2 are intended to facilitate the complex process of extrusion blow molding process and selection of optimal thickness blowing parison, in order to obtain a uniform wall thickness distribution of the final blow product. Properly designed geometry features, including the parison thickness, allow to specify the minimum plastic demand for the implementation of plastic container.

The purpose of the simulation are axially symmetric products whose shape and dimensions are presented in Figure 1. Due to the complex structure of blow modeling process in Polyflow environment, the methodology of the case was briefly mentioned in order to focus on the results of the simulation.
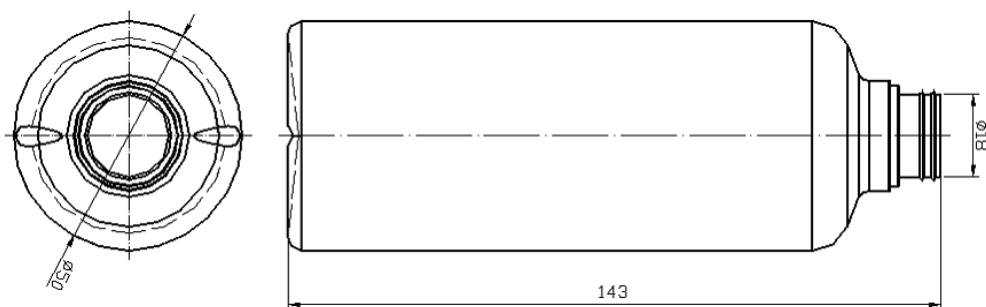
*Fig. 1. The shape and dimensions of axially symmetric bottle*

The simulation was carried out for a parison-shaped circular cross section: parison diameter d = 14 mm, thickness g = 2 mm. In order to carry out blowing simulation of the object, with the parison was separated geometry quarter, which significantly reduced the time of calculation. In order to determine the parting lines form in a later stage of modeling, for each of the objects has been added the reference plane. This plane in the longitudinal direction of the bottle is equal to the parison length. The final bottle geometry model is shown in Figure 2.
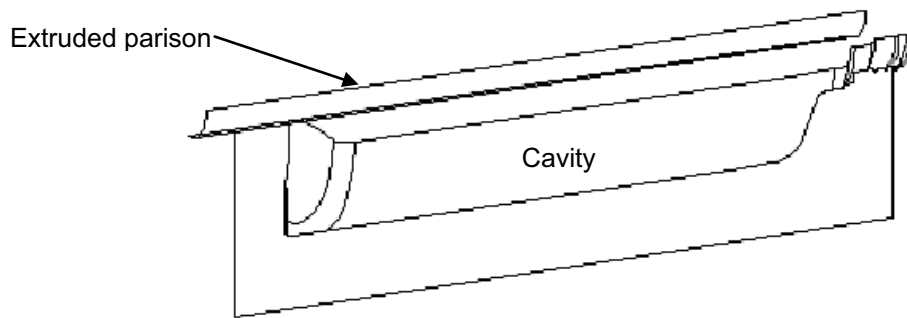
Fig. 2. The model of cavity with parison

4. Stages and results of blowing extrusion in Polyflow simulation

At a pre-arranged geometrical object were imposed grid finite elements in Gambit module. After the imposition of FEM, the mesh object is divided into separate sub domains for the parison and the cavity. The division is necessary to continue the modeling phase of the flow. Defining the problem was implemented in the module Polydata, which establishes the data: a physical model of parison and cavity, parison blowing range, the relative movement of the mold (cavity), the flow boundary conditions, and type of calculations. Adopted material for extruded parison is PE-HD, density $\rho=0.96$ g/cm³ and the viscosity $\mu = 92140$ Pa•s for the temperature T = 190 ºC. The adopted initial thickness of the parison was g = 2 mm. Blowing pressure p = 0,9 MPa. Simulations were also put down the distribution of wall thickness of blowing bottles, and optimize a uniform distribution of wall thickness. The criterion of the optimization was the wall final thickness g = 1 mm. The obtained results allowed the simulation module Fieldview to create models depicting the spatial distribution of container wall thickness before (Fig. 3) and after the blow optimization of the initial thickness of extruded parison (Fig. 4). On the charts we can see that in the case of constant parison
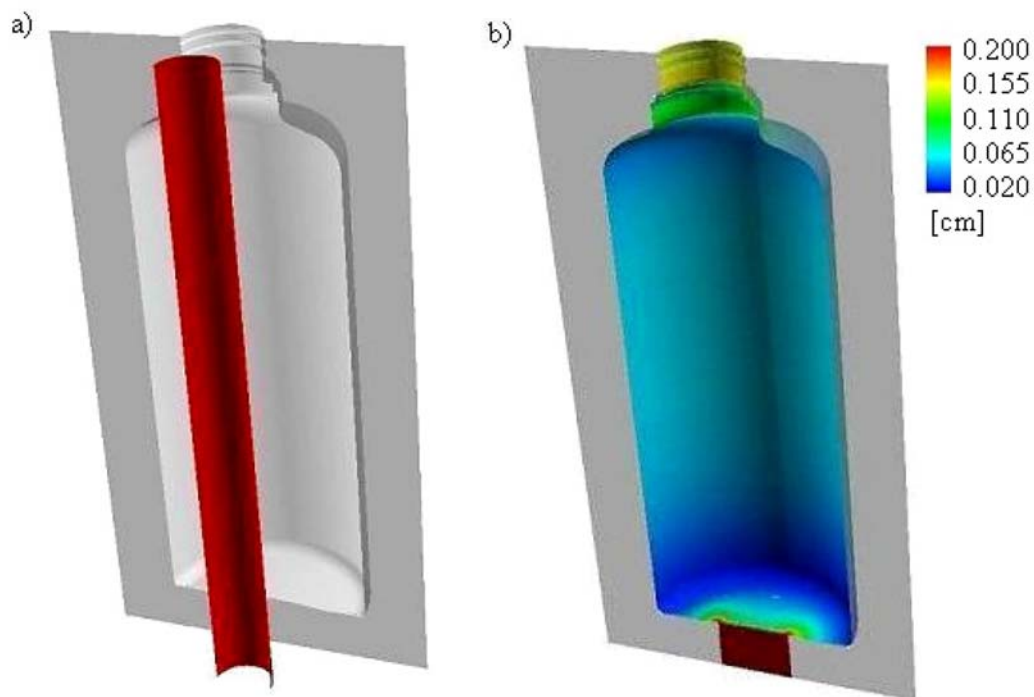
Fig. 3. Schedule parison wall thickness: a) before blowing (g = 2 mm), b) after blowing ($g_i \cong 0,2 \div 1,5$mm)

thickness g = 2mm, occurs an excessive wall thickness reduction in the corners $g_i \cong 0,2 \div 0,3$mm. This is an unacceptable value in terms of packaging design, as it can lead to corner deformation for its use. An alternative to this was a generation of such extruded parison which prevents the emergence of such thickness reduction during blowing. The result of this approach is to obtain a significant thickness improvement in the wall corners ($g_o \cong 0,9 \div 1,1$mm). Also in the rest of the container wall thickness was similar to the value of 1 mm, only the bottom of the bottle in the area increased to 1,8 mm.
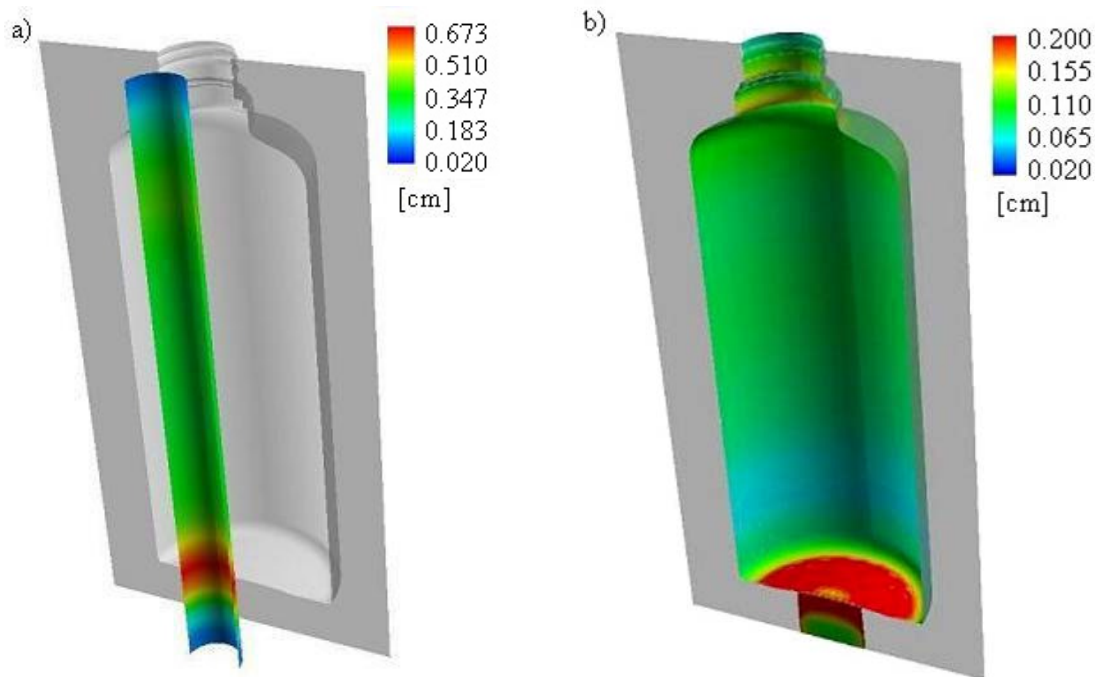

Fig. 4. Optimizing the parison wall thickness: a) before blowing ($g_o \cong 6,7 \div 1$mm), b) after blowing ($g_o \cong 0,9 \div 1,8$mm)

5. Summary

The blowing container simulations in Polyflow environment offer an opportunity to predict the shape and geometrical characteristics (thickness of the wall) of the intended form, thanks to the optimization of the profile thickness extruded parison. Using a simulation can be assessed at the design stage of the packaging, or its geometry form will not rise to unacceptable wall thickness, or even to tears at the stage of production. Using the Polyflow software at the initial stage of the design process, it is possible to propose an alternative form of parison profile geometry.

References

[1] Attara A., Bhuiyanb N., Thomsonc V., *Manufacturing in blow molding: Time reduction and part quality improvement*, Journal of materials processing technology 204 (2008) pp. 284÷289.
[2] Glenn L. B., James L., *Hollow Plastic Parts: Manufacture & Design*, Hanser Publisher, Munich 2004.
[3] Kalyon D. M., Kamal M., Tan V., *The Dynamics of Parison Development in Blow Molding*, Polymer Engineering and Science, 20, 1980, 12, pp. 773÷777.

[4]   Kondziela J., *Wspomaganie komputerowe procesu wytłaczania z rozdmuchiwaniem w formie*, Praca dyplomowa, UTP Bydgoszcz 2008.

[5]   Norman C. L., *Practical guide to blow moulding*, Smithers Rapra Technology, 2006.

[6]   Pepliński K., *Badania wpływu warunków przetwórstwa na cechy wytworów wytłaczanych z rozdmuchiwaniem*, Rozprawa doktorska, UTP Bydgoszcz 2008.

[7]   Pepliński K., Bieliński M., *Ocena rozkładu grubości ścianki i odwzorowania powierzchni formy w pojemnikach wytłaczanych z rozdmuchiwaniem*, Inżynieria i Aparatura Chemiczna. 3, 2008, pp. 8÷10.

[8]   Pepliński K., Bieliński M., *Ocena wybranych właściwości przetwórczych i użytkowych wytworów wytłaczanych z rozdmuchiwaniem*, pp. 115÷118, Polska Akademia Nauk oddział w Lublinie, Komisja Budowy i Eksploatacji Maszyn, elektrotechniki i Budownictwa, Tom II, Lublin 2008.

[9]   Pepliński K., Bieliński M., *Właściwości przetwórcze i użytkowe pojemników wytwarzanych w procesie wytłaczania z rozdmuchiwaniem w zmiennych warunkach przetwórstwa - ocena wydajności i jakości procesu*, Polimery 2009, 54, nr 6, pp. 44÷52.

[10]   Rosato D. V., *Blow Molding Handbook*, Hanser Publisher, wyd. 2., Munich 2004.

[11]   Sikora J. W., *Wpływ elementów konstrukcyjnych ślimaka na charakterystykę procesu wytłaczania z rozdmuchiwaniem*, Polimery, 47, 2002, 6, s. 435÷440.

[12]   Szczepański K., *Modelowanie zjawisk zachodzących podczas procesu wytłaczania z rozdmuchiwaniem tworzyw termoplastycznych*, Rozprawa doktorska, Częstochowa 2005.

[13]   Wilczyński K., *Reologia w przetwórstwie tworzyw sztucznych*, WNT Warszawa 2001.

[14]   Wilczyński K., Łączyński B., Czaplarski A., *Modelowanie uogólnionych przepływów newtonowskich za pomocą systemu Polyflow*, Polimery, 43, 1998, 2, pp. 115÷120.

[15]   www.ansys.com/products/polyflow/default.asp

[16]   www.plasticseurope.org, The Compelling Facts About Plastics 2007, Plastics Europe, Brussels – Belgium 2008.

TECHNICAL CONDITION MONITORING
OF HOR 6002 PRODUCTION LINE

Henryk Tylicki, Rafał Bochen

University of Technology and Life Science
ul. S. Kaliskiego 7, 85-789 Bydgoszcz, Poland
tel.: +48 52 340828, fax: +48 52 3408286
e-mail:tylicki@utp.edu.pl, e-mail:r_bochen@wp.pl

Abstract

Article concerns technical condition monitoring procedures dedicated to production line HOR 6002 which are realized during operating and maintenance of the machines. The main goal of the article is to formulate the algorithm of determination of control procedures of the condition of damage location and genesis and prognosis of the machine condition on the production line.

Keywords: *production line HOR6002, monitoring the condition of machine engines, the procedure of the state opinion, procedure genesis and prognosis of the state.*

1. Introduction

Employing the optimum technical state evaluation which is the basis of automation of machines' condition monitoring process in machines' exploitation process, requires optimizing diagnostic parameters set, diagnostic tests, genesis and forecasting methods. State monitoring of HOR6002 production line is the process which should allow to:
 a) determine machines' technical states in real time, on the basis of diagnostic examination results, and to identify defects' localization in case of machine breakdown;
  b) in the future, predict machines' states, based on not complete historical results of diagnostic examinations, which allows to estimate machines error-free running time;
  c) in the future, predict machines' state, based on incomplete historical results of diagnostic examinations, which allows to estimate machines' state, or value of their previous work

This article discusses the above problems in the light of their influence on machines' technical readiness in HOR6002 line, and suggests certain solutions.

2. HOR6002 line production characteristics

HOR6002 line is one of five HOR type production lines, placed in Philips Lighting Poland production plant in Pila, Poland. All HOR lines are capable of producing fluorescent, linear lamps with 8/8" diameter and 0,5 to 1,8 meters long. Thanks to many modifications made by Polish engineers, mechanics, setters and operators, and with significant support from Dutch engineers, HOR6002 is able to produce 7200 lamp pieces per hour. In HOR lines, we can distinguish six modules (Fig. 1): coating module, inside production module, assembling module, control and

measuring module, packaging module, cap filing module [5]. Modules are connected via mechanical conveyers adjusted to the kind of the especially to carried products, semi products or materials which are transported.
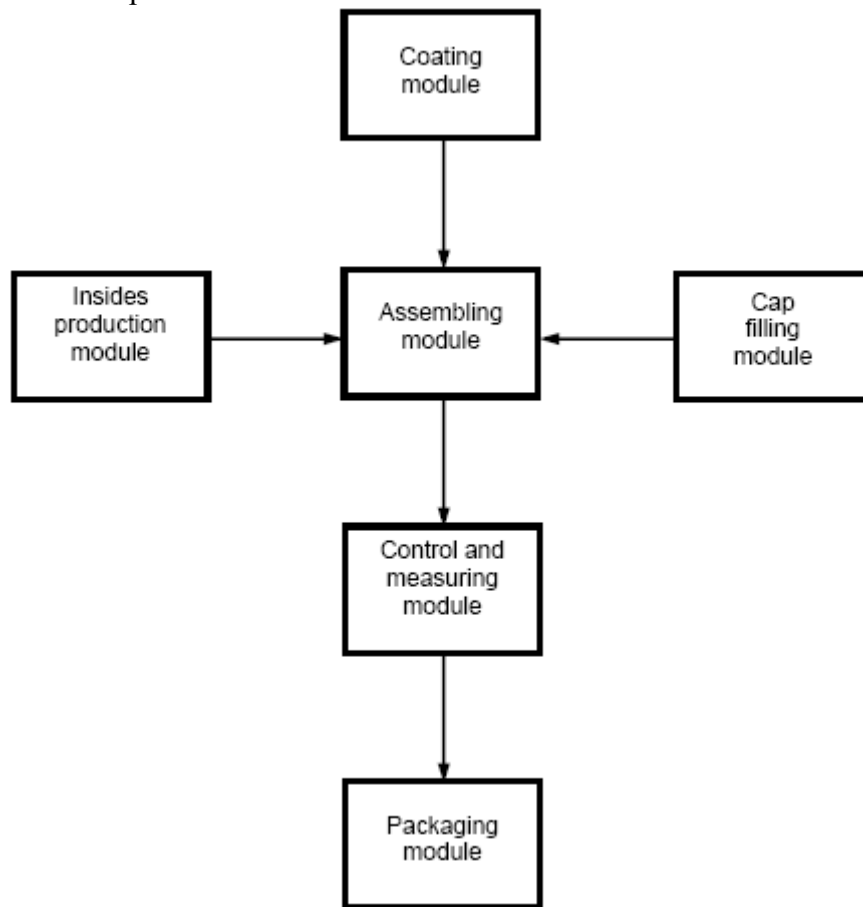
Fig. 1 .Modules of HOR6002 production line

Each of the modules consists of high specialized machines which include sub-assemblies responsible for particular operations made by machines on product. In case of a breakdown, these are replaced so that there is no downtime, and repaired off-line. State monitoring of particular sub-assemblies is done via production process control (each machine product parameters measuring).

In coating module (Fig. 2), the controlled parameters are: coating weight, Top-Bottom (top coating weight – in the injection point, to bottom coating weight ratio), temperature of suspension, in coating and pre-drying chambers), suspension viscosity, color point (correctness of luminofors mixture used in suspension). Among these parameters, only the temperature is controlled automatically, while other parameters are controlled according to statistical process control (SPM). In case of sudden value change of measured parameter, there is no unambiguous answer regarding sub-assemblies states of each machines. There is possibility to correct process parameters, without any certainty if that state was only some kind of disturbance (transient state), or if it is the beginning of breakdown of one of sub-assemblies of modules machines. Measured parameters values are identified, but there is no information about their value changes between measures. If there is any sub-assembly breakdown, the machine or whole line must be stopped to allow its replacement, which causes financial losses.
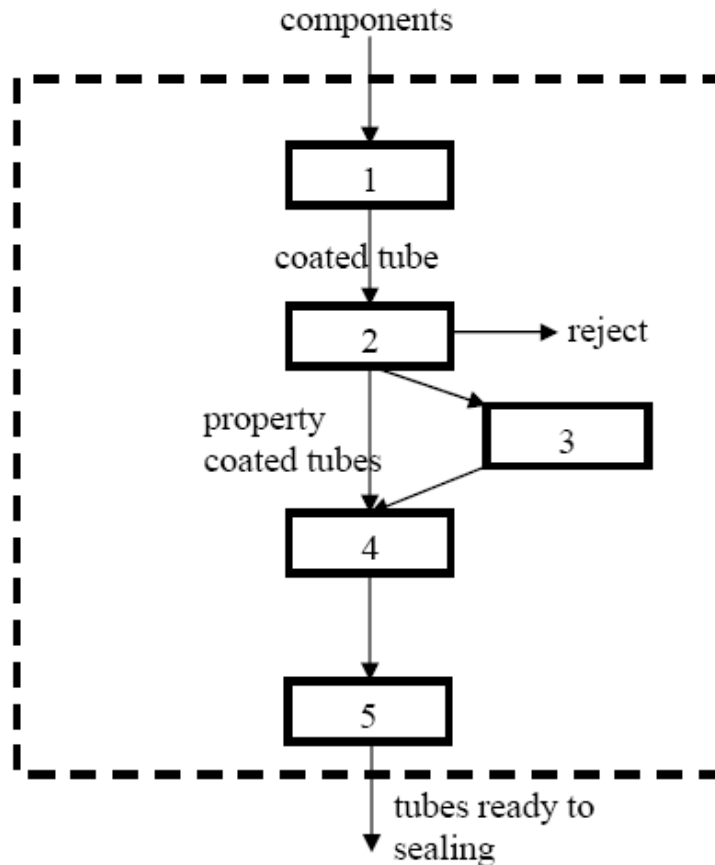
Fig. 2. Coating module: 1 coating machine; 2 –visual controls system; 3 –robotized buffer; 4 –brushing machine; 5 – sintering oven

Interior production module (Fig. 3) is responsible for coated tube closing. Machines' states control in this module is realized via statistical process control. Glass tenses, inside strength, coil coating weight are statistically controlled parameters. Only emitter's viscosity (emitter coats coil) is controlled automatically and continuously. Measurement results are not registered and done only for the sake of continuous, automatic emitter viscosity correction. In case of breakdown any machines of insides production modules, sub-assemblies in broken machine are replaced with fully efficient sub-assembly, however there is not any data which allow to unambiguously determine the cause of breakdown and time of its occurrence.
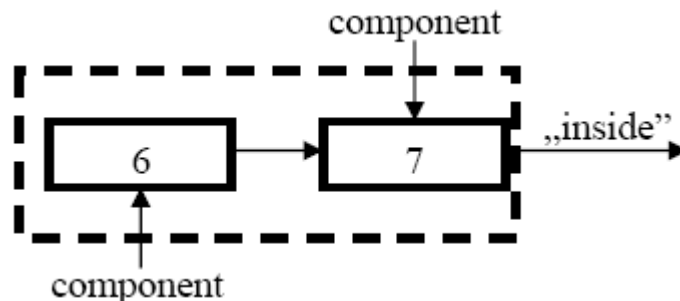

Fig. 3. Interior production module: 6 – steam making machine; 7 – mounting machine

Assembling module (Fig. 4) is responsible for making the lamp from delivered components. It assemblies coated tube with inside (sealing process), which tightens the lamp. After that, the lamp is filled with special gas mixture (pumping process) and coil (part of inside responsible for electrons emission) is prepared (forming process). If the burner complies with its specification, it

is transferred to assembling machine in which burner is assembled with cap (this is the moment in which the burner becomes a lamp). By means of high temperature (~200 Celsius degrees) the cap is permanently connected with the burner.

Also, in the assembling module, machine's sub-assemblies state is estimated in accordance with product parameters values, made on each machine. Failures are shown in the binary system, which means that we can only indicate how many laps are discarded because of particular failures, without information about the value of parameter on which lamp was eliminated. For instance, forming process failure can be caused by coil, but the primal reason can be located in pumping machine or in the interior production module. The primary reason can be declared after a careful lamp investigation. The condition of each machine in assembling module is estimated by reject/waste value of each machine, but there is no certainty that the reject/waste is generated because of the machine, component quality or operator fault. If it is assumed that an excessive rise in waste is a result of the machine sub-assembly failure, the machine which generates reject is stopped for the faulty sub-assembly(ies) replacement. It is always related with the whole line stopping and no production. It is obvious that it has some impact on financial results.
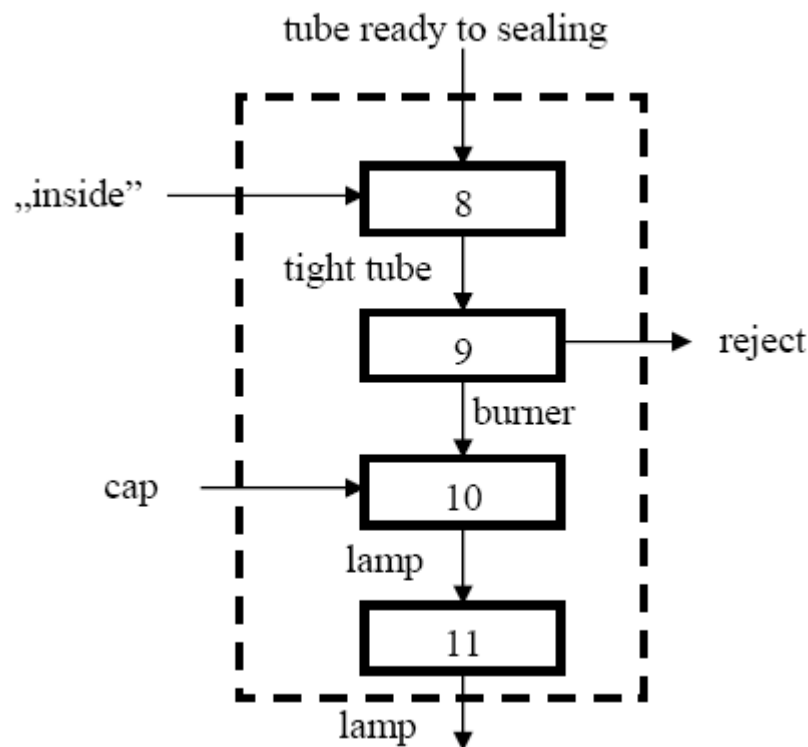

Fig. 4. *Assembling module: 8 –sealing machine; 9 – pumping machine; 10 – capping machine; 11 – hardening machine*

Control and measuring module (Fig. 5) is the module which, by definition, is not supposed to influence the product and it should only control whether the lamps are compatible with technical specifications (whether the preceding process has gone properly), but it doesn't exclude a situation in which the module becomes inefficient, which can be identified by sudden growth of excluded lamps, qualified by flashing and testing the machine as incompatible with technical specifications (reject).
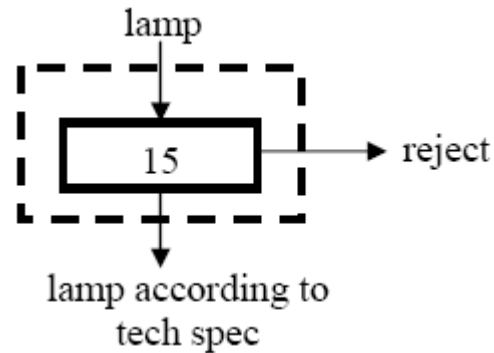
Fig. 5. Control and measuring module: 15 –flashing and testing machine

Inefficient state is easily recognizable by production line setters or operators, because of the appreciable reject. It has got financial consequences, because all eliminated lamps, from the period between inefficient state start and its notification, are qualified as rejects and must be, after the machine becomes efficient, flashed and tested once again. The situation in which proper lamps are wrongly eliminated is better than the situation when incompatible lamps are accepted, which may result in the "call back" (lamps withdraw from the market) and generate the costs of production.

Cap filling module (Fig. 6) is another machine only module. The machine's state is determined on the basis of the products. Visual control system continuously controls cement (glue) layout, done by cementing machine. Caps with improper layout ale eliminated by a special mechanism and gathered in a dedicated container in order to be analyzed. Inefficient state is recognized by a number of eliminated caps, but when it occurs during some time (buffers fulfilled time), the whole line is stopped.
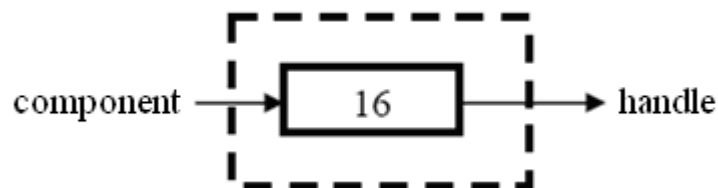

Fig. 6. Cap filling module: 16 – cementing machine

Packaging module (Fig. 7) is the last in HOR6002 line. In this module, proper lamps are packed and prepared to be shipped. The module state is recognized by lamp packaging quality, but it is only a recognition of efficient or inefficient state. This recognition is done by an operator who places group boxes on pallets. Machines which are part of this module are not very complicated, and in case of their inefficiency there is no need for the whole line to cease. By the time packaging machines are functioning again, complete and proper lamps can be gathered by buffer or by operators into special containers. However, such conduct generates extra cost because of bigger labor, additionally, after retrieving the machines' efficiency, the buffered lamps must be placed on the transporter before the packaging module.

Such conduct generates extra cost because of bigger labour, additionally, after packaging machines have become efficient, the buffered lamps must be placed on the transporter before the packaging module.
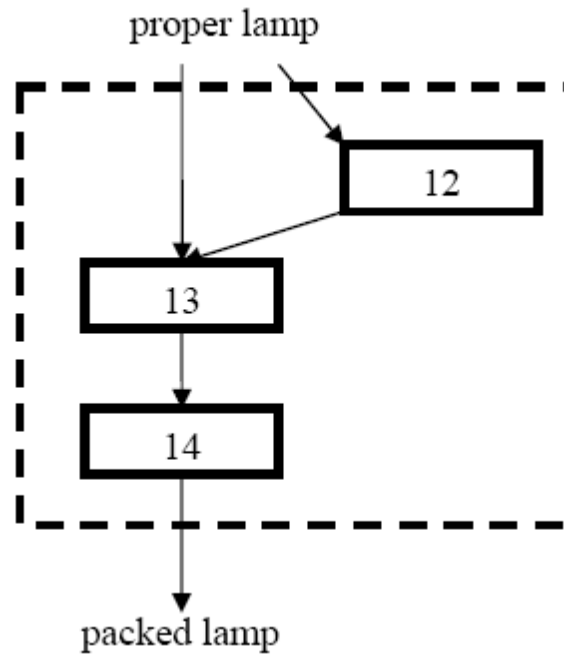
Fig. 7. Packaging module: 12 –robotized buffer; 13 – single packaging machine; 14 – gropu packaging machine

HOR6002 line undergoes regular, weekly checks. Thanks to high-tech industrial Siemens controllers of seventh generation, it is possible to make weekly maintenance plan for particular modules, machines or even sub-assemblies. It is possible because the program is written in the way which allows to sum up machine working hours and the number of products. For the proper functioning of the maintenance process, nine highly specialized mechanics are required. During a maintenance shift, parts of sub-assemblies for which probability of breakdown calculated by producer is very high, are replaced by new or regenerated parts. Replaced parts are generally very expensive, which is noticeable in the maintenance budget calculated only for HOR6002 line (approximately hundreds of thousands Euros). After a sub-assembly, or part, has worked for the producer-calculated number of hours, it is replaced no matter the condition of sub-assembly or part.

HOR6002 production line state monitoring could be alternative to weekly maintenance. However, it needs production line machines' technical state monitoring and suitable sensors deployment (e.g. generated frequencies spectrum, temperatures, dimensions, currents etc.). Thanks to historical values of the diagnostic parameters, it is possible to predict their value in the future, and determine, with a probability dependent on quantity and quality of data, whether a sub-assembly will be efficient until the next maintenance shift, or whether it needs to be replaced. Thanks to such a prediction, high savings can be generated by a lower number of replaced sub-assemblies/parts, no need to keep a large parts storage, maintenance brigade wouldn't be so large. It would be easy to predict when a particular part will break down, and order the part from a supplier in advance

3. Problem characteristics

The problem of production line state monitoring (state evaluation, state prognosis and genesis of machine) is very essential at the designing stage, as well as production and operation stages. While determining state monitoring procedures which serve as tests of state control and damages localization, machine state prognosis and genesis will encounter certain obstacles which are reflected in the following questions [1, 2, 6, 7, 10]:

a) does the optimal set of diagnostic parameters unambiguously describe machine state; does it correlate with machine state change, does it include enough information on the machine's state?
b) is optimal diagnostic parameters set stable, or does it fluctuate, and if so, what is the nature of these changes depending on machine's operating conditions?
c) what is the influence of characteristic factors on machine operating, over optimal test stability and state control program: machine diagnostic susceptibility, diagnosis reliability
d) level (which can be decided by operator), change of machine operating conditions and change in sub-assemblies reliability?
e) what is the influence of machine operating characteristic factors on optimal forecast stability: value of forecast or genesis range (which can be decided by the operator), change of machine operating conditions and change in sub-assemblies reliability?

Accurate solutions to the indicated problems are essential to highly effective HOR6002 machines' state monitoring and requires necessary examination of sensitivity of procedures to the conditions described. If the examination shows that the determined procedures are stable, they can be used to set programs to state control, damages localization, machine state prognosis and genesis. In other cases, assumptions and limits regarding state monitoring procedure setting should be modified, e.g. by conscious exclusion of the factors which cause solution instability; but it makes the solution less universal.

4. Monitoring state line production HOR6002

We can distinguish in diagnostics examination methodology the following phases of evaluating examination which have the following diagnostic mechanism forms:
a) diagnosis – machine state determination in Θ_b time;
b) genesis – as the machine historical states recovering, e.g. in order to determine the primal reason for damage which appeared during machine examination;
c) forecasting – as future machine state prognosis, e.g. in order to determine the next maintenance shift time (Θ_d);
Main problems which can appear during machine state monitoring task realization are:
a) determination of goals of machine state diagnosing, forecasting and genesis making;
b) machine state changing during operating;
c) machine state description by means of state features and relations between state features and diagnostic parameters;
d) state diagnosis task realization;
e) state forecasting task realization;
f) state genesis task realization;
Main problems occurring during task realization shown above are:
a) most suitable parameters choice, which describe best, actual machine state and its future change;
b) diagnostic test setting;
c) forecasting value of diagnostic parameter setting, for forecast range τ_1, $s_{jp}(\Theta_b+\tau_1)$ with best forecasting method and with the next diagnostic and maintenance time Θ_d setting;
d) determination of the value of diagnostic parameter genesis for genesis range τ_2, $y_{jp}(\Theta_b-\tau_2)$ with the best genesis method and machine state estimating, valuation of the work done by machine, determination of primal reason of machine damage occurring during machine examination.
The term "best" used here relates to the established suitable criteria, and takes them into consideration in optimal solution research, and because of many valuation criteria. There is a need

to look at problems in a multi-optimal solution [8] for particular tasks (local optimum) or for machine state monitoring task (global criteria).

5. Conclusion

To summarize, the solutions to certain problems described require formulation and solution to consecutive sub-tasks according to the algorithm shown below:
1) analysis of the production line machine's state monitoring process;
2) development of the production line machine state monitoring model;
3) optimization of the production line machine's state monitoring process;
4) verification of the state monitoring procedures for selected production line machines;
5) employment of monitoring procedures in operating and maintenance of sub-systems of the production line HOR6002.

The algorithm presented above is the basis for future authors' publications in which, thanks to modern diagnostic tools from modeling area, experiments and development of statistical data, one may expect solutions to the problems described in the article.

References

[1] Batko, W., *Metody syntezy diagnoz predykcyjnych w diagnostyce technicznej*, AGH, Kraków 1984.
[2] Będkowski, L*., Elementy diagnostyki technicznej*, WAT, Warszawa 1991.
[3] Box, G., Jenkins G., *Time series analysis forecasting and control*, London 1970.
[4] Cempel, C.: *Ewolucyjne modele symptomowe w diagnostyce maszyn*, Materiały I Kongresu Diagnostyki Technicznej, Gdańsk 1996.
[5] *Linia produkcyjna HOR 6002,* Materiały Philips Lighting Poland S.A., Piła 2006.
[6] Staszewski W.J., Boller C., Tomlinson G.R., *Health Monitoring of Aerospace Structures*. John Wiley & Sons, Ltd. Munich, Germany 2004.
[7] Theil, H., *Applied economic forecasting*, North-Holland, Amsterdam 1971.
[8] Tylicki, H., *Optimization of the prognosis method of mechanical vehicles technical state*, Wydawnictwa uczelniane ATR, Bydgoszcz 1998.
[9] Tylicki H. i inni, *Sprawozdanie z projektu badawczego KBN nr 4 T07B 033 26*. UTP, Bydgoszcz 2007.
[10] Żółtowski B., *Podstawy diagnostyki maszyn*. Wydawnictwa Uczelniane ATR, Bydgoszcz 1997.

STUDY OF THE TECHNICAL STATE OF A FRANCIS TURBINE BY ROTOR DYNAMIC SIMULATIONS

Bogdan Żółtowski
Jaime Leonardo Barbosa Perez
Leonel Francisco Castañeda Heredia

Abstract

This paper presents a methodology to evaluate the technical state of a Francis turbine by shaft rotor dynamic simulation. There are several rotor dynamic criteria that define the technical state of a turbomachine. To feed the shaft rotor dynamic model this delivers the required information to accomplish the technical assessment. The numerical rotor dynamic model uses as input, the field forces obtained by the fluid-solid interaction analysis undertaken over the blades of the runner.

The rotor dynamic numerical simulations allow to determinate the record-in-time of the displacements of any point along the shaft. This information is relevant for diagnosis tasks, because it is possible to decompose it spectrally and to estimate the severity of the vibrations. Comparing the results of the numerical model against those obtained from machines that operates under normal conditions, it is possible to determinate the technical state of the turbomachine. This allows studying the stability of the turbine working on several operation ranges.

A Francis turbine is a very complex machine that involves many physical phenomena of different nature. In this way, the hydraulic input forces needed by the rotor dynamic model should not be assumed but calculated directly from the fluid interaction over the turbine structure.

Keywords: *FEM, Francis turbine, Diagnosis, Fluctuations, Hydrodynamic*

1. INTRODUCTION

The technical diagnosis is a set organized of methods and a half that allow the evaluation of the technical condition state (his reason, evolution and consequence) of systems of engineering. In most cases they are systems in operation, designed to fulfill a principal function. These appliances generate and transform information, which is used later to study his technical condition state.

For the definition of the field of application of the technical diagnosis, are studied the processes of destruction of the objects during the whole period of his existence and certain situations, in which it is necessary to consider the actions (shares) of diagnosis. The term "period of existence of the machines" refers to the cycle that initiates in the instant that there are formulated the requirements of design that must fulfill the new object up to his respective liquidation (residues, felling and reutilization). (Żółtowski B., 2002).

The current technology (skill) is a result of the models' analysis, which they describe with certain degree of accuracy. The process, which takes as an aim the construction of the best model of operation (mathematical or empirical), is named a process of identification, and includes shaped, you try, estimation and check. The methodology of the studies of diagnosis includes the heuristic and mathematical models (Żółtowski B., 1996).

"The identification in the diagnosis is a process of searching complex, in that, based on the knowledge of the structure and the functioning of the object, there are realized the analysis and the

synthesis of the model of the object for the obtaining of the information of diagnosis". The idea on the methodical construction of the dynamic model of the mechanical system is supported of the information of the modal experiment and the information of the measurements of the quantities of vibration (acceleration of the vibration, moment rotational, you force and etc.) in conditions of exploitation development. The models of analysis of loads (charges) are constructed depending on his application in the procedures of dynamic optimization and diagnosis of exploitation development. (Żółtowski B., Cempel C., 2004).

During the electric generation process, the turbines develop hydraulic phenomena that extend along all the components of the machine represented in vibrations, sound and instabilities. Recently, the evaluation of the machine state using modern diagnosis techniques has become important. These diagnosis techniques, expert systems in particular, are based on the knowledge of the technical system and on the use of artificial intelligence. To enlarge the understanding of machines for failure detection, the study of their dynamical behavior plays a significant role. This methodology is known as maintenance based on models and pretends to achieve the failure identification by establishing relations between the real object and a virtual model (Kicinski, 2006).

The vibration analysis has been a important tool in the technical diagnosis. Instruments for measuring vibrations (accelerometers) are implemented in large machines and the parameters extracted from the acquired signals are used as effective indicators of the technical state. The rotor dynamical study of turbines, in this case, pretends to develop the knowledge to correctly identify the relations between the symptom and its causes.

The objective of the present study is to develop a study method that allows calculating the displacements of any point along the shaft of the turbine using FEM simulations. This information is relevant for diagnosis tasks, because it is possible to decompose it spectrally and to estimate the severity of the vibrations.

2. CASE OF STUDY

This investigation considers a Francis turbine composed by 20 stay and guide blades and 15 runner blades. It rotates at 900 rpm and generates a maximum output of 10MW. For this case, only the Best Efficiency Point (BEP) is analyzed. The turbine head is 230 m and the discharge at this point is 4.8 m^3/s.

The assembly of the turbine / generator of can be observed in Figure 1. The set is assembled on a rigid shaft, to which are attached: the runner, the flywheel, the generator core and poles, and the exciter. The shaft is supported by three hydrodynamic bearings. The first of them (nearest to the runner) has axial and radial effect; the other two have only radial effect.
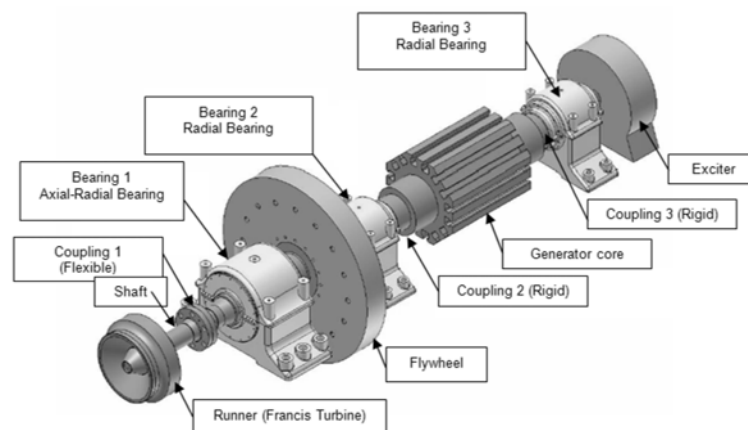
Figure 1. Turbine shaft with bearings and attached mechanical elements

3. METHOD OF EXPERIMENTAL MEASURES

A series of measurements using dynamic pressure sensors arranged along the guide vanes and draft tube were carried out. Also, a set of strain gages installed in the turbine shaft were employed with the purpose of measuring deformations to determine the torque and the radial forces.

There were installed sensors along different components of the turbine. Three of them were installed near the zone where the rotor-stator interaction occurs (between the guide vane and the runner). Figure 2 shows an image of the approximate position of one sensor.
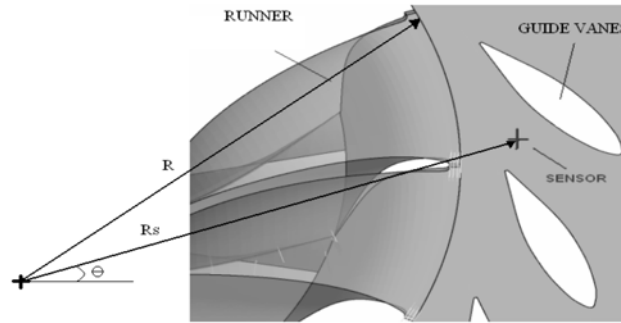

Figure 2. Position of the sensors

The task of these sensors was to capture pressure fluctuations generated by the rotor-stator interactions. Figure 3 shows an image of the experimental assembly carried out. It can be appreciated the physical conditions of the sensor installation.
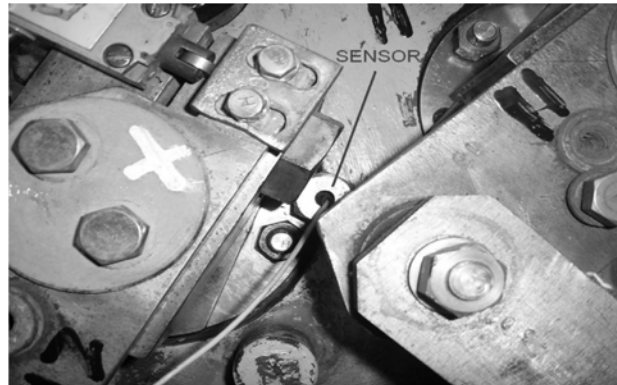

Figure 3. Photo of the experimental location of the sensor

Another six dynamic pressure sensors were installed along the draft tube. The objective of the sensors was to obtain information on the vortex rope generated at the exit of the runner. The sensors were distributed in two cross sections: i.e. A and B; in each section were installed 3 sensors (Fig.4).
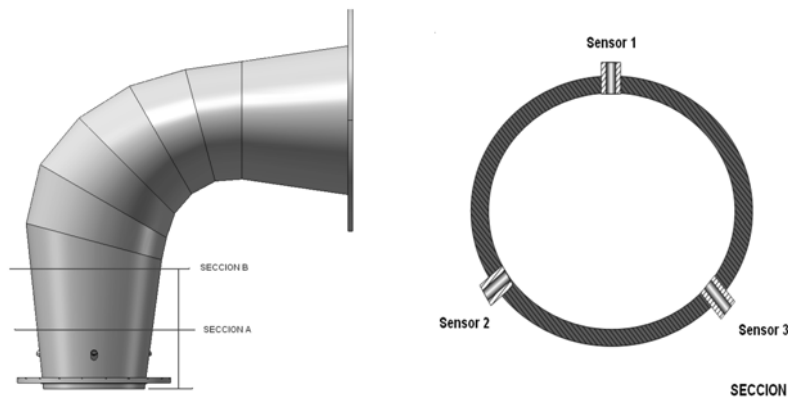

Figure 4. Distribution of the sensors in the draft tube

The measurements were recorded performing a simultaneous sampling during 3 seconds of every channel at 102 kHz, i.e. more than 40 rotor revolution and more than 6500 samples per channel. It allows to capture all the hydraulic phenomena present at low and high frequencies.

For the measurement of the torque and the radial force a strain gage technique applied to the generation shaft was used. The use of this technique did not affect the turbine operation in any way. The strain gage signals were registered via wireless connection.

Figure 5 shows the position in the shaft where the strain gages (SG) were installed. For the measurement of the radial force it was use of four bi axial well dable SG meanwhile the measurement of the torque used one bi axial well dable SG. The strain gages were connected to a transmitter tied to the shaft.
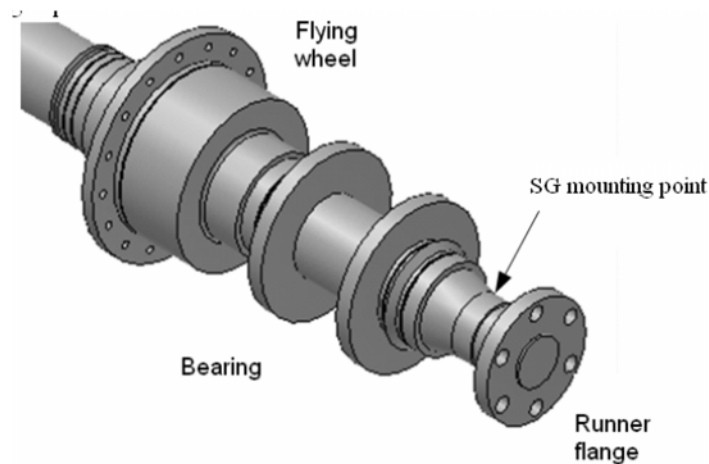

Figure 5. Strain gages position in the shaft

Figure 6 shows an image of the experimental installation of the SG. The distribution of the strain gages and its position in the shaft can be observed.
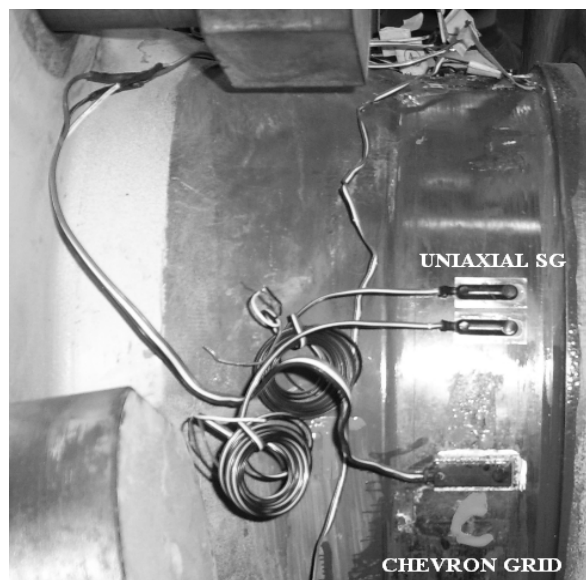

Figure 6. Photo of the experimental installation of the gages in the shaft

The information give by all this pressure sensors and the strain gages is used to validate the CFD numerical model.

4. ROTODYNAMIC METHOD

The goal is to develop a model that accurately predicts the dynamic behavior of the shaft of a Francis turbine by means of numerical methods. To achieve this goal, it is necessary to find an approximated solution to the equations of motion of the system. These equations are a set of non linear differential equations:

$$\mathbf{M\ddot{x}} + \mathbf{D(x,\dot{x})\dot{x}} + \mathbf{K(x,\dot{x})x} = \mathbf{P(t)} \quad [1]$$

Where:

M : Global matrix of inertia.

D : Global matrix of damping.

K : Global matrix of stiffness.

$P(t)$: Generalized vector of external excitations.

x : Generalized vector of position.

The model is implemented in the computational environment MESWIR®. This software was developed by the Institute of Fluid Flow Machinery (IFFM) from the Polish Academy of Science. It composed by a set of codes to determine static and dynamic parameters of rotors, including analysis of the hydrodynamic bearings. The software uses the finite element method to analyze the rotor shaft and the finite difference method to determine the characteristic of the hydrodynamic bearings. With the software it is possible to analyze lateral vibrations with linear and non linear models.

The required entries of the model are: the conditions of support, the forces or external excitations, the mechanical and geometrical properties of the shaft. The shaft is supported in three hydrodynamic bearings but for the rotordynamic model they are represented by springs and dampers. The determination of the oil film stiffness and damping coefficients required additional computation of the fluid dynamics involved. The oil film stiffness and damping coefficients depend on the relative position and velocity of the journal in the bearing causing the non linearity in the equations of motion. However the results obtained under the assumption of linear stiffness and damping coefficients are acceptable. For the purpose of this work, the MESWIR® linear models were used.

The bearings are also attached to a foundation. The foundation is replaced in the mechanical model by springs and dampers, whose coefficients were prior determined by experimental measurements and numerical simulations. The shaft is modeled coupled rigid discs with masses and inertias equivalent to those of the real objects.
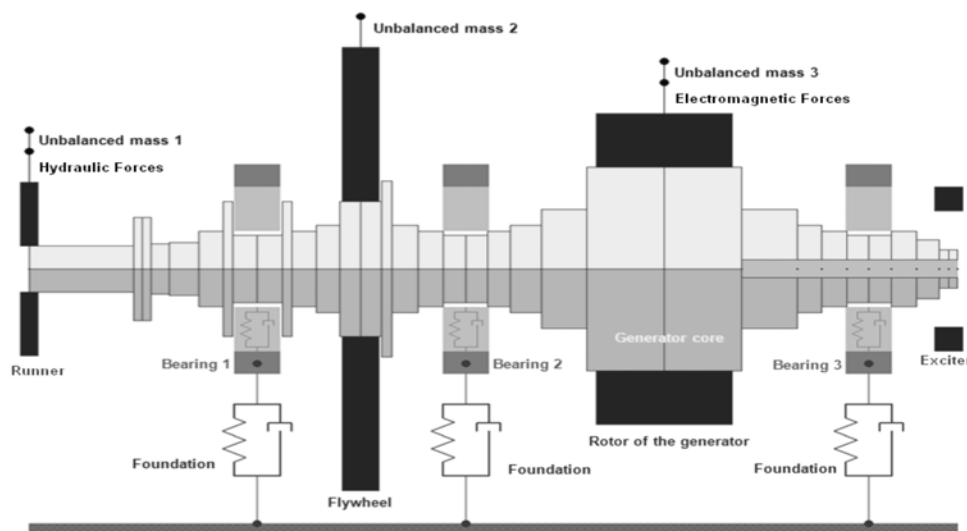

Figure 7. Numerical model

Geometry and physical properties

The real model is simplified in a mechanical model to make possible its analysis (Figure 7). The shaft is discredited into 33 cylindrical Timoshenko beam elements with six degrees of freedom to use the finite element method. These elements are provided of mass, stiffness and damping, which are estimated from the physical properties of the material of the shaft, such as: density, Young modulus, Poisson coefficient and damping coefficients. In the Table are listed the material properties.

Table 1. Physical properties of the material of the shaft

Density	Young modulus	Poisson coefficient	Damping coefficient A	Damping coefficient β
7800 kg/m^3	200 GPa	0.3	1.96 rad/s	5.09*10^{-5}s/rad

Support parameters

In the oil film in the hydrodynamic bearings appears a hydrodynamic pressure distribution induced by the rotation and originating the reaction force. This pressure distribution is described by the Reynolds equation:

$$\frac{1}{R^2}\frac{\partial}{\partial\theta}\left(h^3\frac{\partial p}{\partial\theta}\right)+\frac{\partial}{\partial z}\left(h^3\frac{\partial p}{\partial z}\right)=6\eta\left(\frac{1}{R}\frac{\partial(hU)}{\partial\theta}+2\frac{\partial h}{\partial t}\right) \quad [2]$$

Where:

p : Pressure in the oil film.

h : Film thickness.

U : Oil velocity in tangential direction.

η: Dynamic oil viscosity

R: Radius of journal.

Assuming that the flux is laminar and that the viscosity is constant along the oil film the pressure distribution could be found. The magnitude and orientation of the reaction force depend of the position and velocity of the gravity center of the rotor shaft. The stiffness and damping coefficients are computed based on the reaction force. The stiffness coefficients are the derivatives of the reaction force respect to the displacements.

$$k_{11}=\frac{\partial W_x}{\partial x}, \quad k_{22}=\frac{\partial W_y}{\partial y}$$
$$k_{12}=\frac{\partial W_x}{\partial y}, \quad k_{22}=\frac{\partial W_y}{\partial x} \quad [3]$$

Where:

$k_{11}, k_{22}, k_{12}, k_{22}$: oil film stiffness coefficients

W_x, W_y : Components of the reaction force.

The damping coefficients are found as the derivatives of the reaction force respect to the velocities.

$$c_{11}=\frac{\partial W_x}{\partial \dot{x}}, \quad c_{22}=\frac{\partial W_y}{\partial \dot{y}}$$
$$c_{12}=\frac{\partial W_x}{\partial \dot{y}}, \quad c_{22}=\frac{\partial W_y}{\partial \dot{x}} \quad [4]$$

Where:

$c_{11}, c_{22}, c_{12}, c_{22}$: oil film damping coefficients.

The figure 8 presents a representation of the oil film as springs and dampers.
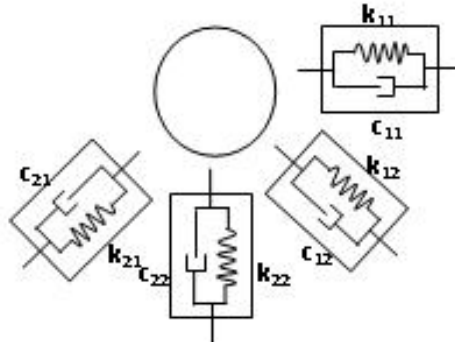

Figure 8. Stiffness and damping coefficients of the oil film

The shaft is affected by static and dynamic loads. The static loads are the masses of the elements attached to the shaft. The dynamic loads are originated by: residual unbalanced masses, the solid-fluid interaction in the runner and electromagnetic phenomena in the generator.

Static and dynamic loads

The static loads are determined by the geometry and physical properties of the discs assembled to the shaft. For the model, it is supposed that these discs are made of steel. The discs add mass and inertia to the system but they do not represent additional stiffness or damping. Other properties of the discs are list in

Table 2. Elements assembled to the shaft

Element	Runner	Flywheel	Generator poles	Exciter
Outer diameter (m)	0.900	2.300	1.614	0.850
Inner diameter (m)	0.240	0.706	1.054	0.600
Thickness (m)	0.146	0.300	1.090	0.225
Mass (kg)	673	8806	9977	500
Inertia (kgm^2)	73	6372	4634	68

As it was mentioned the dynamic loads could be inertial, hydraulic or magnetic. The inertial forces are used to tune the model and the represent an output of the model. The hydraulic forces are estimated by CFD simulations. Regarding to the magnetic forces only unbalanced magnetic pull is considered.

The unbalanced magnetic pull appears when the rotor is eccentrically positioned respect to the stator. This causes asymmetric distribution of the magnetic flux and then an unbalance force in the direction of the smallest air gap. This force depends in a non linear way of the relative eccentricity, which is defined as:

$$\varepsilon = \frac{u_r}{\Delta R} \quad [5]$$

Where:

ε : Relative eccentricity

u_r : Distance between the rotor center line and the stator center line

ΔR : Difference between the stator inner radius (R_s) and the rotor radius (R_r).

The unbalance magnetic pull has a constant and a variable part. The variable force oscillates with a frequency equal to the supply frequency. If the number of poles increases, the variable part decreases. The mean value for the unbalance magnetic pull could be found as (Gustavsson, 2005):

$$F = \frac{\mu_0 S_s^2 R_s^3 h\pi}{2p^2 \Delta R^2} \frac{e}{\sqrt{(1-e^2)^3}} \quad [6]$$

Where:

μ_0 : Magnetic permeability.

S_s : Lineal density of current

R_s : Stator inner radius

h : Rotor length

e : Relative eccentricity

p : Number of poles.

By means of a static analysis the deflection of the shaft in the generator core section is found. With this value and the technical information of the machine the unbalance magnetic pull is computed and is found that it has a value of 4966 N.

5. RESULTS

The experimental data used in rotordynamic calculations is obtained from displacement sensors installed in the bearings. In each bearing are two sensors forming a rectangular angle between them and an angle of 45 degrees respect the horizontal plane as is shown in Figure 9. Then, the vibration is measure in a coordinate system that is 45 degrees rotated respect the general coordinate system and some transformations should be made to compare the results.
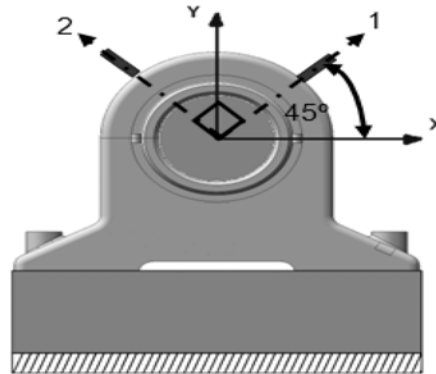

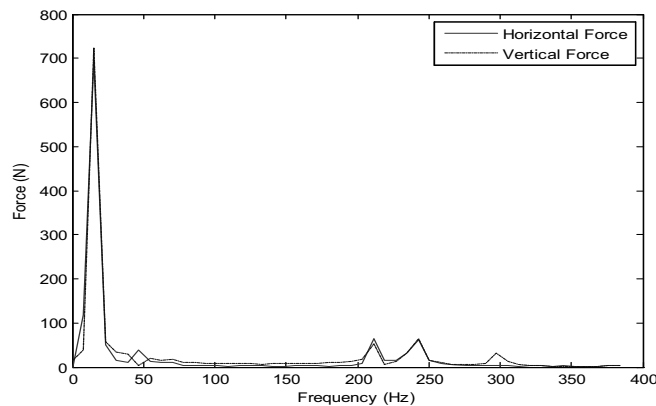Figure 9. Stiffness and damping coefficients of the oil film

Figure 10. Spectral analysis of the radial force

Table 3. Spectral components of the radial force

Frequency (Hz)	Horizontal force (N)	Vertical Force (N)
15	696.2	723.50
210	65.53	53.52
240	61.58	64.93
300	--	30.6

The most relevant component in the spectrum is at 15 Hz, which is the rotational frequency of the machine. The other force components are very low and are not considered in this analysis. In the model the force should be introduced as an unbalanced mass at specific unbalance radius. The transformation is made using the definition of centrifugal acceleration.

The analyses are made with the modules of MESWIR® for studying lateral vibrations with linear models. Hence, only excitations at first harmonic are taken into account and the numerical signals are sine functions with the rotational frequency. In Figure 11, 12 and 13 the experimental and numerical results for the displacement vibration are compared for each bearing.
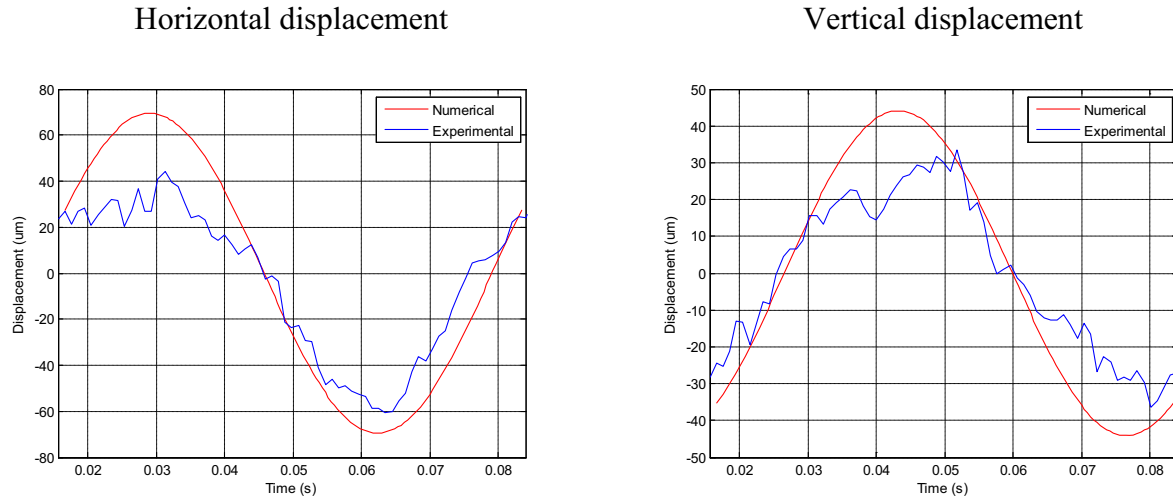
Horizontal displacement   Vertical displacement

Figure 11. Numerical and experimental displacement signals for the bearing 1

Horizontal displacement   Vertical displacement
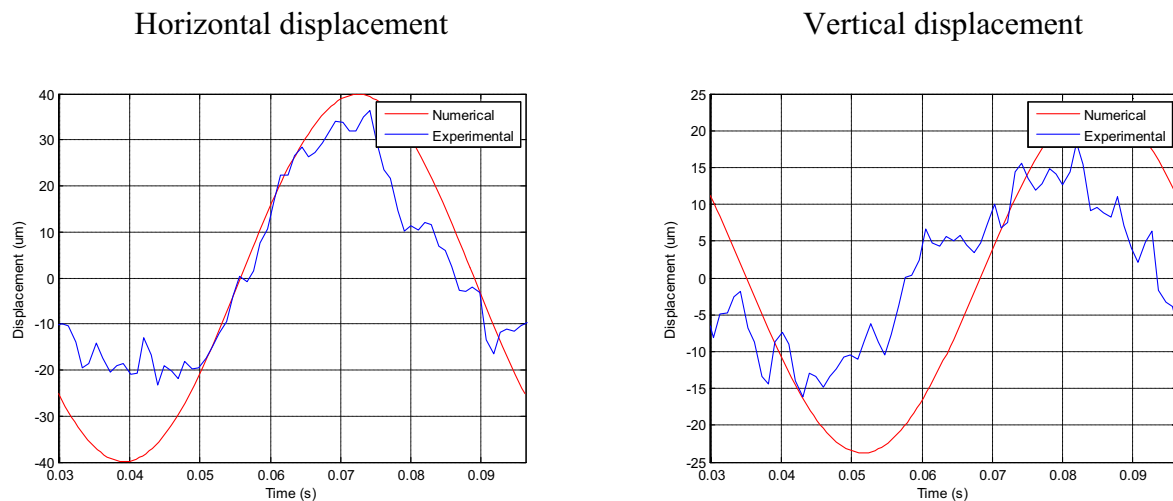
Figure 12. Numerical and experimental displacement signals for the bearing 2

121

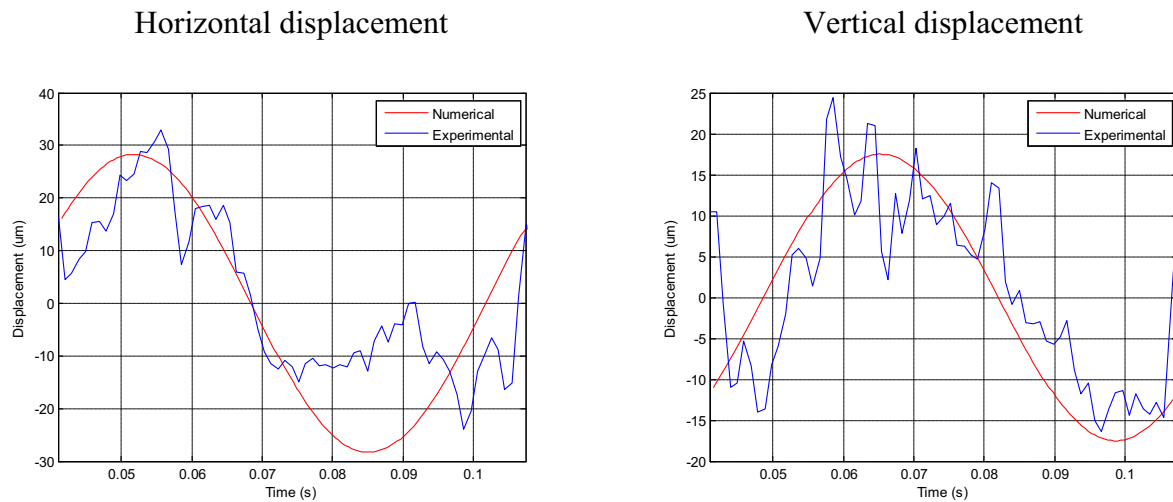| Horizontal displacement	Vertical displacement

Figure 13. Numerical and experimental displacement signals for the bearing 3

As it was mentioned the unbalanced forces are tuned until the numerical vibration amplitudes adjust to those measured in the real technical object. The final required values represent a result from the rotordynamic model.

Table 4. Resultant unbalance masses

Position	Unbalanced mass (kg)	Unbalance radius (m)	Phase (degrees)
Runner	7.000	0,5	0
Flywheel	15.000	0,5	180
Generator poles	12.400	0,5	0
Runner (hydraulic force)	0.157	0,5	0
Runner (hydraulic force)	0.163	0,5	90

6. FINAL CONSIDERATIONS

The radial forces obtained via numerical methods were used to feed the FEM rotordynamic software. These forces have a consistent predominant spectrum component at the frequency of rotation which was used in the linear rotordynamic model. However this resultant radial component has a low magnitude, because for the simulations the runner is completely symmetrical and the unbalance in the pressure distribution is little. If some imperfections of the runner are included in the simulations, the magnitude of force would probably become more significant.

It was possible to develop a rotordynamic model whose results are in agreement with the experimental data. In this case, the unbalance masses required are relative large. This could be caused because the rotor is very rigid and important amounts of residual unbalanced could be bear with acceptable vibration amplitudes.

The amplitudes of vibration for the displacement obtained by the numerical computations and the experimental measures are acceptable according to the standard ISO 7919-5. This standard establishes a maximum limit of 165μm. From the point of view of vibration the technical state of the machine is acceptable.

BIBLIOGRAPHICAL REFERENCES

[1] Egusquiza, E. Nascimento, L.P. Valero, C. Jou, E. (1994) *El diagnostico de daños en grupos hidroeléctricos mediante el análisis de vibraciones*. Revista Ing. del agua Vol 1 Num 3.

[2] Gagnon, J.M, Payette F.A. and Deschenes C. (2007). *Numerical Simulation of a Rotor-Stator Unsteady Interaction in a Propeller Turbine*. CFD Society of Canada, Toronto.

[3] Guedes, A. Kueny, J.L. Ciocan, G. and Avellan, F. (2002). *Unsteady rotor-stator analysis of a hydraulic pump-turbine – CFD and experimental approachl*.

[4] *Proceedings of the XXIst IAHR symposium on hydraulic machinery and systems*, Laussane, Switerland.

[5] Hoffmann, K. (1989). *An introduction to measurements using strain gages*. Hottinger Baldwin Messtechnik GmbH, Darmstadt.

[6] Menter F.R. (1994). *Two-equation eddy viscosity turbulence models for engineering applications*. AIAA Journal.

[7] Nennemann, B. Vu, T. and Farhat, M. (2005). "*CFD prediction of unsteady wicket gate-impeller interaction in Francis turbines: A new standard hydraulic design procedure*. Waterpower XIV, Austin, USA.

[8] Qian, Z. Yang, J. Huai, W. (2007). *Numerical simulation and analysis of pressure fluctuation in Francis hydraulic turbina with air admisión*. Journal of hydrodunamics.

[9] Zobeiri, A. Kueny, J.L. Farhat, M. and Avellan, F. (2006). *Pump turbine rotor-stator interactions in generating mode: pressure fluctuations in distributor channel*. 23th IAHR symposiums, Yokohama, Japan.

[10] Ciocan and others (2007). *Experimental study and numerical simulation of the FLINDT draft tube rotating vortex*. Journal of fluid dynamics. Vol 129.

[11] Kicinski, J. (2006). *Rotor dynamics*. Institute of Fluid-Flow Machinery Polish Academy of Science, Gndask.

[12] Gustavsson, R (2005). *Modelling and Analysis of Hydropower Generator Rotors*. Lulea University of Technology. The Polhem Laboratory. Division of Computer Aided Design.

[13] Żółtowski B., Badania dynamiki maszyn, 2002, Bydgoszcz (Polonia), Akademia Techniczno - Rolnicza w Bydgoszczy, p. 337.ISBN 83-916198-3-4

[14] Żółtowski B., Podstawy diagnostyki maszyn, 1996, Bydgoszcz (Polonia), Akademia Techniczno-Rolnicza w Bydgoszczy. ISBN 83-900853-9-9.

[15] Żółtowski B., Cempel C., Inżynieria diagnostyki maszyn, 2004, Varsovia, Towarzystwo Diagnostyki Technicznej, Instytut Technologii Eksploatacji, pp. 1109.